Kristian Løvås Svalland

Topological phases in proximised magnetic superconductors and related time dependent phenomena

Master's thesis in Applied Physics
Supervisor: Jacob Linder and Mario Cuoco
July 2019

Master's thesis

NTNU
Norwegian University of Science and Technology
Faculty of Natural Sciences
Department of Physics

NTNU
Norwegian University of
Science and Technology

SPIN

Kristian Løvås Svalland

Topological phases in proximised magnetic superconductors and related time dependent phenomena

Master's thesis in Applied Physics
Supervisor: Jacob Linder and Mario Cuoco
July 2019

Norwegian University of Science and Technology
Faculty of Natural Sciences
Department of Physics

NTNU
Norwegian University of
Science and Technology

Abstract

Noncollinear magnetic textures in contact with superconductors have been shown to harbour Majorana modes at their edges. In this thesis we investigate new phenomena related to the generation and control of the topological phase of 1D magnetic chains proximised to superconductors. The topological phases of noncollinear magnetic chains deposited on s-wave superconductors and collinear magnetic chains deposited on p-wave superconductors were analysed in the tight-binding approximation in both the adiabatic and sudden quench limit. For non accidental values in the parameters space that set the character of the magnetic and superconducting order parameters, these types of superconductors are gapless and any symmetry conserving and gap-opening perturbation brings them into a topological phase. This regime in topological superconductors can open up new paths to controlling the topological phase in the future, as arbitrarily small perturbations activates the topological phase. The topological phases of the special case of an elliptical field were analysed in terms of the synthetic dimensions given by the offset and eccentricity of the elliptical texture. When an out-of-plane chiral symmetry breaking field reaches a critical value of Δ_0 the energy gap closes at general points in the Brillouin zone, effectively killing the Majorana bound states. Under quenches in the parameters, critical values of the out-of-plane field also led to fast decay of the survival probability of the Majorana states. We find that by switching the helicity of the ellipse, characteristic length scales are an important factor for the survival of the Majorana bound states.

Sammendrag

Ukolineære magnetiske teksturer i kontakt med superledere har blitt vist å huse Majorana fermioner på kantene. I denne oppgaven undersøker vi nye fenomener relatert til opprettelse og kontroll av den topologiske fasen i 1D magnetiske kjeder i nærhet til superledere. Den topologiske fasen til ukolineære magnetiske kjeder lagt på s-bølge superledere og kolineære magnetiske kjeder lagt på p-bølge superledere ble analysert i 'tight-binding' approksimasjonen både adiabatisk og med plutselige endringer i parametrene. For tilsiktede verdier i mulighetsområdet for parametrene som bestemmer karakteristikken til den magnetiske og superledende ordensparametrene, var disse superlederne uten gap i energispekteren og enhver symmetrikonserverende og energigap-åpnende perturbasjon ledet dem inn i en topologisk fase. Dette regimet innen topologisk superledning kan åpne nye retninger for kontroll av topologiske faser i fremtiden, siden vilkårlig små perturbasjoner er i stand til å aktivere den topologiske fasen. De topologiske fasene til spesialtilfellet av et elliptisk magnetfelt ble analysert i form av syntetiske dimensjoner gitt av ellipsens eksentrisitet og av faseforskyvningen av magnetfeltvektorene på ellipsen. Når et kiral-symmetri-brytende magnetfelt vinkelrett på planet til ellipsen når en kritisk verdi tilsvarende Δ_0, lukker energigapet seg på generelt grunnlag. Derved forsvinner Majorana fermionene fra systemet. Plutselige endringer i denne parameterer førte også til rask nedgang i overlevelsessannsynligheten til Majorana fermionene. Vi oppdaget at ved å endre helisiteten til den elliptiske teksturen i Hamiltonian-en, var karakteristiske lengde skalaer på endringen av stor betydning for skjebnen til de bundne Majorana fermionene.

Acknowledgement

During the spring of 2019 I have had the pleasure of working closely with Mario Cuoco at the University of Salerno on this final part of my Master's degree in applied physics. Mario has welcomed me to the scientific community at the University of Salerno and made sure that my stay in Italy was comfortable and that the transition was an adiabatic one. Mario and I have continuously discussed the goals of the thesis, and dynamically updated them as we obtained results. I want to thank Mario for the great and interesting theoretical discussions in the course of the investigations that went into this master's thesis. I am grateful for helpful discussion on the topics of the thesis with Prof. Maria Teresa Mercaldo at the University of Salerno. I also want to thank Prof. Jacob Linder for all the help he has contributed during the research and for discussing the ideas and goals of the thesis during the last year. Jacob also was my supervisor for the specialisation project in the fall of 2018, which we used as a primer for the work that was done this spring. Without his supervision I would have had a much harder time to do the necessary investigations that went into this work. I am grateful that Jacob was positive to the idea of writing the master's thesis abroad, which turned out to be an awesome experience for me.

Contents

List of Figures

List of Tables

Nomenclature

Pauli matrices

The Pauli matrices, including the identity σ_0, are

$$\sigma_0 = \begin{pmatrix} 1 & 0 \\ 0 & 1 \end{pmatrix} \qquad \sigma_1 = \begin{pmatrix} 0 & 1 \\ 1 & 0 \end{pmatrix}$$
$$\sigma_2 = \begin{pmatrix} 0 & -i \\ i & 0 \end{pmatrix} \qquad \sigma_3 = \begin{pmatrix} 1 & 0 \\ 0 & -1 \end{pmatrix}.$$

The Pauli vector is in terms of the Pauli matrices

$$\boldsymbol{\sigma} = \sigma_1 \hat{\boldsymbol{x}} + \sigma_2 \hat{\boldsymbol{y}} + \sigma_3 \hat{\boldsymbol{z}}$$

Fourier transformation

Unless states otherwise, the fermion operators are Fourier transformed according to the following equations

$$c_{j\sigma} = \frac{1}{\sqrt{N}} \sum_k e^{ikj} c_{k\sigma} \qquad c_{k\sigma} = \frac{1}{\sqrt{N}} \sum_j e^{-ikj} c_{j\sigma} \tag{1}$$

Notation

The imaginary unit is the italic serif roman letter

$$i,$$

to discern from the often used running index for e.g. lattice sites, which is the sans-serif italic letter

$$\mathsf{i}.$$

The *nearest neighbour* sum, $\sum_{\langle ij \rangle}$, counts *both* ways. That is,

$$\sum_{\langle ij \rangle} = \sum_i \sum_{j=i\pm 1}$$

in one dimension. At the boundaries of an open boundary system, it should be understood that only one of the j values are valid.

Winding number

When a Hamiltonian has chiral symmetry, the Hamiltonian matrix is block off-diagonal in the basis that diagonalises the chiral symmetry operator. The Hamiltonian is then written as

$$H(k) = \begin{pmatrix} 0 & A_k \\ A_k^\dagger & 0. \end{pmatrix}$$

The determinant of the matrix A_k is in general a complex number. The winding number is defined as the number of times the complex determinant winds around the origin of the complex plane as k traverses the first Brillouin zone,

$$W = \frac{1}{2\pi i} \int_{\mathcal{C}} \frac{\mathrm{d}|A_k|}{|A_k|} \equiv \frac{1}{2\pi i} \int_{1\mathrm{BZ}} \mathrm{d}k \frac{\mathrm{d}_k|A_k|}{|A_k|}.$$

1 Introduction

1.1 Motivation and background

Topological superconductivity is a field which has been extensively researched for almost two decades and has the potential to lead to decoherence free quantum computing (Kitaev, 2003) due to the topological protection of the information carrying states. One of the topological particles which can emerge in such systems is the Majorana bound state. Such a particle is by definition its own antiparticle. Majorana particles are a theoretical solution to the Dirac equation (Majorana, 1937), but no known particle in the standard model is known to be a Majorana particle, although the neutrinos are interesting propositions (Alicea, 2012). However, in condensed matter Majorana particles may emerge as Bogoliubov quasiparticles in superconductors, where the Majorana excitations are composed of equal amounts of holes and electrons.

Kitaev (2001) theoretically demonstrated this fact by analytically solving a toy model, now known as the Kitaev model, which is a spinless model, and suggested ways to obtain Majorana fermions in a realistic model. The Kitaev model has a p-wave superconducting order parameter, and modeling has been brought to the level of real system. There are three main material paths to realise the Kitaev model: Firstly, by engineering convetional spin singlet pairing with spin-orbit coupling (SOC) and ferromagnetism (Alicea, Oreg, Refael, von Oppen & Fisher, 2011; Lutchyn, Sau & Das Sarma, 2010) or with noncollinear ferromagnetism (Marra & Cuoco, 2017; Nadj-Perge, Drozdov, Bernevig & Yazdani, 2013). Secondly, topological insulators can be combined with superconductivity and magnetism (Fu & Kane, 2008). The third path to topological superconductors is to use intrinsic p-wave superconductors like for instance the Beechgard salts (Jérome, Mazaud, Ribault & Bechgaard, 1980; I. J. Lee et al., 2002), lithium molybdenum purple bronze (Lebed & Sepper, 2013) or the more recent chromium based pnictide (Bao et al., 2015). An example of an intrinsinc p-wave superconductor harbouring Majorana bound states (MBSs) is analysed by Mercaldo, Cuoco and Kotetes (2018) There are indications that MBSs have already been achieved in experiments (Deng et al., 2012; E. J. H. Lee et al., 2014; Mourik et al., 2012).

An alternative to ferromagnetism and SOC is that of noncollinear exchange fields. It turns out that if one locally does a unitary spin rotation so that the spin-axis is aligned with the exchange field vector, the noncollinear exchange field is transformed into a spin-density wave (SDW) with Rashba SOC (Klinovaja & Loss, 2013; Marra & Cuoco, 2017; Sedlmayr, Aguiar-Hualde & Bena, 2015). Additionally, if the angle between neighbouring exchange field vectors is of significant size, the resulting effective SOC is comparable to the Hubbard hopping strength, which often is considerably larger than SOC strengths obtained in semiconductors.

Motivated by the strong focus on the generation and manipulation of topological superconductivity and Majorana modes, we aim to investigate the topological properties

of a quantum system where magnetism and superconductivity can have different character, symmetry and spatial patterns. Especially, we are interested in finding criteria and non-accidental areas in the topological phase diagram where the superconductor has a robust topological character because it is between two topological phases such that it is gapless, yet any symmetry conserving perturbation brings it into a topological phase. We call these types of systems 'marginal topological superconductors'. Such systems could potentially be of special importance since the dynamics of the MBSs can be easily controlled by closing and reopening the gap in these areas in the parameter-space. This way, the control can be as small as possible and still have significant impact on the topological phase of the system, opening ways for new methods to control the MBS in for example quantum gates. The investigation into topological spinful p-wave superconductors is also interesting in itself, as it allows us to understand how odd parity pairing and a vectorial order parameter can be employed to open new paths to control the topology of superconductors.

We also aim to investigate the topological properties of s-wave superconductors subject to noncollinear exchange fields, including elliptical textures. An interesting issue is the importance and interrelation of time reversal breaking and inversion symmetry breaking with respect to the topology of the systems. In addition to looking at the static limit of the topological systems, we investigate the robustness of the MBS during sudden quenches in the model parameters, motivated by the need to understand fast switching of parameters in potential applications.

1.2 Outline

The work presented in this thesis is divided in multiple chapters. At first, in chapter 2, we present basic theory on the tight binding approximation, superconductivity, topology and the relation to global symmetries and the general model formulation as used throughout the thesis. The Kitaev model is also solved in multiple ways to explain the various paths to generate and manipulate MBSs. Each chapter after chapter 2 presents the needed theory, results and discussions.

In chapter 3 we investigate marginal topology in three slightly different models: a p-wave superconductor (SC) in a ferromagnetic field, a p-wave SC in a antiferromagnetic field and an s-wave SC in a noncollinear magnetic field.

In chapter 4, we look at an s-wave superconductor in an elliptical conical exchange field, and the topological properties are analysed in the parameter space given by the form of the elliptic cone.

The same model is subsequently analysed with respect to time-dependent variations in the Hamiltonian in chapter 5, where quenches close to topological phase transitions and quenches that do not change the topological phase are in focus.

2 | Preliminaries

2.1 Tight binding approximation

The tight binding approximation is an effective description of a system of electrons that are tightly bound to the atomic nucleus. This type of modelling was initially proposed by Bloch (1929) and later simplified and parameterised by Slater and Koster (1954). One of the assumptions in the tight binding models is, as the name implies, that the electrons are tightly bound to the nucleus of the atoms. That ensures us that the overlap of orbitals of neighbouring atoms at large distance are negligible, as well as the contribution from neighbouring nucleus potentials. Thus the atomic orbitals may be used as the basis wave functions. The tight binding approximation, due to the assumption of tightly bound electrons, usually works well for inner valence electrons in crystals, while they often are not good approximations for conductance electrons since they are less localised in the crystals (Kittel, 2005). The tight binding approximation has also seen use in conjunction with other methods like the free wave method, thus combining the best of both worlds.

2.1.1 Second quantisation in the tight binding approximation

A usual starting point to obtain the tight binding approximation is to with the first quantised Hamiltonian, which in a simple model is

$$H = \sum_i \frac{\hat{\boldsymbol{p}}_i^2}{2m} + \sum_{i,R_j} V(\boldsymbol{r}_i - \boldsymbol{R}_j) + \frac{1}{2}\sum_{ij} U(\boldsymbol{r}_i - \boldsymbol{r}_j). \tag{2.1}$$

The first term is the familiar kinetic energy term with $\hat{\boldsymbol{p}}_i$ the canonical momentum of particle i, the second is the potential energy of the electrons relative to the lattice atoms, $\boldsymbol{r}_i$ is the position of particle i, $\boldsymbol{R}_j$ is the lattice atoms' positions. The third and last term is the electron-electron interaction (through e.g. Coulomb potential). As we will show later, more terms may exist in the system, like Rashba SOC or phonon-electron interactions, but to keep things simple we will only consider the above terms at the moment. The tight binding model is obtained by considering an effective number of orbitals per atom, $\psi_\nu(\boldsymbol{r}-\boldsymbol{R}_i)$, and solving the Schrödinger equation for single-electron orbitals where just one atom potential $V(\boldsymbol{r}-\boldsymbol{R}_i)$ is considered at a time. Here $\boldsymbol{R}_i$ is the position of the centre of the orbital and nucleus and ν is the orbital quantum number, which can be indexing orbital momentum, radial momentum or other quantum degrees of freedom for the bound states. The number of orbitals that are considered will vary between use cases. For some systems, using only one orbital per atom is accurate enough due to freeze out and filling of the other orbitals that are actually present in the system. When multiple orbital bands cross the chemical potential, more orbitals have to be considered in the tight binding model. In addition to orbital degrees of freedom, a spin degree of

freedom, $\chi_\sigma(s)$, is implied. The set of orbitals used as basis are $\{\psi_\nu(\boldsymbol{r}-\boldsymbol{R}_i)\}$, which satisfy the eigenvalue equation

$$\left(\frac{\hat{\boldsymbol{p}}}{2m} + V(\boldsymbol{r}-\boldsymbol{R}_i)\right)\psi_\nu(r-R_i) = E_\nu\psi_\nu(r-R_i). \tag{2.2}$$

That is, each orbital satisfied the hydrogen like wave equation and is located at a given lattice site, R_i. This implies that the potentials from the other lattice sites and the other potential terms of the Hamiltonian are treated as perturbations. Using the above set of orbitals as the basis, we can transform the Hamiltonian to second quantised form

$$\begin{aligned} H_{\text{2nd}} = \sum_{ij\nu\nu'}\sum_{\sigma\sigma'} c^\dagger_{i\nu\sigma}c_{j\nu'\sigma'}\langle i\nu\sigma|\, H^{\text{single}}_{\text{1st}}\,\big|j\nu'\sigma'\rangle + \\ \sum_{ijkl} c^\dagger_i c^\dagger_j c_k c_l \langle i;j|\, H^{\text{e-e}}_{\text{1st}}\,|k;l\rangle. \end{aligned} \tag{2.3}$$

where the single particle second quantised Hamiltonian is

$$\langle i\nu\sigma|\, H^{\text{single}}_{\text{1st}}\,\big|j\nu'\sigma'\rangle = \int \mathrm{d}^3 r\,\psi_\nu(\boldsymbol{r}-\boldsymbol{R}_i)^* H^{\text{single}}_{\text{1st}}\psi_{\nu'}(\boldsymbol{r}-\boldsymbol{R}_j)$$

and the second quantised two-particle Hamiltonian is

$$\begin{aligned} \langle i_1\nu_1\sigma_1; i_2\nu_2\sigma_2|\, H^{\text{e-e}}_{\text{1st}}\,|i_3\nu_3\sigma_3; i_4\nu_4\sigma_4\rangle = \int \mathrm{d}^3 r\,\mathrm{d}^3 r'\psi^*_{\nu_1\sigma_1}(\boldsymbol{r}-\boldsymbol{R}_{i_1})\psi^*_{\nu_2\sigma_2}(\boldsymbol{r}'-\boldsymbol{R}_{i_2})\times \\ H^{\text{e-e}}_{\text{1st}}(r,r')\psi_{\nu_3\sigma_3}(\boldsymbol{r}'-\boldsymbol{R}_{i_3})\psi_{\nu_4\sigma_4}(\boldsymbol{r}-\boldsymbol{R}_{i_4}). \end{aligned} \tag{2.4}$$

2.1.2 Obtaining the effective Hamiltonian

From now on we will only consider the system to have available one orbital per nucleus, and we omit the orbital label ν. The diagonal part of the second quantised Hamiltonian is simply the part of the Hamiltonian that defined the eigenvectors ψ of the system, with a small correction due to the potential from neighbouring atoms:

$$\begin{aligned} H_0 &= \sum_{i\sigma} c^\dagger_{i\sigma}c_{i\sigma}\langle i\sigma|\left[\frac{\hat{\boldsymbol{p}}}{2m} + \sum_{R_j} V(\boldsymbol{r}-\boldsymbol{R}_j)\right]|i\sigma\rangle \\ &= \sum_{i\sigma} \epsilon\, c^\dagger_{i\sigma}c_{i\sigma} \end{aligned}$$

The Hubbard hopping term (Hubbard, 1963), is obtained similarly, but letting (i,j) be orbitals on different lattice sites:

$$\begin{aligned} H_t &= \sum_{i,j\sigma} c^\dagger_{i\sigma}c_{j\sigma}\langle i\sigma|\sum_{k\neq i} V(\boldsymbol{r}-\boldsymbol{R}_k)|j\sigma\rangle \\ &= -\sum_{i,j\sigma} t_{ij}\, c^\dagger_{i\sigma}c_{j\sigma} \end{aligned}$$

Here the fact that $\left[\frac{\hat{p}^2}{2m} + V(\boldsymbol{r}-\boldsymbol{R}_i)\right]|i\sigma\rangle = \tilde{\epsilon}|i\sigma\rangle$ and that the overlap between neighbouring orbitals are negligible was used to remove them from the sum. Although the pairs (i,j) in principle can denote atoms arbitrary distant away from each other, one usually only consider nearest neighbours, $\langle i,j\rangle$, or next nearest neighbours, $\langle\langle i,j\rangle\rangle$, since the overlap integrals fall off quickly in the tight binding approximation.

The U term

The electron-electron interaction can give rise to various effects, including:

- Superconductivity,
- Ferromagnetism,
- Antiferromagnetism,
- Paramagnetism.

The last three magnetic effects depend on the details of the system, and can also be a result of the relative size of U compared to the Hubbard hopping term above. A pedagogical introduction to the magnetic phases that can arise from the U term is given by Claveau, Arnaud and Di Matteo (2014). Since the U-term of eq. (2.1) is a two-particle operator (it depends on the positions of two electrons), the second quantised Hamiltonian must be expanded according to eq. (2.4). The details of the calculations quickly become complicated and can give rise to effective ferromagnetic or antiferromagnetic interactions depending on the details, so we will point the reader to more thorough works in the field like the pedagogical introduction to magnetism by Timm (2015). A simple approximation to the repulsive U-term in the tight binding model can be obtained by assuming that the overlap integral is much bigger for electrons on the same lattice site. In that case the the second quantised Hamiltonian is

$$H_U = U \sum_i c_{i\uparrow}^\dagger c_{i\downarrow}^\dagger c_{i\downarrow} c_{i\uparrow} = U \sum_i n_{i\uparrow} n_{i\downarrow}.$$

Rashba spin-orbit coupling in the tight binding model

Spin orbit interaction of the Rashba type (Rashba & Sheka, 1959; Bihlmayer, Rader & Winkler, 2015) is a relativistic effect that emerges when expanding the Pauli equation to second order in c^{-1}. Due to the relative motion of a particle with spin in an electric field it feels an effective magnetic field that couples to the spin. In first quantisation the relativistic spin orbit Hamiltonian is

$$\hat{H}_{\mathrm{SO}} = \frac{\mu_{\mathrm{B}}}{2mc^2} \boldsymbol{\sigma} \cdot (\boldsymbol{E} \times \boldsymbol{p}), \tag{2.5}$$

where μ_B is the Bohr magnetic, $e\hbar/2m_e$. Using the fact that $\boldsymbol{E} \times \boldsymbol{p}/mc^2$ has the unit of Tesla, this can be rewritten as $\frac{1}{2}\mu_B \boldsymbol{\sigma} \cdot \boldsymbol{B}'$, i.e. the same form as the Zeeman energy except a factor half, known as the Thomas half (Thomas, 1926). The effective Rashba spin-orbit coupling in a single band model is in first quantisation modelled by

$$\sum_i (\hat{\boldsymbol{n}} \times \hat{\boldsymbol{s}}) \cdot \{\alpha_R(\boldsymbol{r}_i), \hat{\boldsymbol{p}}_i\}, \tag{2.6}$$

where $\hat{\boldsymbol{n}}$ is a vector pointing in the direction of the electrical field, $\hat{\boldsymbol{s}}$ is the spin of the electron and $\alpha_{\mathrm{R}}(\boldsymbol{r}_i)$ is the strength of the Rashba SOC which may vary in space. The anticommutator of the factors $\boldsymbol{p}$ and $\alpha(\boldsymbol{r})$ is used to ensure the hermiticity of the Hamiltonian. Because the Hamiltonian in eq. (2.6) is linear in $\boldsymbol{p}$, this type of Hamiltonian can only exist in systems with broken inversion symmetry.

The Rashba SOC can be calculated straight forward by specifying the orbitals and calculating the overlap integrals of the form $-i\hbar\langle i+\delta|\left(\nabla+\frac{1}{2}\left[\nabla\alpha_R(\boldsymbol{r})\right]\right)|i\rangle$. The final result, written in a similar fashion as J. Linder, Amundsen and Risinggård (2017), is

$$H_{\mathrm{SO}}=i\sum_{\langle i,j\rangle}\alpha_R(i,j)(\boldsymbol{n}\times\hat{\boldsymbol{\sigma}})_{\sigma\sigma'}\cdot\boldsymbol{d}_{ji}c^{\dagger}_{i\sigma}c_{j\sigma'}. \tag{2.7}$$

Here $\alpha_R(i,j)=\alpha_R(j,i)$ and is real, while $\boldsymbol{d}_{ji}$ is a unit vector pointing from j to i with $\boldsymbol{d}_{ji}=-\boldsymbol{d}_{ij}$. Note that the Hamiltonians of eqs. (2.5) to (2.7) all have time reversal symmetry: When the arrow of time is reversed, an electron jumping from i to j jumps instead from j to i (or $\boldsymbol{p}\to-\boldsymbol{p}$), while the spin of the electron also changes direction. Thus since both σ and $\boldsymbol{d}_{ij}$ ($\boldsymbol{p}$) changes sign, the Hamiltonians are left unchanged.

2.2 Superconductivity

2.2.1 BCS theory

Cooper (1956) showed that an arbitrarily small attractive interaction between two electrons just above the Fermi sea would create bound states between them, Cooper pairs. This would happen even in the presence of a repulsive Coulomb potential. The isotope effect discovered by Maxwell (1950) indicated that the attractive potential was due to electron-phonon interactions. The interaction is a result of the dipole moment due to oscillations of the lattice nuclei from the equilibrium position, which interacts with the negative charge of the electrons, and is

$$\hat{H}_{\text{ph-e}} = \sum_{\boldsymbol{k}\boldsymbol{q}\sigma} M_{\boldsymbol{q}} \left(a^{\dagger}_{-\boldsymbol{q}} + a_{\boldsymbol{q}} \right) c^{\dagger}_{\boldsymbol{k}+\boldsymbol{q}} c_{\boldsymbol{k}} \tag{2.8}$$

with

$$M_{\boldsymbol{q}} = i(\boldsymbol{q} \cdot \boldsymbol{\xi}_{\lambda}) \sqrt{\frac{\hbar}{2M_{\text{ion}}\omega_{\boldsymbol{q},\lambda}}}. \tag{2.9}$$

Here a_q are boson (phonon) annihilation operators, whereas c_k are fermion (electron) annihilation operators. As can be seen above, the amplitude of the coupling between the electrons and phonons are mass dependent, which led Maxwell to hypothesise that the superconducting effect was a result of coupling to massive particles — the phonons. When treating eq. (2.8) as a perturbation, one has to go to second order in the interaction strength in order to obtain an expression which is nonzero due to the first order Feynman diagrams giving zero contribution to the electrons energy. (Sudbø, n.d.). In doing so, the electron-phonon interaction can be written as an effective electron-electron interaction (Bardeen, Cooper & Schrieffer, 1957; Sudbø, n.d.; Fossheim & Sudbø, 2005).

$$\hat{H}_{\text{ph-e}} = \sum_{\boldsymbol{k}\boldsymbol{k}'\boldsymbol{q}} \sum_{\sigma\sigma'} \frac{2\hbar\omega_{\boldsymbol{q}} |M_{\boldsymbol{q}}|^2}{(\varepsilon_{\boldsymbol{k}+\boldsymbol{q}} - \varepsilon_{\boldsymbol{k}})^2 - (\hbar\omega_{\boldsymbol{q}})^2} c^{\dagger}_{\boldsymbol{k}+\boldsymbol{q},\sigma} c^{\dagger}_{\boldsymbol{k}'-\boldsymbol{q},\sigma'} c_{\boldsymbol{k}'\sigma'} c_{\boldsymbol{k}\sigma}. \tag{2.10}$$

The interaction is depicted in the Feynman diagram of fig. 2.1a which describes the process of two electrons entering the system, which transmits a virtual phonon between them, and leaves again. This process is similar to the Coulomb force which uses the *photon* as force carrier instead. The difference between the two force carriers is that the phonon is massive whereas the photon is not, and that affects the form of the propagator (the fraction in eq. (2.10)), which in the case of photons is always positive (repulsive) while, as fig. 2.1b shows, the phonon propagator is energy dependent and gives an effective attractive potential for small energy transferal between the electrons. The k-dependence in eq. (2.10) is symmetric in the momentum, which means that it only allows even wavefunctions and singlet Cooper pairing. For odd parity wavefunctions to be allowed (symmetric in spin), the pairing mechanism for the electrons must be anisotropic. However, spin fluctuations can be responsible for the anisotropic pairing mechanisms, which is identified for liquid He_3 (Leggett, 1975; Sigrist & Ueda, 1991).

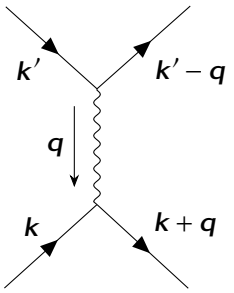

(a) Feynman diagram of the phonon mediated scattering between two electrons.

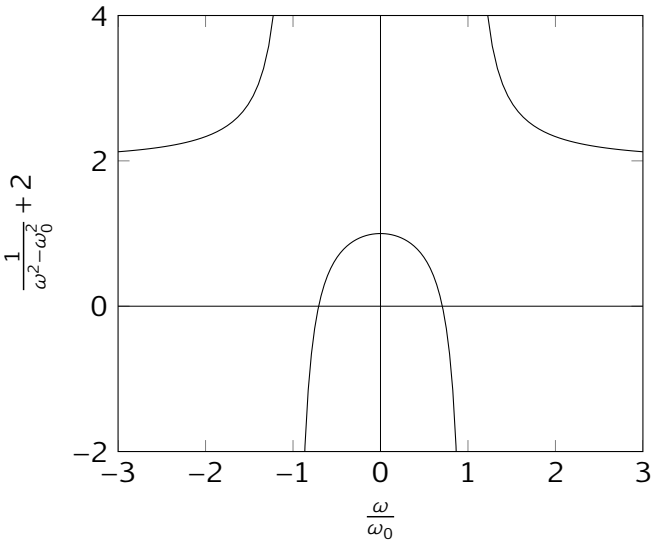

(b) The energy dependence of the effective potential between two electrons.

Figure 2.1: Two electrons can exchange a virtual phonon according to the Feynman diagram in **(a)**. **(b)** The total propagator consists of the exchange of virtual phonons and photons. The figure shows the propagator for a certain $\boldsymbol{k}$, which due to the photon adds a constant term to the frequency dependence, which here is taken to be 2 (the energy is also unitless here).

2.2.2 Second quantisation

The general Bardeen-Cooper-Schrieffer (BCS) quartic superconducting Hamiltonian for any type of superconductivity can be written in momentum ($\boldsymbol{k}$) space as

$$\hat{H}_{\mathrm{BCS}} = \hat{H}_{\mathrm{N}} + \hat{H}_{\mathrm{SC}} = \sum_{\boldsymbol{k}\boldsymbol{k}'\sigma\sigma'} \epsilon_{\sigma\sigma'}(\boldsymbol{k},\boldsymbol{k}') c^\dagger_{\boldsymbol{k}} c_{\boldsymbol{k}'} + \frac{1}{2}\sum_{\boldsymbol{k}\boldsymbol{k}'}\sum_{\substack{s_1 s_2 \\ s_3 s_4}} V_{s_1 s_2 s_3 s_4}(\boldsymbol{k},\boldsymbol{k}') c^\dagger_{-\boldsymbol{k}s_1} c^\dagger_{\boldsymbol{k}s_2} c_{\boldsymbol{k}'s_3} c_{-\boldsymbol{k}'s_4}. \quad (2.11)$$

The derivation of the above Hamiltonian can be found in any complete textbook on supercoductivity, but I refer the reader to the works by Bardeen et al. (1957), Fossheim and Sudbø (2005), Sigrist and Ueda (1991) for a detailed derivation of the Hamiltonian. The following derivations also follow these references closely. The first sum in eq. (2.11) is the normal quadratic terms found in most *normal* systems, and is particle conserving since any annihilation operator is matched by a creation operator. The Hamiltonian could be written in a more general way by including terms of the form $c_{\boldsymbol{k}} c_{\boldsymbol{k}'}$ and hermitian conjugate, which do not conserve particle number, but these terms seldom appear by themselves in nature, furthermore they appear in the mean field superconducting part, which we soon derive. The latter sum in eq. (2.11) is a very general quartic Hamiltonian in that it couples two fermionic annihilation operators with two creation operators. In light of the previous argument this Hamiltonian term is also particle number conserving. By using the anticommutation relations for fermions, we

can derive some symmetries for the electron-electron interaction potential:

$$V_{s_1 s_2 s_3 s_4}(\boldsymbol{k}, \boldsymbol{k}') = -V_{s_2 s_1 s_3 s_4}(-\boldsymbol{k}, \boldsymbol{k}') \tag{2.12}$$
$$= -V_{s_1 s_2 s_4 s_3}(\boldsymbol{k}, -\boldsymbol{k}') \tag{2.13}$$
$$= V_{s_4 s_3 s_2 s_1}(\boldsymbol{k}', \boldsymbol{k}) \tag{2.14}$$

In practice, just a small number of degrees of freedom for a fermionic systems renders a solution to eq. (2.11) intractable, due to the quartic term which means that one has to consider the full Hilbert space of combinations of single particle excitations and not just the single particle excitations independently. The solution to this is describing the particle-particle interaction in terms of mean fields. In this regard there are multiple fields that can be used. If the interaction is attractive and superconductivity is expected, one uses the superconducting fields cc', while if the interaction is repulsive one used the Hartree-Fock fields, $c^\dagger c$. In the context of this chapter, the first are used. Writing

$$cc' = \langle cc' \rangle + \overbrace{cc' - \langle cc' \rangle}^{\delta} \tag{2.15}$$

for any quadratic factor of same type (annihilation or creation), and by assuming that the fluctuations in δ are small and thus only approximating first order in δ, the SC term in the Hamiltonian is approximated as

$$\begin{aligned}
\hat{H}_{\mathrm{SC}} = \frac{1}{2} \sum_{\boldsymbol{k}\boldsymbol{k}'} \sum_{\substack{s_1 s_2 \\ s_3 s_4}} V_{s_1 s_2 s_3 s_4}(\boldsymbol{k}, \boldsymbol{k}') \Big[& \langle c^\dagger_{-\boldsymbol{k} s_1} c^\dagger_{\boldsymbol{k} s_2} \rangle c_{\boldsymbol{k}' s_3} c_{-\boldsymbol{k}' s_4} + \\
& \langle c_{\boldsymbol{k}' s_3} c_{-\boldsymbol{k}' s_4} \rangle c^\dagger_{-\boldsymbol{k} s_1} c^\dagger_{\boldsymbol{k} s_2} - \langle c^\dagger_{-\boldsymbol{k} s_1} c^\dagger_{\boldsymbol{k} s_2} \rangle \langle c_{\boldsymbol{k}' s_3} c_{-\boldsymbol{k}' s_4} \rangle \Big], \\
= \frac{1}{2} \sum_{\boldsymbol{k}\sigma\sigma'} \Bigg[& c_{-\boldsymbol{k}\sigma} c_{\boldsymbol{k}\sigma'} \sum_{\boldsymbol{k}' s s'} V_{s s' \sigma \sigma'}(\boldsymbol{k}', -\boldsymbol{k}) \langle c^\dagger_{-\boldsymbol{k}' s} c^\dagger_{\boldsymbol{k}' s'} \rangle + \\
& c^\dagger_{\boldsymbol{k}\sigma} c^\dagger_{-\boldsymbol{k}\sigma'} \sum_{\boldsymbol{k}' s s'} V_{\sigma \sigma' s s'}(-\boldsymbol{k}, \boldsymbol{k}') \langle c_{\boldsymbol{k}' s} c_{-\boldsymbol{k}' s'} \rangle \Bigg] - \overline{V}
\end{aligned}$$

where a relabeling $\boldsymbol{k} \to -\boldsymbol{k}$ was done in the second equal sign, and the constant term without fermion operators was written as $\overline{V}$. This last term is not important when computing the eigenvectors and energies of the Hamiltonian, but is needed when the superconducting phase is compared to the normal phase concerning the equilibrium phase of the system. The sign of $-\boldsymbol{k}$ in the potential can be removed by using eqs. (2.12) to (2.14). The superconducting term is then

$$\hat{H}_{\mathrm{SC}} = \frac{1}{2} \sum_{\boldsymbol{k}\sigma\sigma'} \left(\Delta_{\sigma\sigma'}(\boldsymbol{k}) c^\dagger_{\boldsymbol{k}\sigma} c^\dagger_{-\boldsymbol{k}\sigma'} - \Delta^*_{\sigma\sigma'}(-\boldsymbol{k}) c_{-\boldsymbol{k}\sigma} c_{\boldsymbol{k}\sigma'} \right), \tag{2.16}$$

with

$$\Delta_{\sigma\sigma'}(\boldsymbol{k}) = -\sum_{\boldsymbol{k}' s s'} V_{\sigma' \sigma s s'}(\boldsymbol{k}, \boldsymbol{k}') \langle c_{\boldsymbol{k}' s} c_{-\boldsymbol{k}' s'} \rangle \tag{2.17}$$

$$\Delta^*_{\sigma\sigma'}(-\boldsymbol{k}) = \sum_{\boldsymbol{k}' s s'} V_{s s' \sigma' \sigma}(\boldsymbol{k}', \boldsymbol{k}) \langle c_{\boldsymbol{k}' s} c_{-\boldsymbol{k}' s'} \rangle. \tag{2.18}$$

These Order Parameters (OPs) must, using eqs. (2.12) to (2.14), satisfy

$$\Delta_{\sigma\sigma'}(\boldsymbol{k}) = -\Delta_{\sigma'\sigma}(-\boldsymbol{k}). \tag{2.19}$$

That is, it must be antisymmetric under a total exchange of spin and momentum coordinates. Until now no restriction has been made on the momentum dependence of $\Delta_{\sigma\sigma'}(\boldsymbol{k})$. Writing it as $\Delta^{\mathrm{S}}_{\sigma\sigma'}(\boldsymbol{k}) + \Delta^{\mathrm{A}}_{\sigma\sigma'}(\boldsymbol{k})$, where superscript S and A denote symmetric and antisymmetric $\boldsymbol{k}$ dependence, we get

$$\begin{aligned}\hat{H}_{\mathrm{SC}} = \sum_{\boldsymbol{k}\geq 0}\Big[&\Delta^{\mathrm{S}}_{\uparrow\downarrow}(\boldsymbol{k})\left(c^\dagger_{\boldsymbol{k}\uparrow}c^\dagger_{-\boldsymbol{k}\downarrow} - c^\dagger_{\boldsymbol{k}\downarrow}c^\dagger_{-\boldsymbol{k}\uparrow}\right)\\ &+\Delta^{\mathrm{A}}_{\uparrow\uparrow}(\boldsymbol{k})c^\dagger_{\boldsymbol{k}\uparrow}c^\dagger_{-\boldsymbol{k}\uparrow}\\ &+\Delta^{\mathrm{A}}_{\uparrow\downarrow}(\boldsymbol{k})\left(c^\dagger_{\boldsymbol{k}\uparrow}c^\dagger_{-\boldsymbol{k}\downarrow} + c^\dagger_{\boldsymbol{k}\downarrow}c^\dagger_{-\boldsymbol{k}\uparrow}\right)\\ &+\Delta^{\mathrm{A}}_{\downarrow\downarrow}(\boldsymbol{k})c^\dagger_{\boldsymbol{k}\downarrow}c^\dagger_{-\boldsymbol{k}\downarrow} + \mathrm{h.c.}\Big].\end{aligned} \tag{2.20}$$

It is straightforward to show using eq. (2.19) that

$$\Delta^{\mathrm{S/A}}_{\sigma\sigma'}(k) = \mp\Delta^{\mathrm{S/A}}_{\sigma'\sigma}(k) \qquad\qquad \Delta^{\mathrm{S/A}}_{\sigma\sigma'}(k) = \pm\Delta^{\mathrm{S/A}}_{\sigma\sigma'}(-k),$$

where $\pm$ and $\mp$ corresponds to S/A. From eq. (2.20) it is clear that the k-symmetric Δ pairs electrons in the singlet configuration while the antisymmetric Δ pairs electrons in the triplet Cooper configuration, of which there are three types ($m_z = 1, 0, -1$). We see that the representation above for the triplet pairs is written in a specific basis: the triplets have a well defined spin z-direction, and the representation is followingly not invariant under SU(2) spin-rotations. Thus we seek a way to write Δ as in terms of a vector that rotates under spin rotations. It turns out (Balian & Werthamer, 1963; Sigrist & Ueda, 1991) that the triplet matrix in spin space can be defined in terms of a vector $\boldsymbol{d}(\boldsymbol{k})$, called the $\boldsymbol{d}$-vector, as

$$\hat{\Delta}^{\mathrm{A}} = \begin{pmatrix}\Delta^{\mathrm{A}}_{\uparrow\uparrow} & \Delta^{\mathrm{A}}_{\uparrow\downarrow}\\ \Delta^{\mathrm{A}}_{\downarrow\uparrow} & \Delta^{\mathrm{A}}_{\downarrow\downarrow}\end{pmatrix} = i(\boldsymbol{d}(\boldsymbol{k})\cdot\boldsymbol{\sigma})\sigma_y = \begin{pmatrix}-d_x(\boldsymbol{k}) + id_y(\boldsymbol{k}) & d_z(\boldsymbol{k})\\ d_z(\boldsymbol{k}) & d_x(\boldsymbol{k}) + id_y(\boldsymbol{k})\end{pmatrix}. \tag{2.21}$$

The $\boldsymbol{d}$-vector has the properties that it always points perpendicular to the pairing potential. Thus, if we rotate the system so that the $\boldsymbol{d}$-vector points in the z-direction, only electrons with opposite spins, e.g. $c^\dagger_\uparrow c^\dagger_\downarrow$, will be paired. These pairs do not have a net spin in the direction of $\boldsymbol{z}$. The singlet pair potential can be written by substituting the dot product in eq. (2.21) by the scalar $\Delta_0(\boldsymbol{k}) = \Delta^{\mathrm{S}}_{\uparrow\downarrow}(\boldsymbol{k})$ which gives

$$\hat{\Delta}^{\mathrm{S}} = i\Delta_0(k)\sigma_y = \begin{pmatrix}0 & \Delta_0(\boldsymbol{k})\\ -\Delta_0(\boldsymbol{k}) & 0\end{pmatrix}. \tag{2.22}$$

Assuming that $\boldsymbol{k}$ is a good quantum number for the normal quadratic terms in eq. (2.11), we define the Nambu spinors $\hat{\psi}_k = (c_{\boldsymbol{k}\uparrow}, c_{\boldsymbol{k}\downarrow}, c^\dagger_{\boldsymbol{k}\uparrow}, c^\dagger_{\boldsymbol{k}\downarrow})^{\mathrm{T}}$, which allows the Hamiltonian to be written in a compact form

$$\hat{H} = \frac{1}{2}\sum_{\boldsymbol{k}}\hat{\psi}^\dagger_k\begin{pmatrix}h(\boldsymbol{k}) & \hat{\Delta}(\boldsymbol{k})\\ -\hat{\Delta}(-\boldsymbol{k})^* & -h(\boldsymbol{k})^*\end{pmatrix}\hat{\psi}_k. \tag{2.23}$$

If the translational symmetry is altered by a spin density wave, one must consider other bases instead when solving the Hamiltonian. For example, when there is an antiferromagnetic ordering in the system one can divide the fermion operators in two sublattices, which leads to two 'types' of Fourier transformed operators on each sublattice, each of which has a reduced Brillouin zone due to the increased lattice constant of each sublattice.

2.2.3 Bogoliubov-de Gennes formalism

The Hamiltonian in eq. (2.60) contains both the usual terms quadratic in creation and annihilation operators like $c^\dagger c$, and terms quadratic in either creation operators or annihilation operators, like cc. The first type conserves the particle number in the system regardless of the type of interaction. The latter on the other hand does not conserve particle number. This implies that the eigensolutions of the Hamiltonian can not be a superposition of only particles, but must be a superposition of both particles and holes. The transformation into a basis consisting of superpositions of particles and holes for simple s-wave systems were first formalised by Bogoliubov (1958) and Valatin (1958), the Bogoliubov-Valatin transformations. Further in the developement of the BCS-theory was the developement of Bogoliubov-de Gennes formalism after de Gennes (1964) and Bogoliubov (1958). In this formalism the Hamiltonian is written with a redundant representation of the states. Defining the column vector of creation operators

$$\hat{\psi} = \left(c_{\nu_1}, c_{\nu_2}, \ldots, c_{\nu_N}, c^\dagger_{\nu_1}, c^\dagger_{\nu_2}, \ldots, c^\dagger_{\nu_N}\right)^{\mathrm{T}}. \tag{2.24}$$

If we denote the first half of this vector as the 'particle part', and the lower half as the 'hole part', and remembering that the τ-denoted Pauli matrices operate in the particle-hole basis, the column vector satisfies

$$\tau_x(\psi^\dagger)^{\mathrm{T}} = \psi, \tag{2.25}$$

which demonstrates the redundancy in the representation and effectively defines a particle-hole symmetry. Here it is assumed that the fermion operators are given in the position basis. In the momentum basis the relation would instead have been $\tau_x(\psi^\dagger(k))^{\mathrm{T}} = \psi(-k)$. In truth, these relations are only particle hole constraints due to the Fermi-Dirac statistics (Chiu, Teo, Schnyder & Ryu, 2016, p. 7).

The Bogoliubov-de Gennes (BdG) Hamiltonian matrix is written like

$$\hat{\psi}^\dagger H_{\mathrm{BdG}}\hat{\psi} = \hat{\psi}^\dagger \begin{pmatrix} H & \Delta \\ \Delta^\dagger & -H^* \end{pmatrix} \hat{\psi}, \tag{2.26}$$

where H is the normal part matrix connecting pairs of creation and annihilation operators, while Δ is the anomalous part due to superconducting pair interactions. Insertion of eq. (2.25) into eq. (2.26) gives the requirement

$$\tau_x H^*_{\mathrm{BdG}}\tau_x = -H_{\mathrm{BdG}} \quad \text{(position basis)} \quad \tau_x H^*_{\mathrm{BdG}}(\boldsymbol{k})\tau_x = -H_{\mathrm{BdG}}(-\boldsymbol{k}) \quad \text{(momentum basis)} \tag{2.27}$$

This implies that the matrix Δ must equal $-\Delta^{\mathrm{T}}$, therefore being an antisymmetric matrix.

What is interesting about the BdG Hamiltonian is that it always has particle-hole symmetry by its very definition. The result as described in section 2.3.2 is that the eigensolutions comes in $(\epsilon, -\epsilon)$-pairs. For any eigenwave function $\gamma = (u, v)$, the negative eigenenergy partner is $\tau_x\gamma^* = (v^*, u^*)$, where u and v are the particle and hole components respectively. The PH symmetry is in this case defined by $\hat{\mathscr{C}}\psi\hat{\mathscr{C}}^{-1} = \tau_x(\psi^\dagger)^{\mathrm{T}}$, which implies that $\hat{\mathscr{C}}^2 = +1$. The Bogoliubov-de Gennes (BdG) Hamiltonian apparently also has too many degrees of freedom in its definition. If we assume that the actual system has two internal spin degrees of freedom and N degrees of additional freedom in terms of e.g. position, there are a total of $2N$ degrees of freedom for the system. However, the Hamiltonian matrix is a $4N \times 4N$ matrix, which implies that there are a total of $4N$

degrees of freedom. That is, the BdG Hamiltonian has twice the number of degrees of freedom as the actual system has. The number of solutions to the Hamiltonian can not exceed the number of degrees of freedom, else we would have a problem when chosing the energy eigenvectors to construct a state from. The solution to this problem is to observe that the particle-hole symmetry connecting electrons and holes by eq. (2.25) in fact limits the degrees of freedom by half since for each solution, there must always exist a solution with the opposite energy.

The BdG equation

The BdG equation is an eigenvalue equation on the matrix Hamiltonian which gives the eigenenergies and eigenvectors when solved. It is

$$H_{\mathrm{BdG}}\phi_\nu = E_\nu \phi_\nu. \tag{2.28}$$

Here the ψ_ν is an eigenvector of the BdG Hamiltonian with the eigenenergy E_ν.

BdG formalism in momentum basis

In systems with translational invariance, $\hat{H}(i+T) = \hat{H}(i)$, fourier transforming the Hamiltonian from the position basis into momentum basis usually simplifies the equations that have to be solved. We then write the Hamiltonian as a function of the momentum: $\hat{H}_{\mathrm{BdG}}(\boldsymbol{k})$. For the following derivation, we assume that the Hamiltonian has a unit cell with one atom and one orbital in its basis, and two spin degrees of freedom. The Hamiltonian then completely decouples to a k-dependent 4×4 matrix of the form

$$H_{\mathrm{BdG}}(\boldsymbol{k}) = \begin{pmatrix} H(\boldsymbol{k}) & \hat{\Delta}(\boldsymbol{k}) \\ -\hat{\Delta}(-\boldsymbol{k})^* & -H(-\boldsymbol{k})^* \end{pmatrix}, \tag{2.29}$$

$$\hat{H}_{\mathrm{BdG}}(\boldsymbol{k}) = \psi_{\boldsymbol{k}}^\dagger H_{\mathrm{BdG}}(\boldsymbol{k})\psi_{\boldsymbol{k}}, \tag{2.30}$$

where $H(k)$ and $\Delta(k)$ are 2×2 matrices, the Nambu spinors are $\psi_k = (c_{k\uparrow}, c_{k\downarrow}, c^\dagger_{-k\uparrow}, c^\dagger_{-k\downarrow})^{\mathrm{T}}$, and the particle hole symmetry is $\tau_x(\psi_k^\dagger)^{\mathrm{T}} = \psi_{-k}$. The BdG equation now takes the form

$$H_{\mathrm{BdG}}(\boldsymbol{k})\phi_{\boldsymbol{k},\pm} = E_{\boldsymbol{k},\pm}. \tag{2.31}$$

The matrix which diagonalises the Hamiltonian can then be written as

$$U(\boldsymbol{k}) = \begin{pmatrix} \phi_{\boldsymbol{k},+} & \phi_{\boldsymbol{k},-} & \tau_x\phi^*_{-\boldsymbol{k},+} & \tau_x\phi^*_{-\boldsymbol{k},-} \end{pmatrix} \tag{2.32}$$

which satisfies

$$U(\boldsymbol{k})^\dagger H_{\mathrm{BdG}}(\boldsymbol{k})U(\boldsymbol{k}) = \begin{pmatrix} E_{\boldsymbol{k},+} & & & \\ & E_{\boldsymbol{k},-} & & \\ & & -E_{-\boldsymbol{k},+} & \\ & & & -E_{-\boldsymbol{k},-} \end{pmatrix}. \tag{2.33}$$

2.3 Global symmetries and the ten-fold way

It can often be a fruitful exercise to discover the intrinsic symmetries of a system before looking for the solutions. The symmetries of a Hamiltonian can reveal much information about a system and the possible phases and topological constants that it can have. This has led to what is called 'The Ten-Fold Way' by the community (Chiu et al., 2016; Ludwig, 2016; Ryu, Schnyder, Furusaki & Ludwig, 2010) which is a 'periodic table' of topological systems that are classified by only three global symmetries: The Time Reversal (TR) symmetry, the Particle-Hole (PH) symmetry also called charge conjugation symmetry and lastly the chiral symmetry which is the product of the first two or it can be associated to a subdivision of the lattice such as the connectivity of the Hamiltonian is only between two separate groups of atoms. In this chapter we review the mentioned symmetries and explain why their combinations exhaust the topological classes. In section 2.3.4 we summarise the symmetries and explain the meaning of the Ten-Fold Way, which is described by the Altland-Zirnbauer (AZ) table.

A fermionic symmetry operator is an operator that commutes with the Hamiltonian in the second quantisation formalism, that is to say that the symmetry operator, $\mathscr{U}$, satisfies

$$\hat{\mathscr{U}}\,\hat{H}\hat{\mathscr{U}}^{-1} = \hat{H}, \tag{2.34}$$

and additionally the anticommutation relations for the fermion operators must be invariant (Chiu et al., 2016),

$$\{\psi_\nu, \psi_\lambda^\dagger\} = \hat{\mathscr{U}}\{\psi_\nu, \psi_\lambda^\dagger\}\hat{\mathscr{U}}^{-1}. \tag{2.35}$$

By Wigner's theorem (Wigner, 1959; Bargmann, 1964), the operator $\hat{\mathscr{U}}$ eqs. (2.34) and (2.35) must be either a unitary or antiunitary transformation, the latter preserving the size but not the phase of inner products in the Hilbert space. The unitary and antiunitary operators are defined by the following two equations:

$$\hat{\mathscr{U}}\,i\hat{\mathscr{U}}^{-1} = i \quad \text{(unitary)} \qquad\qquad \hat{\mathscr{U}}\,i\hat{\mathscr{U}}^{-1} = -i \quad \text{(antiunitary)}. \tag{2.36}$$

The symmetry operator $\hat{\mathscr{U}}$ transforms the second quantised creation and annihilation operators as

$$\psi_\nu \to \psi'_\nu = \hat{\mathscr{U}}\,\psi_\nu\hat{\mathscr{U}}^{-1} = (U\boldsymbol{\psi})_\nu, \tag{2.37}$$

where $\boldsymbol{\psi}$ is the vector containing all annihilation operators (and creation operators in the case of particle hole symmetry). Here, U is not a second quantised operator, but is a unitary matrix (Chiu et al., 2016; Ludwig, 2016).

As mentioned above, there exist arbitrarily many unitary symmetries that a Hamiltonian may have, examples being spin-symmetries, inversion symmetries, mirror symmetries and (discrete) translational symmetries to mention a few. In the study of topological systems three symmetries stand out, Time Reversal (TR), Particle-Hole (PH) and chiral symmetry. The reason why they stand out is that any 'normal' symmetry operator commutes with the Hamiltonian in first quantisation formalism, which is to say that the matrix representation of the operators commute. Followingly, the Hamiltonian can be block diagonalised in blocks corresponding to the eigenvalues of the symmetry operator in question. This procedure can be repeated for each block until all the 'normal' symmetries are gone, which is to say that the blocks of the Hamiltonian matrix does not individually have the symmetries as the Hamiltonian as a whole has. The three special symmetries mentioned above are *global* symmetries of the Hamiltonian that either are antiunitary and commutes or anti-commutes with the Hamiltonian in first quantisation, or are unitary and anti-commutes with the Hamiltonian in first quantisation.

2.3.1 Time reversal symmetry

The first operator we consider in this chapter is the TR operator. The time reversal operator, $\hat{\mathcal{T}}$ is the operator that reverses the direction of time:

$$\hat{\mathcal{T}} : t \to -t. \tag{2.38}$$

The creation and annihilation operators transform under the TR symmetry operator as

$$\hat{\mathcal{T}} c_i \hat{\mathcal{T}}^{-1} = (U_{\mathrm{T}})_{ij} c_j \qquad \hat{\mathcal{T}} c_i^\dagger \hat{\mathcal{T}}^{-1} = (U_{\mathrm{T}})_{ij}^* c_j. \tag{2.39}$$

Time reversal leaves the initial position invariant but flips the momentum, which implies that the canonical position and momentum operators transform according to

$$\hat{\mathcal{T}} \hat{x} \hat{\mathcal{T}}^{-1} = \hat{x} \qquad \hat{\mathcal{T}} \hat{p} \hat{\mathcal{T}}^{-1} = -\hat{p} \tag{2.40}$$

Applying eq. (2.40) to the canonical commutation relation, $[\hat{x}_i, \hat{p}_j] = i\hbar\delta_{ij}$, we get

$$\hat{\mathcal{T}} [\hat{x}_i, \hat{p}_j] \hat{\mathcal{T}}^{-1} = [\hat{x}_i, -\hat{p}_j] = -i\hbar\delta_{ij} = \hat{\mathcal{T}} i\hbar\delta_{ij} \hat{\mathcal{T}}^{-1}. \tag{2.41}$$

The latter equality sign can only be satisfied if $\hat{\mathcal{T}}$ is antiunitary, meaning that it satisfies

$$\hat{\mathcal{T}} i \hat{\mathcal{T}}^{-1} = -i. \tag{2.42}$$

Furthermore it is useful to note that orbital momenta, which are proportional to angular momentum $\hat{\boldsymbol{x}} \times \hat{\boldsymbol{p}}$ is also flipped under time reversal, which is an important fact to consider for fermionic systems. Until now there is nothing that dictates how the intrinsic spins should behave under time reversal symmetry. The most 'physical' case is that the intrinsic spin of the fermion, which is also an angular momentum, should change sign from the same argument as for the real space angular momenta. On the other hand, this is not a requirement for the theory of symmetry operators to work, and time reversal symmetries that do not flip the spin can exist.

Applying the TRS operator twice to a system should leave the system invariant up to a phase factor, since the system reverses time two times and thus should represent the same state. That is we expect that $\hat{\mathcal{T}}^2 |\psi\rangle = e^{i\alpha} |\psi\rangle$. We are therefore interested in finding the values that the phase $e^{i\alpha}$ can have. Equation (2.39) inserted into eq. (2.34) and evaluated with eq. (2.42) gives

$$U_{\mathrm{T}}^\dagger H^* U_{\mathrm{T}} = H, \tag{2.43}$$

where H is the Hamiltonian matrix. Equation (2.43) can be rewritten by the introduction of a *first quantised* operator,

$$T = U_{\mathrm{T}}^\dagger K \qquad THT^{-1} = H \tag{2.44}$$

Equation (2.43) implies that if we have an eigenwave solution u with energy ϵ, then the time reversed partner $U_{\mathrm{T}}^\dagger u^*$ is also an eigenwave solution with the same energy. Following the proof of Chiu et al. (2016, p. 6), we get, by using eq. (2.43) twice, that

$$U_{\mathrm{T}} U_{\mathrm{T}}^* H (U_{\mathrm{T}} U_{\mathrm{T}}^*)^\dagger = H. \tag{2.45}$$

From Schur's lemma, UU^* must be a scalar multiple of the identity matrix, $e^{i\alpha}\mathbb{1}$. Multiplying this with U_{T}^* from the left gives

$$U_{\mathrm{T}}^* U_{\mathrm{T}} U_{\mathrm{T}}^* = e^{-i\alpha} U_{\mathrm{T}}^* = U_{\mathrm{T}}^* e^{i\alpha}, \tag{2.46}$$

where the first equality sign comes from evaluating the product of the first two matrices, while the latter comes from evaluating the product of the latter two matrices. From this fact it follows that $U^* = e^{2i\alpha} U^*$, which implies that $UU^* = \pm 1$. In other words, using the TR operator twice gives the same state up to a sign.

$\mathcal{T}^2 = -1$ for spin-half systems

Any antiunitary operator can be factored into a linear and antilinear operator, $\mathscr{L}$ and $\mathscr{A}$ respectively. The (anti)linearity of the operators mean the same as in eq. (2.36). The form of either operator depends on the basis used, but for the position-spin basis the antilinear operator is often the complex conjugation operator, K. This certainly satisfies eq. (2.42). We see that the position transformation in eq. (2.40) is satisfied under this transformation:

$$K\hat{x}K^{-1}\psi(x) = x\psi(x).$$

Similarly, the momentum relation is also satisfied:

$$K(-i\hbar\nabla)K^{-1}\psi(x) = i\hbar\nabla\psi(x).$$

On the other hand, for systems with spin-$\frac{1}{2}$ the spin axes are asymmetrically treated:

$$K\sigma K^{-1}\psi(x) = K\begin{pmatrix}\sigma_x\\ \sigma_y\\ \sigma_z\end{pmatrix}K^{-1}\psi(x) = \begin{pmatrix}\sigma_x\\ -\sigma_y\\ \sigma_z\end{pmatrix}\psi(x).$$

If the spins are to be equally treated under the time reversal symmetry, then the two other spin axes must be flipped. This can be achieved by a rotation of π around the y-axis,

$$\mathscr{L} = e^{-i\pi\hat{\sigma}_y/2} = \cos(\pi/2)I - i\sin(\pi/2)\hat{\sigma}_y = \begin{pmatrix}0 & -1\\ 1 & 0\end{pmatrix}.$$

The fermionic operators now transform according to

$$\hat{\mathcal{T}}\, c_{i\sigma}\, \hat{\mathcal{T}}^{-1} = (-i\sigma_y)_{\sigma\sigma'} c_{i\sigma'}. \tag{2.47}$$

Applying eq. (2.47) twice, we see that the square of the time reversal operator with spin flipping is $\hat{\mathcal{T}}^2 = -1$.

Many systems do not have a time reversal operator which squares to -1. An example of such systems is when there is a Zeeman field. When the Zeeman field is an external field it does not change sign when time is reversed. Thus, if the spins are flipped in such a model the energy will change. However, for some such systems with one of the requirements being that the Zeeman field lies in a plane, time reversal symmetry can be recovered, but which squares to $+1$.

Kramer's degeneracy theorem

Kramer's degeneracy theorem applies to systems with half-integer spin which have an odd number of fermions, and states that all eigenenergy solutions of such systems are degenerate by a factor of two if there is a time reversal symmetry which squares to -1. This can easily be proved by contradiction: Let $|\psi\rangle$ be an eigensolution of the Hamiltonian. We already know that the time reversed partner $\hat{\mathcal{T}}|\psi\rangle$ is also an eigensolution with the same energy. Assume now that the time reversed partner is the initial state itself up to a phase factor, $\hat{\mathcal{T}}|\psi\rangle = e^{i\alpha}|\psi\rangle$. Applying $\hat{\mathcal{T}}$ once more gives

$$\hat{\mathcal{T}}^2|\psi\rangle = \hat{\mathcal{T}}\, e^{i\alpha}|\psi\rangle = e^{-i\alpha}\hat{\mathcal{T}}|\psi\rangle = |\psi\rangle.$$

This clearly contradicts the fact that $\hat{\mathcal{T}}^2 = -1$. Thus $\hat{\mathcal{T}}|\psi\rangle$ must be an orthogonal state to $|\psi\rangle$, which is what was to be shown.

2.3.2 Particle hole symmetry

The next symmetry of interest is the particle-hole symmetry which is intrinsic to some Hamiltonians, especially the BdG Hamiltonians.

We define the particle-hole symmetry operator $\hat{\mathscr{C}}$ as a *unitary*[1] operator defined as

$$\hat{\mathscr{C}} c_i \hat{\mathscr{C}}^{-1} = U_{\mathrm{P}}^{ij*} c_j^\dagger \qquad\qquad \hat{\mathscr{C}} c_i^\dagger \hat{\mathscr{C}} = U_{\mathrm{P}}^{ij} c_j.$$

Upon the assertion of eq. (2.34), we have

$$\begin{aligned}\hat{H} &= c_i^\dagger H_{ij} c_j \\ &= U_{\mathrm{P}}^{im} c_m H_{ij} U_{\mathrm{P}}^{jn*} c_n^\dagger \\ &= -c_n^\dagger (U_{\mathrm{P}}^\dagger)_{nj} (H^{\mathrm{T}})_{ji} U_{\mathrm{P}}^{im} c_m + H_{ii} \\ &= -\boldsymbol{c}^\dagger U^\dagger H^{\mathrm{T}} U \boldsymbol{c} + \mathrm{Tr}\, H,\end{aligned}$$

where the last equation is written with vector notation. Thus for a Hamiltonian to have PH symmetry, the matrix representation of the Hamiltonian must satisfy

$$U^\dagger H^* U = -H, \quad \text{and} \tag{2.48}$$

$$\mathrm{Tr}\, H = 0, \tag{2.49}$$

where we used the fact that the Hamiltonian is hermitian to write $H^{\mathrm{T}} = H^*$.

We see that this implies that the eigenvalue and eigenvector solutions come in pairs. Let u be an eigen-wave solution of the Hamiltonian with energy ϵ, then we see with the help of eq. (2.48) that

$$HU^\dagger u^* = -U^\dagger H^* U U^\dagger u^* = -U^\dagger (Hu)^* = -\epsilon U^\dagger u^* \tag{2.50}$$

implies that $U^\dagger u^*$ is also an eigensolution with negative energy.

Note that the matrix representation of the PH symmetry operator is *antiunitary*:

$$\mathcal{C} = U_{\mathrm{P}}^\dagger K, \qquad\qquad \mathcal{C} H \mathcal{C}^{-1} = -H.$$

Zero energy level crossings

It was just established that systems with PH symmetry have eigensolutions that come in pairs with opposite energy. This means that any time a perturbation of a system leads to a zero-energy crossing of one of the eigensolutions, the PH partner must also cross zero-energy, only in the opposite direction. This means that the determinant of the Hamiltonian can never change sign, which will constantly be $(-1)^{N/2}$ where N is the number of degrees of freedom for the system. This is a consequence of the the fact that the determinant of a matrix is invariant to basis transformation. Followingly, in the basis that diagonalises the Hamiltonian it is a diagonal matrix with all the energies on the diagonal. The determinant is just the product of all the diagonal entries, and since there are N energies, where they come in pairs of positive and negative energy, the product of each pair can never change and followingly the determinant of the matrix can never change. On the other hand, whenever such a zero-energy crossing occurs, the Pfaffian of the Hamiltonian changes sign. This is a result of the fact that the Hamiltonian can be written in tridiagonal skew-symmetric form with the energies in the upper

[1] While the *second quantised* operator is *unitary*, the first quantised (matrix) operator is antiunitary, as later derived.

diagonal part, and the particle hole partner energies in the lower diagonal part. The Pfaffian is in this basis a product of the elements in the upper diagonal, and as a result changes sign when one of the energies changes sign. Furthermore, the Pfaffian of a matrix A, $\mathrm{Pf}(A)$, satisfies $\mathrm{Pf}(A)^2 = \det(A)$. This further cements the understanding that the determinant can not change sign when the Pfaffian does.

2.3.3 Chiral symmetry

The last symmetry of special significance in the tenfold way is the chiral symmetry. In the second quantisation formalism, the chiral operator is a *antiunitary*[2] operator. The chiral symmetry operator can be defined as the product of the two other symmetry operators, that is

$$\hat{\mathcal{S}} = \hat{\mathcal{T}}\,\hat{\mathcal{C}}. \tag{2.51}$$

The order at which the operators are applied is not important, but will give a different but equivalent operator. Thus the operator is given by

$$\hat{\mathcal{S}}\, c_i\, \hat{\mathcal{S}}^{-1} = (U_{\mathrm{S}}^*)^{ij} c_j^\dagger = (U_{\mathrm{C}} U_{\mathrm{T}}^*)^{ij} c_j^\dagger. \tag{2.52}$$

Doing the same computation that lead to eqs. (2.48) and (2.49), we get that the *first quantised* (matrix) Hamiltonian transforms as

$$U_{\mathrm{S}}^\dagger H \mathcal{U}_{\mathrm{S}} = -H, \quad U_{\mathrm{S}} = U_{\mathrm{C}}^* U_{\mathrm{T}} \tag{2.53}$$

Using eq. (2.53), we see that if the vector u is an eigenenergy solution with energy E, then

$$U_{\mathrm{S}}^\dagger u \tag{2.54}$$

is also a solution, but with energy $-E$. This means that all energy bands comes in pairs with opposite signed energy of each other.

The implications of eq. (2.53) is that whenever a zero energy crossing occurs due to a parameter change, an energy with opposite sign also crosses zero energy. Again, this means that the sign of the determinant is a conserved quantity of the Hamiltonian.

The topological winding number

A useful consequence of the presence of a chiral symmetry is that we are allowed to define a winding number on the Hamiltonian. Since the chiral symmetry relation is an anti-commutation relation, we know that when the Hamiltonian is rotated into the basis where the chiral operator is diagonal,

$$U_{\mathrm{S}} = \mathrm{diag}(-1,\ldots,-1,+1,\ldots,+1),$$

it becomes an off-diagonal matrix,

$$H(k) = \begin{pmatrix} 0 & A_k \\ A_k^\dagger & 0 \end{pmatrix}$$

Subsequently, we can compute the determinant of the off-diagonal matrix A_k, which in general is a complex number,

$$|A_k| = r(k) e^{i\theta(k)}.$$

[2]While the *second quantised* operator is *antiunitary*, the first quantised (matrix) operator is unitary, as later derived.

When k traverses the 1BZ, it follows a path in the complex plane. The argument of the determinant, $\theta(k)$, is defined up to a multiplicity of 2π. If we define it in such a way that it is a *continuous* function, we can compute a unique and discrete topological number in one dimension as

$$n_{\mathrm{W}} = \frac{\theta(2\pi) - \theta(0)}{2\pi}. \tag{2.55}$$

Here we have assumed that the unit cell length is normalised. The number W is the winding of the curve the determinant takes in the complex plane around the origin, and is therefore called the topological winding number. One way to understand why this number is a topological number and distinguishes phases from each other is by firstly noticing that the product $|A_k||A_k^\dagger| = |H(k)| = \prod_i \epsilon_i(k)$. Followingly, whenever $|A_k|$ is zero, at least one of the energies in the Hamiltonian has to be zero. Secondly, if two curves have a different winding number, the only way to continuously transform them into each other is by letting the curve intersect the origin at least on time. For example, consider a CCW curve lying outside the origin, that is the winding is zero. Now, imagine that we want to wrap the curve around the origin by doing continuous transformation of the curve. This exercise is impossible to do without forcing a part of the curve to pass through the origin, thereby closing the gap. This example may not at first seem representative of all the phase transitions (like e.g. going from $n_{\mathrm{W}} = 1$ to $n_{\mathrm{W}} = 2$), but it is a fact for any change in the winding number. The facts and example just presented imply that two Hamiltonians with different winding numbers can only be transformed into each other by closing the gap. Thus, we say that the topological winding number is protected by the gap as long as the chiral symmetry remains unbroken. Lastly, we emphasise an equivalent way to compute the winding of the Hamiltonian by an integral

$$n_{\mathrm{W}} = \frac{1}{2\pi i}\int_{1\mathrm{BZ}} \mathrm{d}k \frac{\mathrm{d}_k|A_k|}{|A_k|} \equiv \frac{1}{2\pi i}\int_{\mathcal{C}} \frac{\mathrm{d}|A_k|}{|A_k|}. \tag{2.56}$$

This integral resembles the known integral $\oint_{\mathcal{C}} \mathrm{d}z/z$, which from Cauchy's residue theorem (Kreyzig, 2011) is $2\pi i$ for each counterclockwise winding around the origin.

As a brief and final note on winding numbers, we mention that there exist yet another method to compute the winding number by creating what is known as the Q-matrix (Chiu et al., 2016; Ryu et al., 2010) which is also block off-diagonal in the chiral basis. This matrix is constructed from the projection operator onto the occupied states ($E < 0$). However, we will not give the formulas for this method as the methods mentioned above were the ones used throughout this paper.

2.3.4 Topological classification of systems

The symmetries as explained above can easily be summarised in terms of first quantised operators as

$$\mathcal{T} = U_{\mathrm{T}} K, \qquad \mathcal{T} H \mathcal{T}^{-1} = H, \qquad \text{TRS}, \tag{2.57}$$

$$\mathcal{C} = U_{\mathrm{C}} K, \qquad \mathcal{C} H \mathcal{C}^{-1} = -H, \qquad \text{PHS}, \tag{2.58}$$

$$\mathcal{S} = \mathcal{C}\mathcal{T} = U_{\mathrm{C}} U_{\mathrm{T}}^*, \qquad \mathcal{S} H \mathcal{S}^{-1}, = -H \qquad \text{Chiral symmetry}, \tag{2.59}$$

or by fig. 2.2 demonstrating how the Hamiltonian transforms under the operators in the momentum basis. The first two symmetries can square to either +1 or −1, whereas the chiral symmetry is always present when both of the other two are present, is never

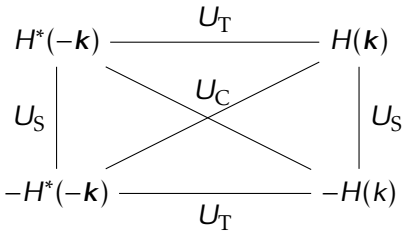

Figure 2.2: The Hamiltonian can be transformed to opposite momentum and or energy by the global symmetry operators. The unitary operators in the figure are the same as the ones described in the text, i.e. the unitary part of the time reversal operator U_T, the unitary part of the particle-hole operator U_C and the chiral operator U_S. The figure also gives a visual reason for how a third operator can be described as the combination (product) of the other two. The lines only indicate possibilities, not all relations have to be present, cf. table 2.1.

present when only one of the other two is present, and can be either present or non-present when neither of the first two are present. Thus for eight of the combinations of TR and PH the chiral symmetry is totally defined from the other two, while the last combination of TR and PH (0 and 0) can have two values of chiral symmetry: 1 and 0. Thus the total is $3 \times 3 - 1 + 2 = 10$ different combinations of the three symmetries of interest. Altland and Zirnbauer (1997) were the first to thoroughly explain the classes of Hamiltonian having each combination of symmetries, and defined the group of which they belong. The resulting table is called the AZ table, and is part of a theory often referred to as *the Ten-Fold Way*, named after the number of different groups. The AZ table is given in table 2.1 The symmetry operators and their accompanying transformations on the Hamiltonian are summarised in fig. 2.2 which demonstrates how the sign of the energy and momentum are changed by the operators, and also how the complex conjugation of the Hamiltonian itself is affected. The AZ classes can be arranged in a grid on a coordinate system with one axis being $\mathcal{T}^2$ and the other axis being $\mathcal{C}^2$ as shown in fig. 2.3. In this representation the real classes are located on the periphery, where the Hamiltonians with chiral symmetry are located in the corners (except one in the center). The complex classes are then located on the origin. The representation then shows how the classes are related to each other by difference in symmetries. In addition, by going CCW around the figure and adding one dimension each step, the topological invariant is the same. As an example, a one dimensional Hamiltonian in the BDI class has a $\mathbb{Z}$ number, and a two dimensional Hamiltonian in the D class also has a $\mathbb{Z}$ number. The way the topological invariants are derived are by e.g. K-theory, but this goes beyond the scope of this thesis. However, the results by Altland and Zirnbauer (1997), Chiu et al. (2016) as presented here makes for a great tool for evaluating if a system of interest can be topological without going into the details of the model.

In this thesis we mainly focus on the BDI class, which consists of spinless systems (Kitaev model) or easy-plane magnetic systems with s-wave or easy-plane p-wave superconductivity ($\boldsymbol{d}$-vector is restricted to a plane and additional realness or imaginary restrictions are applied) with out-of-plane Rashba SOC.

Table 2.1: Altland-Zirnbauer (AZ) table of topological classes. The first column lists the classes, the second to fourth displays the sign and presence of the symmetries, while the fifth to twelfth rows displays the symmetries for a given symmetry for the number $\delta = d - D$, where d is the dimensionality of the system and $D + 1$ is the codimension of defects. As may be seen from the table, the two complex classes A and AIII have a periodicity of 2, while the 8 real classes AI to CI have Bott periodicities of 8. In addition, the rows are arranged so that only one of the TR or PH operators change between two rows, going counterclockwise (CCW) in fig. 2.3. Created from Altland and Zirnbauer (1997), Chiu, Teo, Schnyder and Ryu (2016).

Class\δ	$\hat{\mathscr{T}}$	$\hat{\mathscr{C}}$	$\hat{\mathscr{S}}$	0	1	2	3	4	5	6	7
A				$\mathbb{Z}$		$\mathbb{Z}$		$\mathbb{Z}$		$\mathbb{Z}$	
AIII			1		$\mathbb{Z}$		$\mathbb{Z}$		$\mathbb{Z}$		$\mathbb{Z}$
AI	+			$\mathbb{Z}$				$2\mathbb{Z}$		$\mathbb{Z}_2$	$\mathbb{Z}_2$
BDI	+	+	1	$\mathbb{Z}_2$	$\mathbb{Z}$				$2\mathbb{Z}$		$\mathbb{Z}_2$
D		+		$\mathbb{Z}_2$	$\mathbb{Z}_2$	$\mathbb{Z}$				$2\mathbb{Z}$	
DIII	-	+	1		$\mathbb{Z}_2$	$\mathbb{Z}_2$	$\mathbb{Z}$				$2\mathbb{Z}$
AII	-			$2\mathbb{Z}$		$\mathbb{Z}_2$	$\mathbb{Z}_2$	$\mathbb{Z}$			
CII	-	-	1		$2\mathbb{Z}$		$\mathbb{Z}_2$	$\mathbb{Z}_2$	$\mathbb{Z}$		
C		-				$2\mathbb{Z}$		$\mathbb{Z}_2$	$\mathbb{Z}_2$	$\mathbb{Z}$	
CI	+	-	1				$2\mathbb{Z}$		$\mathbb{Z}_2$	$\mathbb{Z}_2$	$\mathbb{Z}$

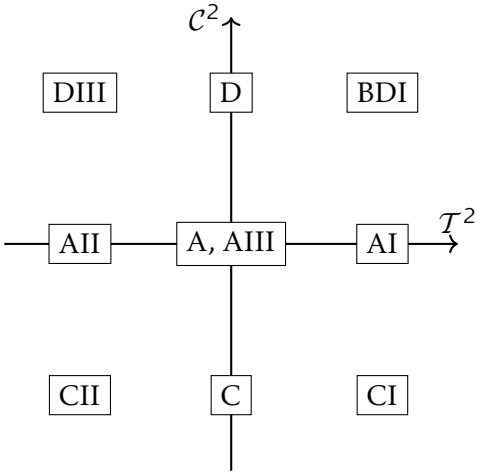

Figure 2.3: Graphical representation of the AZ classes and their symmetries.

2.4 Marginal topological superconductors

As mentioned in section 2.3, a topological system has discrete properties protected by the gap. Followingly, any time the gap closes, the system may change the topological number. An interesting edge case arrises from considering the following question: what can we say about gapless systems? In two dimensions, gaplessness does not necessarily mean that the system does not have topological phases, since the nodal points can be protected by symmetries and give rise to topological edge states (Chiu & Schnyder, 2014). In one dimension however, gaplessness means that even if there *were* zero-energy states characterised by some topological number, they would interact strongly with the bulk and would as a consequence gap out or be delocalised. But we ask, what happens if we could perturb the system in a symmetry conserving way that opens the gap? We speculate if such a gap opening will localise the potential MBS on the boundaries of a finite size system. This could potentially also work if the gapless system has an undefined topological number, but when the gap is opened it immediately obtains a well defined topological number. Take for example systems characterised by the winding number. The winding number is ill defined for any path that passes through the origin (gapless), but is well defined for all gapfull systems where the path does not pass through the origin. Or consider systems characterised by the sign of the Pfaffian. Again, if the system is gapless, the Pfaffian being proportional to the square root of the product of the energies is zero. Since it is the sign of the Pfaffian which is of interest, the topological number is ill defined since $-0 = +0$ and thus -1 and $+1$ are both allowed quantum numbers at the same time. When the gap is opened, the Pfaffian can not be zero, and thus has an unequivocal sign.

We wonder, does there exist systems that a) are gapless, b) have a symmetry conserving small perturbation which opens the gap, c) any such perturbation will bring the system into a topological phase, and d) does not rely on fine-tuning. The three first requirements are quite natural considering the previous paragraph, but the last is added to differentiate these types of systems from any topological system. The reason is that any topological system is a) gapless when transitioning between different phases, b) has symmetry conserving perturbations which opens these same gaps, and sometimes c) brings the system into a topological phase independent of the specifics of perturbation. In addition, including d) has the added benefit of making such systems more easily obtainable experimentally. For a systems gaplessness to not rely on fine-tuning, we require that the gap stays closed for a connected range of the parameters. For example, a gapless ferromagnetic system needs to stay gapless when the amplitude of the field changes or the electron concentration changes, which is in contrast to the usual case where the gap closes at a specific point in parameter space. Certainly, the question of whether a system relies on fine-tuning or not does not have a clear cut answer, and will be a subject for discussion.

To be more specific, we consider superconducting systems with a global chiral symmetry which has a topological number defined by the winding number (eq. (2.56)). When the winding number, n_{W}, is non-zero, the off-diagonal determinant in general encloses the origin, e.g. fig. 2.4a1). The determinant consists of a real and imaginary part. There are two 'ways' that the gap may close. The first is the most general way which discerns topologically different phases from each other, which is shown as when some parameter, here labelled δ, obtains the value of δ_{crit}. In this case the gap closes and reopens again, with an accompanying change of the topological number. The value of δ_{crit} in general depends on all the other parameters of the Hamiltonian, in which case

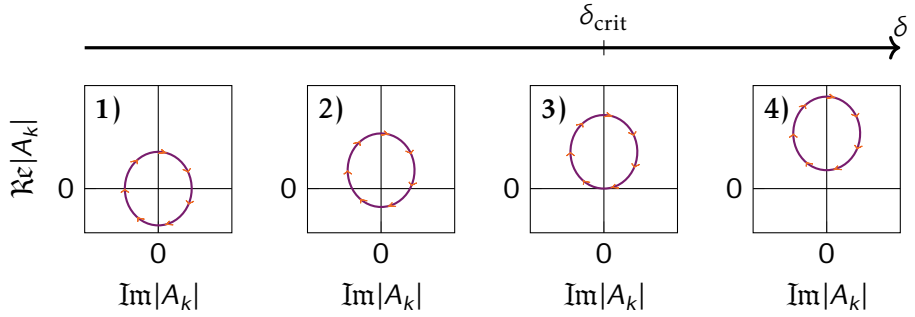

(a) Schematic winding number for normal topological phase transition. At the transition point, the winding number is allowed to change absolute value.

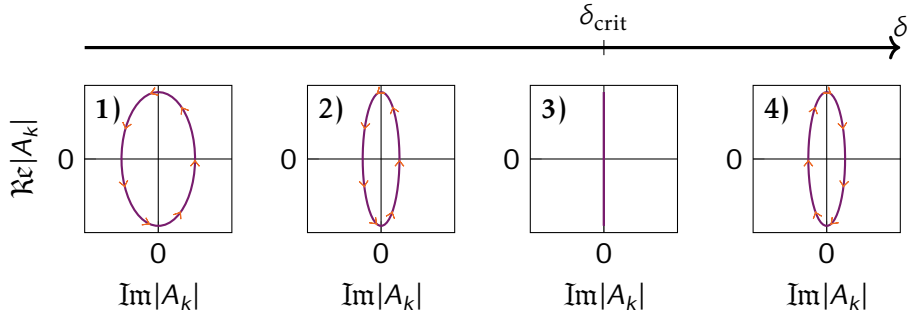

(b) Schematic winding number for marginal topological phase transition. At the transition point, the winding number may changes sign.

Figure 2.4: Schematic phase transtion for 'normal' and marginal superconductors. The closed curves are the determinant $|A_k|$ parameterised by k in 1BZ, and the evolution with respect to a parameter δ is shown for a normal topological phase transition (top) and marginal (bottom) for topological superconductors.

we claim that the gap closing is dependent on fine-tuning. In fact, any time a gap closes due to the origin passing through the path made by the off-diagonal element, the gap closes and reopens again. On the other hand, if the origin were to move along the curve, the gap would stay closed. In most cases, such motion along a curve requires fine-tuning. In the case that such a curve is straight, it is much more feasible to follow it. This leads us to consider cases were the $|A_k|$ is purely real for all k in the 1BZ. If the realness-criteria relies only on a subset of the parameters of the Hamiltonian (shown as δ in fig. 2.4b), any change in the remaining parameters will not add any imaginary part. Followingly, if the real part has both positive and negative values, it means that the curve must pass through the origin at some point due to the intermediate value theorem, which implies that the Hamiltonian is gapless. In addition, because the matrix A_k is a continuous function in the Hamiltonian and the determinant is continuous in the matrix, the gap will stay closed for any change in the parameters not limited by the realness criteria. We would argue that such 'freeness' of some of the parameters means that d) above is satisfied, i.e. fine-tuning these parameters is not required. The only fine-tuning needed is in the parameters which ensures the realness of the Hamiltonian. Thus, the fine-tuning argument should still be discussed in terms of restricted parameters: Are the values easily obtainable? An example of an easily obtainable value is the value of 0, which one may claim is not a 'fine-tuned' value. There may exist other cases where one can argue that the values are easily obtainable. We point out that if the

imaginary part is odd in the perturbation, δ, in close proximity to the critical value, we expect the winding number to be an odd function in the perturbation in the immediate neighbourhood. If the imaginary part is even in the vicinity, we expect the winding number to be even in the immediate neighbourhood.

We argue that the topological systems which are gapless due to the realness of the winding curve, which we from now on refer to as marginal topological systems, are interesting in their own right. These types of systems may prove useful for manipulating MBSs by opening and closing the gap if the gap opening parameter(s) are easily manipulated by external measures. Since only small perturbations will bring marginal topological systems into topological phases, we may say that the systems show a distinct response to the external perturbation which always drives the gapless phase into a topological one.

2.5 Spinless Kitaev model in 1D

Kitaev (2001) analysed a one dimensional toy model of spinless electrons with an anisotropic p-wave superconducting order parameter. This toy model has the same symmetries as the models we analyse later in this thesis and belong to the AZ class BDI. Therefore we here present the work by Kitaev in his paper as a primer and introduction for the later analysis on more realistic topological superconductors.

2.5.1 Model

Consider a simple model of a one dimensional spinless p-wave superconductor with nearest neighbour hopping described by the Hamiltonian

$$\hat{H} = -t\sum_{\langle i,j\rangle} c_j^\dagger c_i - \mu\sum_i\left(\hat{n}_i - \frac{1}{2}\right) + \sum_i\left(\Delta c_1 c_{i+1} + \Delta^* c_{i+1}^\dagger c_i^\dagger\right), \tag{2.60}$$

where t is the usual hopping parameter, μ is the chemical potential and $\Delta = |\Delta|e^{i\theta}$ is the superconducting order parameter. Such an effective spinless model can be due to for example a freeze out of one of the electrons spins in a p-wave superconductor, or more realistically can be achieved by creating an effective p-wave superconductor by combining a superconductor and a semiconductor with SOC in a ferromagnetic field, which is analysed in section 3.3

Any fermionic operator can be transformed into a superposition of two Majorana fermions by the transformation

$$\gamma_1 = \frac{1}{\sqrt{2}}\left(ce^{i\theta/2} + c^\dagger e^{-i\theta/2}\right) \qquad \gamma_2 = \frac{i}{\sqrt{2}}\left(-ce^{i\theta/2} + c^\dagger e^{-i\theta/2}\right) \tag{2.61}$$

Here $c \to ce^{i\theta/2}$ is used to gauge away the phase of Δ, which simplifies the Hamiltonian and of course leaves the physics unchanged. It is however useful to note that a full rotation of the phase by 2π does not leave the Majorana fermions unchanged, but are themselves rotated by π. Thus a full rotation of 4π is needed to rotate the Majorana operators back to the initial point. This phenomenon is not of much importance in this thesis, but we note that it is an important effect in systems with Josepshon junctions (Kitaev, 2001). It can be shown that these new operators obey the anticommutator relations

$$\{\gamma_i,\ \gamma_j\} = \delta_{i,j} \tag{2.62}$$

From the definitions of eq. (2.61) it is clear that both fermionic operators obey $\gamma_{1,2} = \gamma_{1,2}^\dagger$, which is the requirement for Majorana fermions. A simple unitary transformation of the Hamiltonian clearly should not change the physics of the system involved. Thus even though Majorana fermions have unexpectedly appeared in the model, they are not free, but interact in pairs.

Applying the transformations of eq. (2.61) to eq. (2.60), the Hamiltonian becomes

$$\hat{H} = i\left[-\mu\sum_i \gamma_1^i\gamma_2^i + (-t+|\Delta|)\sum_i \gamma_1^i\gamma_2^{i+1} + (t+|\Delta|)\sum_i \gamma_2^i\gamma_1^{i+1}\right]. \tag{2.63}$$

The imaginary unit which appears ensures the hermiticity of the Hamiltonian, since a hermitian conjugation of eq. (2.63) negates the sign and interchanges the Majorana

fermions, but otherwise keep them unchanged since they are their own antiparticles. Therefore, when we anticommute the Majorana operators to bring the Hamiltonian to the initial form, a new negation of the sign occurs and the total sign is the same as it initially had.

It is instructive to consider special cases of the parameter space of the Hamiltonian in eq. (2.63) in a finite size system before solving the system for arbitrary values of these.

In the first case, let $|\Delta| = t > 0$ and μ=0. These parameters leaves only the term

$$\hat{H} = 2it \sum_{i=1}^{N-1} \gamma_2^i \gamma_1^{i+1}. \tag{2.64}$$

Inspecting the above Hamiltonian we realise that γ_1^1 and γ_2^N are missing, i.e. they are unpaired. These two unpaired Majorana fermions are thus free eigensolutions to the problem and have energies equal to 0. This case is depicted in fig. 2.5b. Furthermore, the Hamiltonian of eq. (2.64) can be rewritten by transforming it to new fermion operators $a_i = \frac{1}{\sqrt{2}}\left(\gamma_2^i + i\gamma_1^{i+1}\right)$, giving

$$\hat{H} = 2t \sum_{i=1}^{N-1} (a_i^\dagger a_i - \frac{1}{2}). \tag{2.65}$$

Since we have assumed that t is positive, the system minimises the energy when $a_i \left|\psi\right\rangle = 0$ for all sites i. In the basis of the lattice sites, the operators $a_i = \frac{i}{2}(-c_i + c_i^\dagger + c_{i+1} + c_{i+1}^\dagger)$. As Kitaev (2001) showed, there exist two ground states $\left|\psi_0\right\rangle$ and $\left|\psi_1\right\rangle$ with the relations

$$-i\gamma_1^1\gamma_2^N \left|\psi_0\right\rangle = \frac{1}{2}\left|\psi_0\right\rangle \qquad\qquad -i\gamma_1^1\gamma_2^N \left|\psi_1\right\rangle = -\frac{1}{2}\left|\psi_1\right\rangle. \tag{2.66}$$

These two states have opposite parity measured by the parity operator

$$P = \prod_i (1 - 2\hat{n}_i) = \prod_i (-2i\gamma_1^i\gamma_2^i), \tag{2.67}$$

where the former has even parity, i.e. an even number of electrons, and the latter has odd parity.

In the second case, let $|\Delta| = t = 0$ and $\mu < 0$. Now the Hamiltonian is

$$-i\mu \sum_i \gamma_1^i \gamma_2^i, \tag{2.68}$$

which couples all Majorana fermions on the same site in pairs, thus leaving no unpaired Majorana fermions. This case is depicted in fig. 2.5a. Furthermore the Hamiltonian is diagonal in the original basis of electrons located at the lattice sites, meaning that all sites are unoccupied.

The two cases mentioned above represents two different phases of the Kitaev model, where the former phase has unpaired Majorana fermions bound to the edges whereas the latter does not. Until now we have only described the system for two specific points in parameter space. Thus it is of interest to investigate whether these two phases extend into the ($|\Delta|$, t, μ) space. As we will soon show, the unpaired Majorana fermions are topologically protected by the gap in the bulk energy spectrum, and can not be removed by symmetry-conserving perturbations without closing the gap. The two phases are

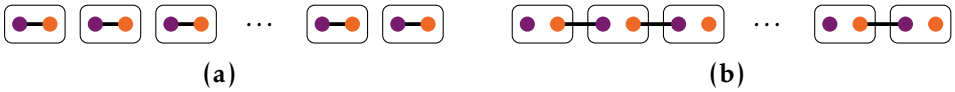

(a) (b)

Figure 2.5: The Kitaev model can have (a) all the fermions paired up or (b) can have two unpaired Majorana fermions at the ends (b).

two distinct topological phases and can thus be described by a topological quantum number.

As mentioned, Majorana fermions are Bogoliubov quasiparticles with zero energy, and it is natural to look for zero energy solutions of the Hamiltonian as written in eq. (2.63). Kitaev (2001) did look for such zero energy solutions, and the following uses the same procedure as Kitaev. Such an eigensolution is a superposition of Majorana fermions, $\psi = A_i\gamma_1^i + B_i\gamma_2^i$. Inserting them into eq. (2.63), we obtain two linear equations:

$$\mu(A_i\gamma_2^i - B_i\gamma_1^i) + (\Delta - t)(B_{i+1}\gamma_1^i - A_{i-1}\gamma_2^i) + (t+\Delta)(A_{i+1}\gamma_2^i - B_{i-1}\gamma_1^i) = 0. \tag{2.69}$$

This gives rise to two independent equations for the A's and B's

$$\mu A_i + (t-\Delta)A_{i-1} + (t+\Delta)A_{i+1} = 0, \tag{2.70}$$
$$-\mu B_i + (\Delta - t)B_{i+1} - (t+\Delta)B_{i-1} = 0, \tag{2.71}$$

where the indices are only valid for $i \in [1, N]$. Trying the ansatz $A_i = xA_{i-1}$ and $B_i = x^{-1}B_{i-1}$ as solutions to the equations, we get a second order equation for a, which has the two solutions

$$x_\pm = \frac{-\mu \pm \sqrt{\mu^2 - 4t^2 + 4|\Delta|^2}}{2(t+|\Delta|)}. \tag{2.72}$$

The resulting eigenvectors are then of the form

$$\psi = \sum_i A_+ x_+^i \gamma_1^i + A_- x_-^i \gamma_1^i, \tag{2.73}$$
$$\psi = \sum_i B_+ x_+^{-i} \gamma_1^i + B_- x_-^{-i} \gamma_1^i. \tag{2.74}$$

This is in correspondence with what Kitaev (2001, eq. (14)) obtained. One must be careful with the boundaries, as some of the indices will be out of bounds and the corresponding terms must be omitted from the equations. In general, both boundaries (left and right) must be satisfied, which is not possible with only two coefficients. However, if we assume that the wavefunction decays from one boundary to the other, only one of the boundaries will contribute with boundary conditions. Still, to satisfy both the normalisation requirement and the remaining boundary condition, we need two degrees of freedom in the choise of coefficients. Thus both of the solutions ($\pm$) must exponentially decrease (located on the left edge, a-solution) or increase (located at the right edge, b-solution) together. Thus we require that $|x_\pm| < 1$. As Kitaev showed, this only happens if $|\mu| < 2|t|$, which can be seen from eq. (2.72).

This way of analytically finding the critical values of the parameters in a model using the Majorana basis and solving for the nullspace of the resulting antisymmetric Hamiltonian was easy with the Kitaev model, but in general the resulting equations are more complicated when spin-degrees of freedom are included.

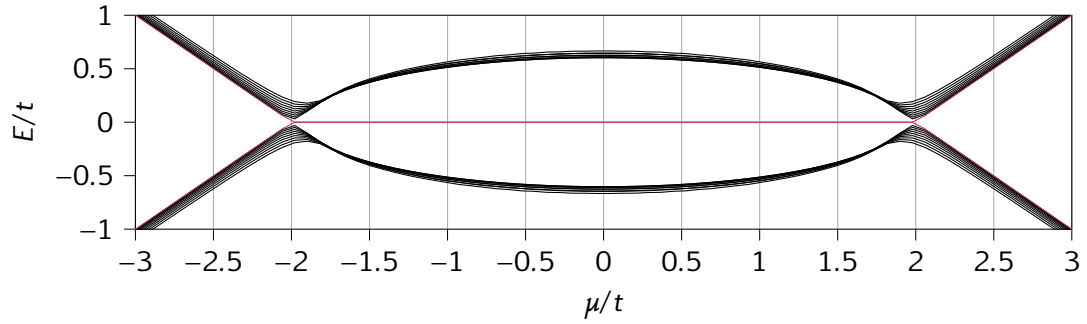

Figure 2.6: Energy bands as a function of the chemical potential with open boundaries. The two energy bands closest to 0 are black, while all other bands are red (light). Here the OP is $\Delta = 0.3t$. The zero-energy Majorana fermions are present until $\mu = 2t$ occurs, which was predicted by Kitaev (2001).

2.5.2 Symmetries of the Kitaev model

As mentioned in section 2.3, the symmetries of a Hamiltonian can reveal much information about a system and the possible phases and topological constants. Therefore, before solving the Kitaev model for arbitrary values of the parameters involved, I will focus the attention on the symmetries intrinsic to the Kitaev model.

Since the Kitaev model is a spinless model (there is no spin index in eq. (2.60)), the time reversal operator is defined in the lattice site basis as

$$\hat{\mathcal{T}}\, c\, \hat{\mathcal{T}}^{-1} = c, \tag{2.75}$$

together with the fact that it should be antiunitary. Thus it is described simply by the complex conjugation operator $\hat{\mathcal{T}} = K$. This operator commutes with the Hamiltonian in eq. (2.60) only if the phase of the superconducting order parameter $\Delta = |\Delta| e^{i\theta}$ is gauged away by the transformation $c \to c e^{i\theta/2}$, or optionally included in the transformation itself ($\hat{\mathcal{T}}\, c\, \hat{\mathcal{T}}^{-1} = e^{i\theta} c$). As mentioned previously, such a gauge transformation is admissible since the overall phase of the system is not measurabe, only the probabilities, i.e. the amplitudes. Furthermore in this model we have

$$\hat{\mathcal{T}}^2 = K^2 = +1, \tag{2.76}$$

since complex conjugation twice leaves all complex numbers invariant.

Written in the BdG formalism the Kitaev model also has particle-hole symmetry as explained in section 2.2.3. The result is that the energies of the Hamiltonian comes in degenerate pairs, $(\epsilon, -\epsilon)$. From section 2.3.1 we could perhaps have expected degenerate energy eigenvalues. This, however, can only apply to systems with half-integer spin particles. As the particles in the model at hand are spinless, Kramer's theorem (Kramer, 1930) does not apply after all. Since both PH and TR symmetries are present, their product $\hat{\mathcal{T}}\hat{\mathcal{C}} = \hat{\mathcal{S}}$ which is the chiral symmetry operator, must also be a symmetry of the Hamiltonian. Reading from table 2.1, we can establish that the Kitaev model belongs to the class BDI, and has a topological invariant described by $\mathbb{Z}$.

2.5.3 Bulk-edge correspondence

While the Majorana fermions appearing in this model are bound edge states, the model can be extended to the periodic lattice by joining the two ends together by the introduction of parameterised hopping between the two links. In other words the chain

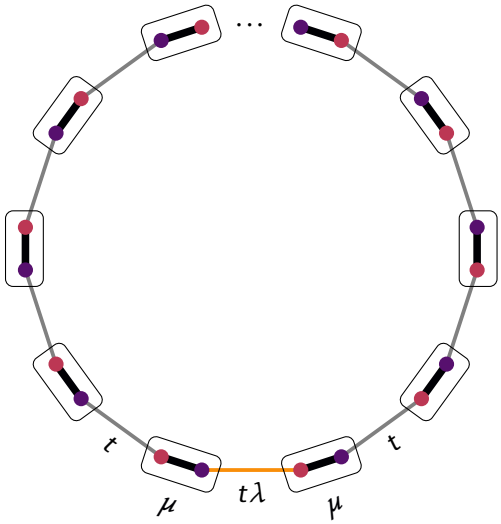

Figure 2.7: Kitaev chain coiled into a ring, with a variable link strength between the two ends, shown in the bottom middle link. The variable strength of the connecting link allows for continuous transformation between periodic and antiperiodic boundary conditions.

is coiled back on itself, like in fig. 2.7 where the added link has variable strength $t\lambda$ where λ is allowed to vary in the range $[-1,1]$. The reason for adding the parameter λ is that it allows us to continuously transform between the two cases of periodic and anti-periodic boundary conditions. For specificity, let there be N orbital sites in the Kitaev ring. Periodic boundary conditions require that the allowed momentum numbers k are given by $Nk = 2\pi m, m \in [0, N-1]$. Antiperiodic boundary conditions on the other hand require that k is given by $Nk - \pi = 2\pi m, m \in [0, N-1]$. The first boundary condition can be obtained by letting $\lambda = 1$, while the latter can be obtained by $\lambda = -1$. For arbitrary values inbetween, k is no longer a well defined quantum number. At $\lambda = 0$ we obtain the Kitaev chain again. In the special cases of $\lambda = \pm 1$, the Hamiltonian can easily be Fourier transformed by introducing the fourier transformed fermion creation operators

$$c_i = \frac{1}{\sqrt{N}} \sum_k c_k e^{iki} \qquad\qquad c_k = \frac{1}{\sqrt{N}} \sum_i c_i e^{-iki}. \tag{2.77}$$

Inserting eq. (2.77) into eq. (2.60) we obtain

$$\hat{H} = \sum_k \left\{ (-2t\cos(k) - \mu)\, c_k^\dagger c_k + 2i|\Delta| c_{-k} c_k \sin(k) - 2i|\Delta| c_k^\dagger c_{-k}^\dagger \sin(k) \right\} - \frac{N\mu}{2}. \tag{2.78}$$

Equation (2.78) can be cast into the BdG formalism to give

$$\hat{H} = \frac{1}{2} \sum_k D_k^\dagger \begin{pmatrix} -2t\cos(k) - \mu & -2i|\Delta|\sin(k) \\ 2i|\Delta|\sin(k) & 2t\cos(k) + \mu \end{pmatrix} D_k, \tag{2.79}$$

with D_k being the column vector $(c_k, c_{-k})^{\mathrm{T}}$. The matrix representation of the Hamiltonian in eq. (2.79) can be rewritten as

$$(-2t\cos(k) - \mu)\tau_z + 2|\Delta|\sin(k)\tau_y, \tag{2.80}$$

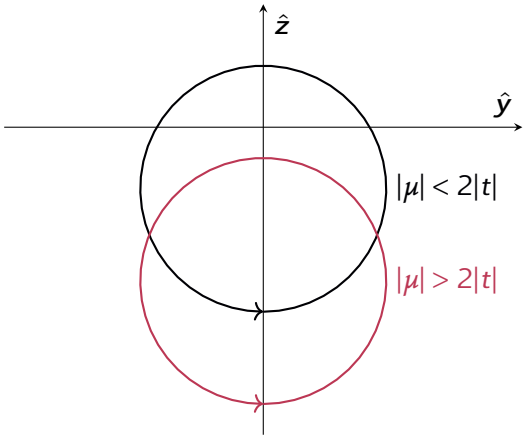

Figure 2.8: The vector representation of the Hamiltonian (eq. (2.81)) creates ellipses in the yz-plane, and a winding number about the origin can be defined. Depending on the relative size of the absolute values of μ and t, the winding number is ± 1 or 0.

where the τ matrices are particle-hole operators.

From here on there are two ways to categorise the topological phase the system is in. Since the system belongs to the class of BDI we expect it to have a winding number in $\mathbb{Z}$ (Sticlet, 2012), while it may also have a $\mathbb{Z}_2$ invariant due to the PH symmetry. Looking at eq. (2.80), it appears as a sort of vector if we interpret the Pauli matrices as components in the three dimensional space. In other words, the Hamiltonian is written like a vector product

$$H = (0, 2|\Delta|\sin(k), -2t\cos(k) - \mu) \cdot \boldsymbol{\tau}. \tag{2.81}$$

The first vector in the dot product is a vector that rotates in the y-z plane when k changes, and creates a closed path when k goes from 0 to 2π. The winding number in this case is defined as the number of times the vector rotates around the x-axis when k traverses the first Brillouin zone. This number in general belongs to the group of $\mathbb{Z}$, yet in this model the only allowed values are -1, 0 and 1. The winding number can only be non-zero for certain pairs of t and μ, as shown in fig. 2.8. For $|\mu| > 2|t|$ the ellipses never encloses the origin, and consequently the winding number is zero. This corresponds with the previous results for the edge states which only existed for $|\mu| < 2|t|$.

The other way to classify the topological phase is to look at the previous mentioned $\mathbb{Z}_2$ topological charge. From the definition of D_k it is clear that the transformation $\tau_x (D_k^\dagger)^{\mathrm{T}} = D_{-k}$ is a *antiunitary* symmetry operation, which, following a similar procedure to that in section 2.3.2, leads to the following requirement on the Hamiltonian,

$$\tau_x H(-k)^{\mathrm{T}} \tau_x = -H(k).$$

Thus, if a wave-function solution to the problem is of the form $uc_k + vc_{-k}^\dagger$ with energy ϵ, then the solution $v^* c_{-k} + u^* c_k^\dagger$ is also obviously a solution with the opposite signed energy ϵ. This implies that the energy spectrum is antisymmetric with respect to the momentum. Furthermore, the chiral symmetry implies that the energy spectrum should also be symmetric around zero energy at the same k. Followingly we expect at least two k-symmetric bands with opposite energy. The implications of this is that any time an energy eigensolution changes sign of the energy, so too does the opposite k-partner and opposite-energy partner, that is two pairs of eigenenergy-solutions become zero simultaneously. There is an exception: At $k = -k$, the k-symmetric partner is itself,

thus any time the energy eigensolutions at these points cross zero energy it happens in pairs of two, not groups of four. Thus the Pfaffian at these points are allowed to change under such crossings. Any time a single energy solution crosses at these points, there is an accompanying topological phase change. Kitaev (2001) showed that the topological charge of the system can be defined as

$$\mathcal{M}(\hat{H}) = \text{sign}\left[\text{Pf}(A(0))\,\text{Pf}(A(\pi))\right] \tag{2.82}$$

where A is the skew symmetric matrix defined by

$$iA(k) = \begin{pmatrix} 1 & 1 \\ -i & i \end{pmatrix} H(k) \begin{pmatrix} 1 & i \\ 1 & -i \end{pmatrix}. \tag{2.83}$$

Now we are interested in knowing how this translational invariant system can be connected to that of a system with boundaries. We note that when the system has periodic boundary conditions, $k = 0$ is always a solution to $k = -k$. For antiperiodic boundary conditions, $k = 0$ is not a solution. On the other hand, $k = \pi$ is a solution to $k = -k$ (modulo 2π) for even N in the periodic case, or odd N in the antiperiodic case. Thus changing λ from 1 to -1 means that the system changes topological charge depending on if N is even or not:

- Even N: Topological charge $\mathcal{M}$ changes from $\text{sign}\left[\text{Pf}(A(0))\,\text{Pf}(A(\pi))\right]$ to 1.
- Odd N: Topological charge $\mathcal{M}$ changes from $\text{sign}\left[\text{Pf}(A(0))\right]$ to $\text{sign}\left[\text{Pf}(A(\pi))\right]$ with a total change in sign of $\text{sign}\left[\text{Pf}(A(0))\,\text{Pf}(A(\pi))\right]$.

Either way the topological charge changes by $\text{sign}\left[\text{Pf}(A(0))\,\text{Pf}(A(\pi))\right]$, meaning that a zero-energy mode appears between $\lambda = 1$ and $\lambda = -1$. The actual place of the crossing happens close to $\lambda = 0$ which is the Kitaev chain with boundaries. Thus if the topological charge is -1 in the periodic structure, there exist a zero energy Majorana fermion at the edges in the Kitaev chain. This is then explains the bulk-boundary correspondence.

Evaluating eq. (2.83) at $k = 0$ and $k = \pi$, gives

$$A(k) = \begin{pmatrix} 0 & \epsilon_k \\ -\epsilon_k & 0 \end{pmatrix}.$$

Thus the topological charge defined in eq. (2.82) is evaluated to

$$\mathcal{M}(\hat{H}) = \text{sign}\left[(-2t - \mu)(2t - \mu)\right].$$

And, as expected we see that the first product changes sign for $\mu < -2t$ and the latter for $\mu > 2t$ in the case that $t > 0$, or opposite for opposite sign of t. The result is that for $|\mu| < 2|t|$ the topological charge is $\mathcal{M} = -1$, while it is 1 otherwise. This is the same boundaries as we have seen two times previously with other methods of computing the topological quantum number.

We have thus established three methods for classifying the topological phase of a Hamiltonian in the AZ class BDI: Computing the winding number, solving the nullspace of the Hamiltonian and look for Majorana solutions, and the third is to compute the $\mathbb{Z}_2$ invariant defined as the Pfaffian of the Hamiltonian in the Majorana basis. Although the Kitaev model is a spinless model, the methods described here can be used in spinfull models as we will demonstrate later in this thesis. As mentioned, one way to achieve a realistic Kitaev model is to obtain effective p-wave superconductivity and

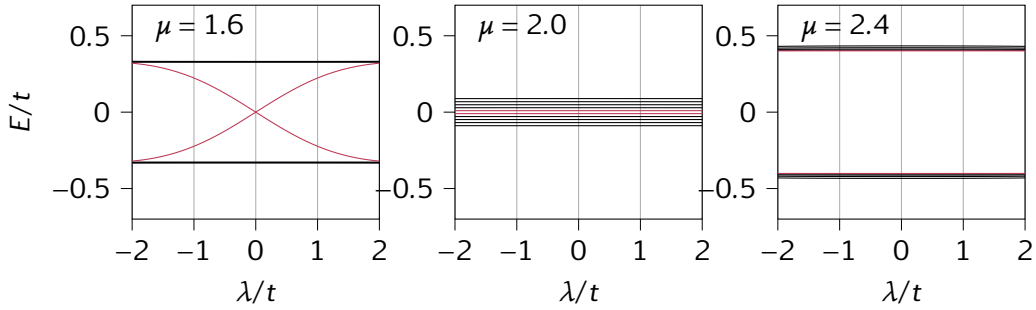

Figure 2.9: Energy bands as a function of coiling link strength λ for three values of μ. Only the five energy bands closest to 0 on each side is shown. The two energy bands closest to 0 are purple (dark) while all other bands are teal (light). Here $\Delta = 0.3t$ and μ is $1.6t$, $2.0t$ and $2.4t$ for left, middle and right subfigure respectively. When λ changes from $2t$ to $-2t$ the system transits from periodic to antiperiodic boundary conditions, which then gives a interpretation of the bulk-boundary correspondence.

use magnetism to lift the degeneracy of the two spin-modes. In the later chapters, we describe both topological intrinsic p-wave superconductors and topological s-wave superconductors in noncollinear fields. Both of these models are examples of Kitaev equivalent models belonging to the BDI class.

2.6 General model

In this thesis we will consider chains of magnetically active atoms deposited on top of a two dimensional slab of superconducting material, cf. fig. 2.10. In the analysis, only the chain will be considered and thus be solved, while the superconducting material acts only to impinge superconductivity into the chain via the proximity effect (Sigrist & Ueda, 1991). Self consistency in the model is, as a consequence of this, not part of the analysis. The electrons in the chain are allowed to hop with a spin-independent amplitude and a spin-dependent Rashba SOC amplitude between neighbouring atoms. In addition, the magnetically active atoms have local exchange fields, h_i, which in general are not constrained.

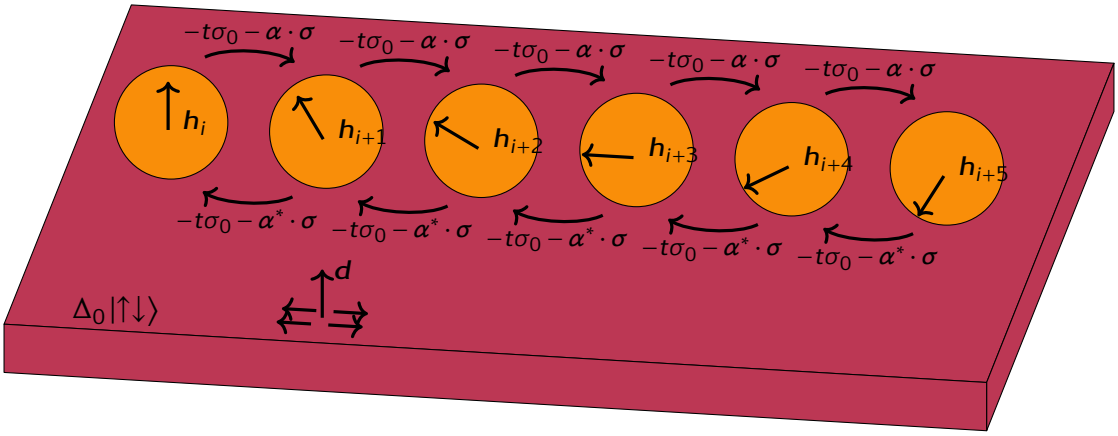

Figure 2.10: A schematic representation of the general system in consideration. The systems consist of a chain of magnetically active atoms (orange spheres) deposited on top of a superconducting 2D slab (red). The chain is described in the tight-binding approximation, whereas the slab of superconducting material is present only to impinge superconductivity in the chain, and is thus not part of the equations. Inside the chain, the electrons are in general free to move to neighbouring atoms (in some cases next nearest neighbours etc.) with a spin*independent* amplitude t and a spin *dependent* Rashba SOC amplitude described by a 3D vector $\boldsymbol{\alpha}$. On each site, there is a local exchange field given by h_i. The superconducting part is described by a s-wave superconducting OP and a three dimensional vector $\boldsymbol{d}$ describing the (p-wave) triplet coupling. The interpretation of the d-vector is that it points in the direction of zero net spin of the cooper pairs, which is shown schematically as Cooper pairs ($|\uparrow\uparrow\rangle$) lying in the plane perpendicular to d.

In the following we will consider the Hamiltonian on a lattice. Instead of explicitly writing the spin indices on the creation and annihilation operators, we write them as vectors, $\hat{c}_i = (c_{i\uparrow}\ c_{i\downarrow})^{\mathrm{T}}$. The spin-independent hopping term allows electrons to 'hop' to atoms in the proximity, which gives rise to an effective kinetic energy and momentum. If there is only nearest neighbour hopping in the system, the hopping Hamiltonian is written

$$\hat{H}_{\mathrm{K}} = -\sum_{\langle ij\rangle} t_{ji}\hat{c}_i^{\dagger}\sigma_0\hat{c}_j - \mu\sum_i \hat{n}_i. \tag{2.84}$$

If there is significant next nearest neighbour hopping, additional sums of the same form can be added, but instead of $\langle ij\rangle$, the more distant pairs, $\langle\langle ij\rangle\rangle$ are used. The

spin-dependent hopping is described by

$$\hat{H}_{\mathrm{SOC}} = i \sum_i \left(\hat{c}_{i+1}^\dagger \boldsymbol{\alpha}_{i,i+1} \cdot \boldsymbol{\sigma} \hat{c}_i - \hat{c}_i^\dagger \boldsymbol{\alpha}_{i,i+1}^* \cdot \boldsymbol{\sigma} \hat{c}_{i+1} \right). \tag{2.85}$$

As can be seen, this term treats electrons differently depending on the direction of motion and the spin: The effect is negative for an electron going the opposite direction or having the opposite spin direction.

The exchange field is given by

$$\hat{H}_{\mathrm{Mag}} = -\sum_i \hat{c}_i^\dagger \boldsymbol{h}_i \cdot \boldsymbol{\sigma} \hat{c}_i. \tag{2.86}$$

The superconducting OPs can be condensed into a four component vector

$$\boldsymbol{\Delta} = (\Delta_0, d_x, d_y, d_z) \tag{2.87}$$

where the first component is the singlet order parameter, and the $\boldsymbol{d}$-vector is defined such that the expectation value of the projection of the Cooper pairs along this vector is always zero. The same applies for the scalar Δ_0, but since it is directionless, the Cooper pairs have zero net spin in all directions, which is a general fact about singlet pairs. In this thesis, we only consider s-wave (excluding extended s-wave) and p-wave superconductivity pairing electron pairs only on neighbouring atoms. This means that in momentum space, the Δ_0 component is constant whereas the d-vector has is proportional to $\sin(k)$, were we have assumed a lattice constant of unity. In lattice space, the superconducting Hamiltonian is written

$$\hat{H}_{\mathrm{SC}} = \frac{1}{2} \sum_i \left(i\Delta_0 \hat{c}_i^\dagger \sigma_y \hat{c}_i^{\dagger \mathrm{T}} - i\Delta_0^* \hat{c}_i^{\mathrm{T}} \sigma_y \hat{c}_i \right) + \frac{1}{2} \sum_{\langle ij \rangle} \left(\hat{c}_j^\dagger (i\boldsymbol{d}_i j \cdot \boldsymbol{\sigma}\sigma_y) \hat{c}_i^{\dagger \mathrm{T}} - \hat{c}_i^{\mathrm{T}} \sigma_y (i\boldsymbol{d}_i j^* \cdot \boldsymbol{\sigma}\sigma_y) \hat{c}_j \right) \tag{2.88}$$

where the factor half is to compensate for double counting.

3 | Marginal topological superconductors

Any time a topological phase transition occurs in a system, effectively changing the number of topological objects on the boundary, the gap must close. If the Hamiltonian stays gapless, the topological invariant is in general not defined, but any perturbation which opens the gap again will simultaneously make the invariant defined. If the gaplessness of the Hamiltonian is due to a realness criterion on the winding curve the system may be a marginal topological superconductor. Any perturbation which adds an imaginary part to the winding curve can in general open the gap and thus push the system into a topological phase. Such types of systems are interesting to investigate since they can open up new paths to obtain and manipulate topological systems by arbitrarily small perturbations, and in addition they are easy to obtain since they gaplessness is not dependent on fine-tuning.

In this chapter we analyse three special cases of the model presented in section 2.6, namely a

- p-wave superconductor in a ferromagnetic field (Mercaldo, Cuoco & Kotetes, 2018),
- p-wave superconductor in a antiferromagnetic field (Mercaldo, Kotetes & Cuoco, 2018), and
- s-wave superconductor in a noncollinear exchange field, including helical fields.

All models are chiral symmetric and belong to the AZ class BDI. We look for the requirements for realness of the winding curve and realisations of marginal topological behaviour in the phase diagram.

3.1 p-wave superconductivity in coexistence with FM ordering

In this section we will consider how time reversal symmetry can be intact also in the presence of a ferromagnetic field in a superconductor. This type of system has been firstly considered by Mercaldo, Cuoco and Kotetes (2018). Here, we will start by recalling the basic topological properties of the model and the phase diagram (Mercaldo, Cuoco & Kotetes, 2018) and then we will expand their model to consider the conditions which can lead to a marginal topological behaviour.

3.1.1 Model

Let the Hamiltonian of a p-wave superconductor in the presence of a ferromagnetic (FM) field be given in lattice space by

$$\begin{aligned}\hat{H} = &\sum_{ij\sigma} W(i-j)c^\dagger_{i\sigma}c_{j\sigma} - \sum_{iss'}(\mu\sigma_0 + \boldsymbol{h}\cdot\boldsymbol{\sigma})_{ss'}c^\dagger_{is}c_{is'} \\ &+ \sum_{i\sigma\sigma'}\left[\Delta_{\sigma\sigma'}c^\dagger_{i\sigma}c^\dagger_{i+1,\sigma'} + \text{h.c.}\right].\end{aligned} \tag{3.1}$$

Here $W(i-j) = W(j-i)$ is a real parameter describing the hopping strength between lattice site i and j, $\boldsymbol{h}$ is the FM field strength, μ is the chemical potential and $\Delta_{\sigma\sigma'} = \Delta_{\sigma'\sigma}$ are the triplet spin superconducting OPs. In the case of periodic boundary conditions, the Hamiltonian can be simplified by introducing the Fourier transformed fermion operators as given in eq. (1) in the nomenclature. Here a unit lattice constant was assumed. Periodic boundary conditions imply that for a system of size N, the allowed k-numbers are $\frac{2\pi m}{N}, m \in [-\lfloor\frac{N-1}{2}\rfloor, \lfloor\frac{N}{2}\rfloor]$. Inserting these transformations in eq. (3.1), we get

$$\begin{aligned}\hat{H} = &\sum_{k\sigma}\epsilon_k c^\dagger_{k\sigma}c_{k\sigma} - \sum_{kss'}c^\dagger_{ks}(\boldsymbol{h}\cdot\boldsymbol{\sigma})_{ss'}c_{ks'} \\ &+ \frac{1}{2}\sum_{k\sigma\sigma'}\left(2i\sin(k)\Delta_{\sigma\sigma'}c^\dagger_{k\sigma}c^\dagger_{-k\sigma'} + \text{h.c.}\right),\end{aligned} \tag{3.2}$$

where ϵ_k is the Fourier transform of $W(i)-\mu$, especially we define $W(i) = -\delta_{1,|i|}t - \delta_{2,|i|}t' - \delta_{3,|i|}t''$, where t, t' and t'' are the nearest neighbour hopping strength, next nearest neighbour hopping strength and the third nearest neighbour hopping strength respectively. Thus ϵ_k is

$$\epsilon_k = -2t\cos(k) - 2t'\cos(2k) - 2t''\cos(3k) - \mu.$$

This Hamiltonian can be cast in tensor form by defining the Nambu spinor

$$\psi_k = (c_{k\uparrow},\ c_{k\downarrow},\ c_{-k\downarrow},\ -c_{-k\uparrow})^{\mathrm{T}},$$

which gives

$$\hat{H} = \frac{1}{2}\sum_k \psi^\dagger_k h_k \psi_k \tag{3.3}$$

$$h_k = \tau_z\epsilon_k - \boldsymbol{h}\cdot\boldsymbol{\sigma} + (\boldsymbol{d}_k\tau_+ + \boldsymbol{d}^*_k\tau_-)\cdot\boldsymbol{\sigma}. \tag{3.4}$$

with $\boldsymbol{d}_k = 2\sin(k)\boldsymbol{d}$. Notice that the hole part of the Nambu spinor has been multiplied by the operator $-i\sigma_y$, which simplifies the tensor form of the Hamiltonian. Here the superconducting OPs are defined in terms of the d-vector as $\Delta_{\uparrow\uparrow,\downarrow\downarrow} = \frac{\Delta_{\uparrow\uparrow,\downarrow\downarrow}(k)}{2i\sin(k)} = \pm id_x + d_y$ and $\Delta_{\uparrow\downarrow} = -id_z$. Provided that $h_x = 0$ and $d_x = -d^*_x$, $d_y = d^*_y$, $h_z = h^*_z$, the Hamiltonian satisfies the symmetries in eq. (2.59) with

$$\mathcal{T} = \tau_z\sigma_z K \qquad \mathcal{C} = \tau_y\sigma_y K \qquad \mathcal{S} = \tau_x\sigma_x.$$

Furthermore, the PH and TR symmetries square to +1. Reading from table 2.1, we see that this Hamiltonian belongs to the BDI class, and in 1D we expect it to have a $\mathbb{Z}$ number, which in this case is a winding number. One way to obtain the winding number is to rotate the Hamiltonian into the basis where the chiral operator is diagonal,

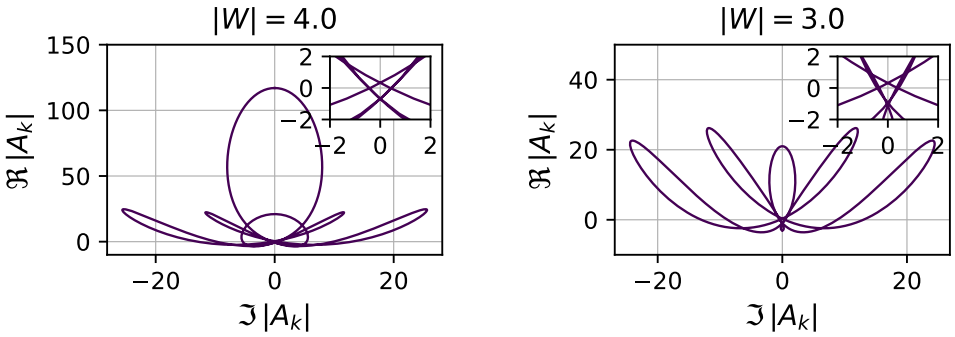

Figure 3.1: Curves of $\det A_k$ in the complex plane parameterised by k in the 1BZ. The insets in the figures shows a small area around the origin to clearly show that they go around it. The common parameters between the two subfigures were $\hat{\Delta} = (2.2, 0, 0.18)t$, $h = 2t$, $\theta = \pi/4$ and ($\mu = t' = t$, while in **(a)** the third nearest neighbour hopping strength was $t'' = 3$, and in **(b)** the third nearest hopping strength was $t'' = -2$.

$\mathcal{S} = \mathrm{diag}(-1, -1, 1, 1)$, with the basis transformation U. Rotating the Hamiltonian into the basis of the eigenvectors of the chiral symmetry operator, that is

$$H \to H' = U^\dagger H U \qquad\qquad U^\dagger \mathcal{S} U = \mathrm{diag}(-1, -1, 1, 1),$$

we get a block off-diagonal matrix

$$H = \begin{pmatrix} 0 & A_k \\ A_k^\dagger & 0 \end{pmatrix}, \tag{3.5}$$

with

$$A_k = \begin{pmatrix} 2i\Delta_{\uparrow\uparrow}\sin(k) - \epsilon_k + h_z & -ih_y \\ -ih_y & 2i\Delta_{\downarrow\downarrow}\sin(k) + \epsilon_k + h_z \end{pmatrix} \tag{3.6}$$

3.1.2 The phase diagram

The next step is to compute the determinant of A_k, and define the winding as the number of times the determinant winds around the origin in the complex plane as the parameter k traverses the first Brillouin zone. We repeat the winding integral first given in the nomenclature, which is

$$W = \frac{1}{2\pi i}\int \mathrm{d}k \frac{\mathrm{d}_k |A_k|}{|A_k|}, \tag{3.7}$$

where the integral is parameterised by the wavenumber k. In contrast with the 1D spinless Kitaev model on the chain, the winding number in this model can vary between -4 and 4, and a phase change can be accompanied by a difference in winding number being

- even, for band gap closing at $k \neq -k$, or
- odd or even, for energy gap closing at $k = -k$.

The latter case is in general odd, but can be even in the case that $k = 0$ and $k = \pi$ closings happen simultaneously. The reason for why the winding number changes with an even

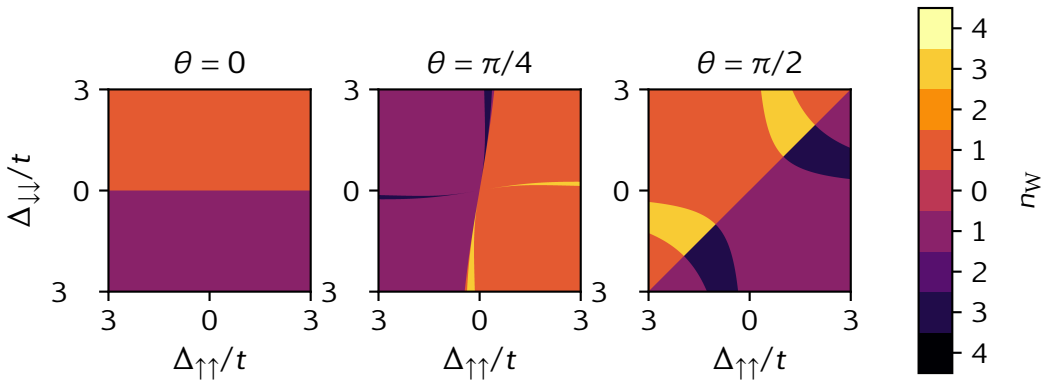

Figure 3.2: Phase diagram in $\Delta_{\uparrow\uparrow,\downarrow\downarrow}$-space for $\mu = t' = t$, $t'' = -2t$, $h = 2t$ and $\theta = 0$, $\theta = \pi/4$ $\theta = \pi/2$ for left, middle and right subfigure respectively. As explained in the text, the parameters Δ are not able to change the parity of the winding number because their contribution vanish at $k = 0, \pi$.

number for gap closings at $k \neq -k$ is similar as to the argument used in section 2.5: TR symmetry and chiral symmetry dictates that when the Pfaffian of the matrix at k changes sign, so to does the Pfaffian at $-k$. That is, in the BdG formalism with chiral symmetry all energy crossings at $k \neq -k$ happens in groups of 4.

What is interesting to note about the last item in the list above is that the $\hat{\Delta}$ contribution at $k = -k$ is zero because of the sine factor. Thus for any set of the other parameters, no amount of change in the superconducting OPs can change the parity of the winding number. Examples of two phases with different winding number parity is shown in fig. 3.1. What is not shown in the figures is that $k = 0$ and $k = \pi$ are located at the tops of the 'flower buds'. The only difference between the two subfigures is the value of t'', which removes one of the 'flower buds', but leaves the overall shape of the 'leaves' intact. For instance, the variable t'' can change the parity of the winding number.

As the absolute value of the winding number encodes the number of Majorana fermions at each edge, the parity of the winding number is an important value as it decides whether there are single Majorana fermions at the edges or if all can be paired in Majorana doublets. If some local symmetry breaking perturbation at the edges couple Majoranas to each other, they will split in energy. The difference between an odd and even parity winding number therefore decides if there still exist an unbound Majorana fermion at the edge. If the number of Majoranas is odd, then there will be at least one Majorana left on each edge, whereas in the case of an even number of Majoranas, no such statement can be given. This can be deduced from the fact that any skew-symmetric $N \times N$ has a Pfaffian of 0 when N is odd. Since the effective perturbation Hamiltonian between the Majoranas at the edge has $N = |W|$, there exist at least one unbound Majorana after the local perturbation is added.

The resulting phase diagram defined by the winding number is quite complex, being a function of the parameters in the Hamiltonian. The phase diagram in $\Delta_{\uparrow\uparrow}\Delta_{\downarrow\downarrow}$-space is given for one set of parameters in fig. 3.2 and for another set in fig. 3.3. An interesting difference between the two phase diagrams is that the first has solely odd winding numbers, whereas the latter has solely even winding numbers due to the vanishing superconducting OP at time reversal invariant momenta. Mercaldo, Cuoco and Kotetes (2016) showed that if one lets the superconducting OP reorganise inside the su-

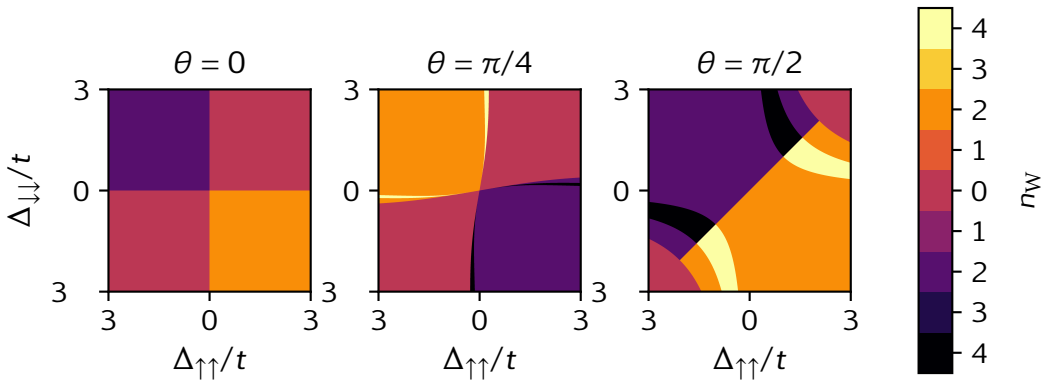

Figure 3.3: Phase diagram in $\Delta_{\uparrow\uparrow,\downarrow\downarrow}$-space for $\mu = t' = t$, $t'' = 3t$, $h = 2t$ and $\theta = 0$, $\theta = \pi/4$ $\theta = \pi/2$ for left, middle and right subfigure respectively. As explained in the text, the parameters Δ are not able to change the parity of the winding number because their contribution vanish at $k = 0, \pi$.

perconductor as a response to the applied magnetic field, the conventional bulk boundary correspondence does straightforwardly apply because the states at the boundary can change the order parameter in the inner side of the superconductor, this leading to topological transition without gap closing. For now, we will assume that reorganisation effects are negligible, thereby not solve the Hamiltonian self consistently. There are multiple ways one can reason that this is an admissible assumption. One way to reason about this is that many proposed 1D Kitaev like systems capable of harbouring Majorana fermions rely on depositing chains of metal with the necessary properties on top of a 2D or 3D superconductor due to the inefficiency of 1D systems to be superconducting on their own. Thus the general idea is that the Cooper pairs in the superconductor diffuse into the 1D chains by means of the proximity effect, thereby making the chain superconducting also. Since the superconducting OP in the chain is to a large degree dominated by the extrinsic OP, one can argue that the competition between the bulk and boundary of the chain has little effects on the total OP, and we can assume that they are given and constant for the time being. This does not apply to all systems, but is assumed here for simplicity.

3.1.3 Marginal topological behaviour

Under certain conditions, the p-wave superconductor in a ferromagnetic field can be gapless for an extended range of parameters. Furthermore, this gaplessness can be removed by perturbing the system in a way which opens the gap. When the gap is opened from the gapless state, the system may end up in a topological state in which the gap opening localizes the state(s) at the edge, thus giving MBSs. We are interested in finding such possibilities for the system. Since the winding number determines the topology of the Hamiltonian, we already know that whenever the winding number changes the gap has to close. One way to ensure that the determinant is zero is by enforcing the imaginary part to be zero. Then we only have to care about the real part. Computing the determinant of A_k (eq. (3.5), we get

$$\begin{aligned}\mathfrak{Re}|A_k| &= h_z^2 + h_y^2 - 4\sin^2(k)|\Delta_{\uparrow\uparrow}\Delta_{\downarrow\downarrow}| - \epsilon_k^2 \\ \mathfrak{Im}|A_k| &= 2\sin(k)\Big[h_z(\Delta_{\uparrow\uparrow} + \Delta_{\downarrow\downarrow}) + \epsilon_k(\Delta_{\uparrow\uparrow} - \Delta_{\downarrow\downarrow})\Big] = 4\sin(k)\Big[h_z d_y + i\epsilon_k d_x\Big]\end{aligned}$$

Looking at the equations above, we see that we can ensure that the imaginary part is zero by setting $h_z = 0$ and $d_x = \frac{\Delta_{\uparrow\uparrow} - \Delta_{\downarrow\downarrow}}{2i} = 0$. This simultaneously gives us a tool to open the gap by externally perturbing the system. One can either apply an out of plane magnetic field h_z, or alternatively alter the superconducting OP. The first method is probably the simplest experimentally. As explained previously, the superconducting OP are not able to change the parity of the winding number at all. This means that if the parity is odd, and the gap at $k = -k$ is far from being zero, we are guaranteed that the system is in a marginal topological phase. Looking at fig. 3.2, we see that the line $\Delta_{\uparrow\uparrow} = \Delta_{\downarrow\downarrow}$ differentiates between topological phases for all OP combinations along that line. Thus any system along that line is a marginal topological superconductor. One way to guarantee that the system enters a topological state when we open the gap is by ensuring that the topological constant

$$M = \operatorname{sign} \mathfrak{Re}|A_0| \cdot \mathfrak{Re}|A_\pi|, \tag{3.8}$$

$$= \operatorname{sign}\left[(-\epsilon_0^2 + |h|^2)(-\epsilon_\pi^2 + |h|^2)\right] \tag{3.9}$$

is negative. Since $\mathfrak{Im}|A_k|$ is odd in k, whereas $\mathfrak{Re}|A_k|$ is even, the system is forced to have an odd winding number (except in the gapless case where it is ill defined). Thus, as long as the perturbation does not change the sign of $|A_k|$ at either time reversal invariant points, the gap opening immediately brings the system into a topological phase. An example is shown in fig. 3.4 where the gap is opened by an out-of-plane magnetic field along the z-direction. The figure consists of fig. 3.4a which shows the first 50 excited and occupied energy bands for an open boundary system, clearly showing that as the gap is gradually opened by the out-of-plane magnetic field, the bulk energy bands gaps out, while a single state is left at zero energy, which according to fig. 3.4b becomes increasingly localised at the boundaries as the magnetic field is increased. Even for a relatively small value of $h_z = 0.01t$ (purple), the decay length of the Majorana density function into the bulk is the order of 100 lattice sites. When the out-of-plane field is increased to $0.1t$, the decay length is even shorter, being about the order of only tens of lattice sites.

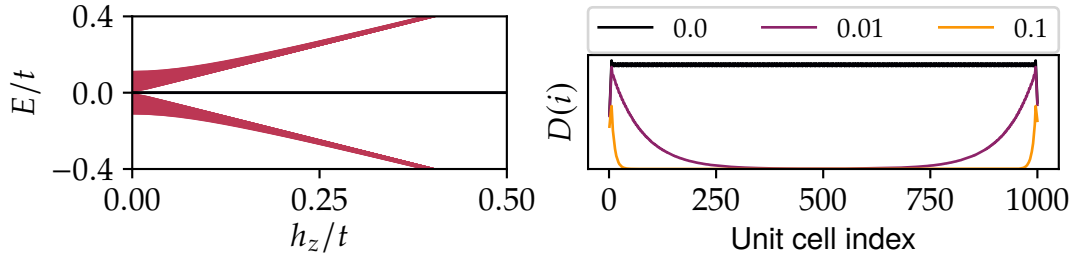

(a) Energy bands for open boundary system of 1000 lattice sites as function of the perturbation h_z.

(b) Probability distribution of first excited states. The lines are given by the moving average with a window width of ten lattice sites.

Figure 3.4: Marginal topological system with only nearest neighbour hopping. The parameters used relative to t was $t' = t'' = 0$, $\mu = 1$, $h_y = 2$, $d_y = 1.3$, $d_x = 0$ and h_z as given in the figures.

Instead of applying an out-of-plane magnetic field as in fig. 3.4, we can change the OP by adding a d_x component. This is experimentally harder to do, but we show the results to highlight that this is a possible way to open the gap. In the following we use

the same values as in the last example, but perturb the OP instead of the out-of-plane magnetic field. We hypothesise that if this perturbation is able to open the gap, then the system will be topological with an odd winding number since the other case was odd. We already know that adding a d_x component will add an imaginary part to the determinant $|A_k|$. This is clearly shown in fig. 3.5b where the winding curve is initially flat against the real axis, but as soon as the perturbation is applied the imaginary part becomes non-zero (red and orange curves). As seen in fig. 3.5a, the bulk band gap (red) is opened when the d_x component is increased from 0. In addition, the system goes into a topological phase, as indicated by the presence of the zero energy state for a range of values of d_x. When the d_x component reaches approximately $0.6t$, the gap closes again at some $k \neq -k$. However, although the gap closes, the system is still in a topological phase when the gap reopens, with a winding number of $|w| = 1$, except that the sign changed. This band gap closing is due to the point where the curve (fig. 3.5b) intersects it self going through the origin. In this process, the winding direction of the curve changes.

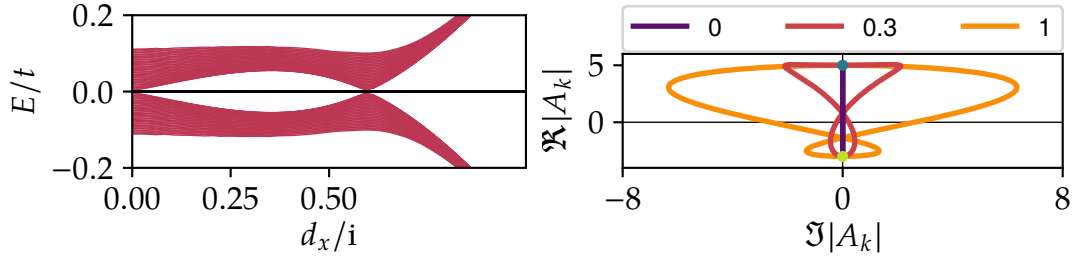

(a) Energy bands for open boundary system of 1000 lattice sites as function of the perturbation d_x.

(b) Winding curves for different values of d_x/i.

Figure 3.5: Marginal topological superconductivity by varying d_x. The parameters used relative to t was $t' = t'' = 0$, $\mu = 1$, $h_y = 2$, $h_z = 0$, $d_y = 1.3$ and d_x as given in the figures.

In fig. 3.6 we show a case where the system can be marginally topological when perturbed in one variable, but be marginally trivial when perturbed in another. The reason for this is that the variable $\mathcal{M}$ given in eq. (3.8) is positive in the case considered, which means that the winding number can only be even as long as the gap stays open at time reversal invariant k, i.e. $k = -k$. The evenness of the winding number does include zero as a possibility, which is the actual winding number that is achieved when the gap is opened by applying an out of plane magnetic field, h_z (going from **(c)** to **(d)** in fig. 3.6). This is in contrast to the case when the gap is opened by adding a non-zero d_x component (arrow in fig. 3.6**(c)**), which achieves a winding of $|w| = 4$, depending on the sign of d_x. This difference in the topological phase in the perturbations can be explained by looking at paths that $|A_k|$ takes in the complex plane in each case. As seen in figs. 3.6a and 3.6b, the shapes of the curves are qualitatively different in each of the cases, which is due to a difference in the dependence of the imaginary part on the perturbations, whereas the effects of the perturbations on the real part are negligible in the limit of small perturbations. In fig. 3.7 the open boundary energy bands are shown as a function of the d_x component, which is moving along the arrow in section 3.1.3. This is located at a marginal point with a marginal winding number of $|n_W| = 4$, meaning there are four MBS when we open the gap. Close to the marginal point, the MBS can be seen to interact significantly with each other leading to them gapping a little, and

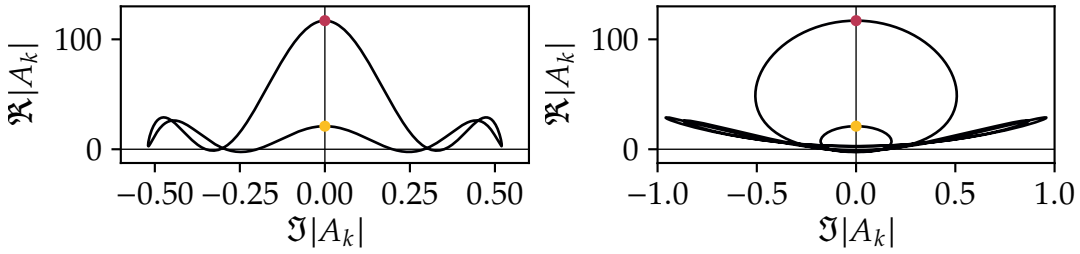

(a) Winding curve for $h_z = 0.1t$. **(b)** Winding curve for $d_x/i = -0.05t$.

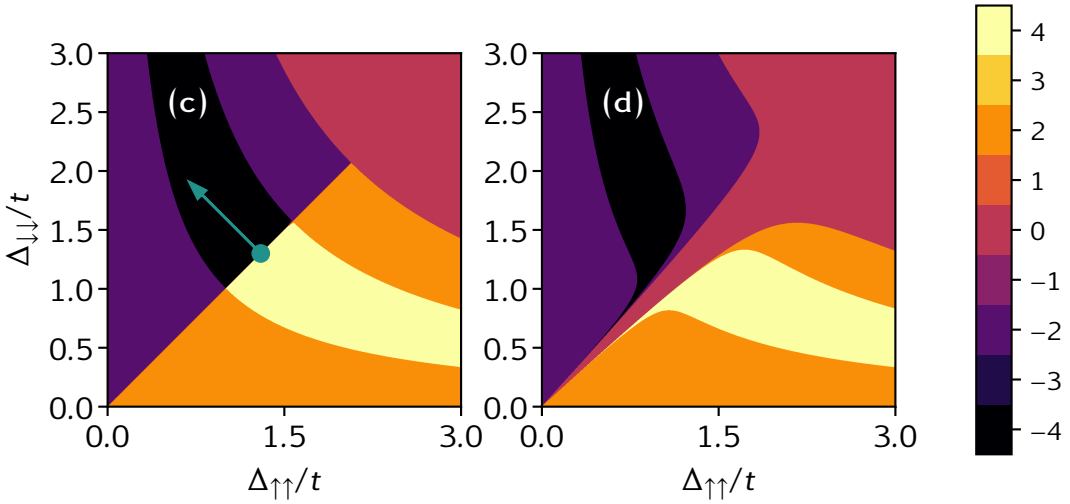

(c) and (d) Phase diagram for **(c)** $h_z = 0$ and **(d)** $h_z = 0.1t$. The colors indicate the winding number (colorbar). The point shows the point in phase space that is perturbed, lying between two topologically nontrivial phases, and the arrow points in the direction of d_x change.

Figure 3.6: The superconductor can be marginal topological in one variable and trivial in another. When $\mathcal{M}$ is positive, the marginal topological nature of the system depends on the form the parametric curve $|A_k|$ takes when the system is perturbed. Here, the system is marginally topological in one variable (d_x) and switched between winding numbers 4 and -4, but is trivial in another (h_z). The reason for the trivial nature of the perturbation h_z can be seen in the transition from **(c)** to **(d)**, where the trivial area extends into the marginal topological area. in the phase diagram. The parameters used were $t' = t$, $t'' = 3t$, $\mu = 1.0t$, $h_y = 0$, $d_y = 1.3$; and $h_z = 0$ and $d_x = 0$ unless stated otherwise.

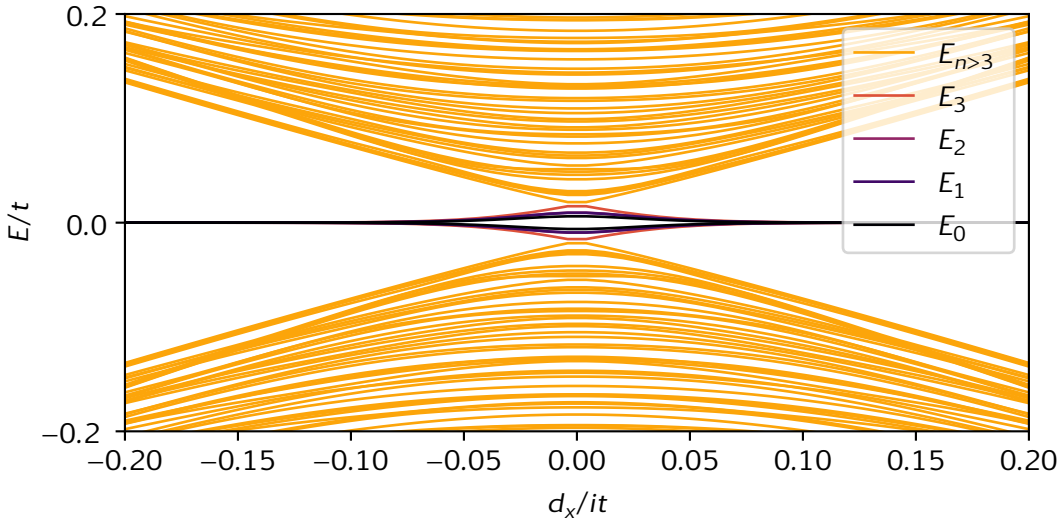

Figure 3.7: Open boundary energy bands as a function of d_x for the parameters in section 3.1.3.

becoming extended states.

From the observations above, we note the following: When the constant $\mathcal{M}$ is positive, the winding number is always even. This depends on the assumption that the determinant $|A_k| = |A_{-k}|^*$. When this is the case, we can cut the curve of $|A_k|$ in two by cutting at $k = 0$ and $k = \pi$. Looking at each curve separately, it has to start and end at the same side of the origin on the real axis, and as a result has half-integer winding numbers each. This means that each half has an integer winding number, and since there are two, the winding number of the total curve can only be even. A similar geometrical argument applies to the case when $\mathcal{M} = -1$, where each of the points are on opposite sides of the origin on the real axis. We speculate whether the constant $\mathcal{M}$, which is computed at time reversal invariant momentum $k = -k$ is linked to the product of the Pfaffians of the Hamiltonian at these two momenta or not. If this is the case, then it is no surprise that a negative $\mathcal{M}$ always gives a marginal topological state. The fact that a gapless superconductor with a positive $\mathcal{M}$ can be marginally topological and trivial at the same time implies that the topological nature of gapless systems is not as robust as when the parity of the winding number is odd, in which case *any* gap opening (and symmetry conserving) perturbation pushed the system into a topological phase. When $\mathcal{M}$ is positive, we can only say for sure that the winding number is even, but it is harder to state whether the winding number is zero or non-zero. To do this, one must evaluate the exact dependence of the imaginary and real part of the determinant $|A_k|$, in which case it is equally simple to just evaluate the winding number numerically by applying an infinitesimal perturbation in the parameter of interest.

3.2 p-wave superconductivity in coexistence with AFM ordering

The next type of topological superconductor we investigate is the p-wave superconductor in proximity to an antiferromagnetic chain. This type of system was investigated by Mercaldo, Kotetes and Cuoco (2018), and we firstly recreate the phase diagram and then expand the model to investigate possible marginal topological phases in these types of systems. Their model is also expanded to include a ferromagnetic exchange field, which further allows the control of the topological phases, as antiferromagnetic exchange field are in general harder to control or to impinge on a specimen.

3.2.1 Model definition

Let a one dimensional intrinsic p-wave superconductor with a coexisting antiferromagnetic (AFM) field be given by the Hamiltonian in lattice space

$$\begin{aligned}\hat{H} = -t\sum_{i\sigma}\left(c^\dagger_{\mathrm{A}i\sigma}c_{\mathrm{B},i+1,\sigma} + c^\dagger_{\mathrm{A}i\sigma}c_{\mathrm{B},i,\sigma} + \mathrm{h.c.}\right) \\ + \sum_{i\alpha ss'}(-\mu\sigma^0_{ss'} - \rho^z_{\alpha\alpha}\boldsymbol{M}\cdot\boldsymbol{\sigma}_{ss'} - \boldsymbol{h}\cdot\boldsymbol{\sigma}_{ss'})c^\dagger_{\alpha is}c_{\alpha is'} \\ + \sum_{i\sigma\sigma'}\left[\Delta_{\sigma\sigma'}\left(c^\dagger_{\mathrm{A}i\sigma}c^\dagger_{\mathrm{B},i+1,\sigma'} + c^\dagger_{\mathrm{B}i\sigma}c^\dagger_{\mathrm{A}i,\sigma'}\right) + \mathrm{h.c.}\right]. \quad (3.10)\end{aligned}$$

Here the subscripts A and B denote two sublattices with corresponding operators, with the mapping

$$c_{\mathrm{A}i\sigma} = c_{2i,\sigma} \qquad\qquad c_{\mathrm{B}i\sigma} = c_{2i-1,\sigma}.$$

in terms of the original fermion lattice operators. The parameters are as before, with an additional antiferromagnetic OP, $\boldsymbol{M}$. Since there are two sublattices, we introduce the sublattice space and accompanying Pauli operators, ρ, which operate in this space. We introduce the Fourier transformed fermion operators by

$$c_{\mathrm{A}i\sigma} = \frac{1}{N_\mathrm{A}}\sum_k e^{2iki}c_{\mathrm{A}k\sigma} \qquad\qquad c_{\mathrm{B}i\sigma} = \frac{1}{N_\mathrm{B}}\sum_k e^{2iki}c_{\mathrm{B}k\sigma}, \quad (3.11)$$

where the factor two in the exponent comes from the fact that each sublattice has twice as big lattice constant as the original. There are equal numbers of lattice site in each sublattice, so we set $N_\mathrm{A} = N_\mathrm{B} \equiv N$. In addition, the Brillouin zones are reduced to $k = \frac{m\pi}{N}$ with $m \in [-\frac{N}{2}, \frac{N}{2}]$. Inserted into eq. (3.10) we get

$$\begin{aligned}\hat{H} = -2t\sum_{k\sigma}\cos(k)\left(c^\dagger_{\mathrm{A}k\sigma}c_{\mathrm{B}k\sigma}e^{ik} + c^\dagger_{\mathrm{B}k\sigma}c_{\mathrm{A}k\sigma}e^{-ik}\right) \\ + \sum_{\alpha k\sigma}(-\mu\sigma^0_{ss'} - \rho^z_{\alpha\alpha}\boldsymbol{M}\cdot\boldsymbol{\sigma}_{ss'} - \boldsymbol{h}\cdot\boldsymbol{\sigma}_{ss'})c^\dagger_{\alpha ks}c_{\alpha ks} \\ + \sum_{kss'}\left[2i\sin(k)\Delta_{ss'}\left(e^{ik}c^\dagger_{\mathrm{A}ks}c^\dagger_{\mathrm{B}-ks'} + e^{-ik}c^\dagger_{\mathrm{B}ks}c^\dagger_{\mathrm{A}-ks'}\right) + \mathrm{h.c.}\right]. \quad (3.12)\end{aligned}$$

Defining the column vector

$$\hat{\psi}_k = (c_{\mathrm{A}k\uparrow}, c_{\mathrm{A}k\downarrow}, c_{\mathrm{B}k\uparrow}, c_{\mathrm{B}k\downarrow}, c^\dagger_{\mathrm{A}-k\downarrow}, -c^\dagger_{\mathrm{A}-k\uparrow}, c^\dagger_{\mathrm{B}-k\downarrow}, -c^\dagger_{\mathrm{B}-k\uparrow})^\mathrm{T}, \quad (3.13)$$

we write the BdG Hamiltonian as

$$\hat{H} = \sum_k \hat{\psi}^\dagger h_k \hat{\psi} \tag{3.14}$$

with

$$h_k = -\mu\tau_z - 2t\cos(k)\tau_z\rho_x e^{-ik\rho_z} - \rho_z \boldsymbol{M}\cdot\boldsymbol{\sigma} - \boldsymbol{h}\cdot\boldsymbol{\sigma} + \rho_x e^{-ik\rho_z}(\boldsymbol{d}_k\tau_+ + \boldsymbol{d}_k^*\tau_-)\cdot\boldsymbol{\sigma} \tag{3.15}$$

being a 8×8 matrix. Here it is understood that τ, ρ and σ operate in particle-hole space, sublattice space and spin space respectively. Furthermore this definition means that the OPs are defined as $\Delta_{\uparrow\uparrow,\downarrow\downarrow} = d_y \pm i d_x$ and $\Delta_{\uparrow\downarrow} = -i d_z$. The hole part of eq. (3.13) is transformed by $-i\sigma_y$ to simplify the tensor notation. Provided that $\boldsymbol{M}$ lies in the yz-plane and $\boldsymbol{d}$ lies in the xy-plane, that is

$$\boldsymbol{d} = |d|(i\cos\alpha, \sin\alpha, 0) \qquad \boldsymbol{M} = |M|(0, \sin\theta, \cos\theta) \qquad \boldsymbol{h} = |h|(0, \sin\phi, \cos\phi), \tag{3.16}$$

it can be shown that the Hamiltonian above has the symmetries $\hat{\mathscr{T}}^2 = +1$, $\hat{\mathscr{C}}^2 = +1$ and $\hat{\mathscr{S}}$ given in first quantised form by

$$\mathcal{T} = -\tau_z\sigma_z K \tag{3.17}$$

$$\mathcal{P} = \tau_y\sigma_y K \tag{3.18}$$

$$\mathcal{S} = \tau_x\sigma_x \tag{3.19}$$

Followingly, the system belong to the class BDI (table 2.1) for this restraint and should have a $\mathbb{Z}$ topological quantum number.

As explained in section 2.3.3, the chiral symmetry means that the Hamiltonian can be written in block off-diagonal form, by sandwiching it between the eigenvector matrix V of the chiral operator, defined by $V^{\mathrm{T}}\mathcal{S}V = \mathrm{diag}(\pm 1)$,

$$V^{\mathrm{T}} h_k V = \begin{pmatrix} 0 & A_k \\ A_k^\dagger & 0 \end{pmatrix},$$

which allows us to define a Winding number on the determinant of either off-diagonal block,

$$W = \frac{1}{2\pi i}\int_{k=0}^{\pi} \frac{\mathrm{d}(\det(A_k))}{\det(A_k)}. \tag{3.20}$$

The winding number for the bulk of this system depends on both the angle θ and α, and the resulting phase diagram for this system as first obtained in Mercaldo, Kotetes and Cuoco (2018) was recreated and is given in fig. 3.8. The phase diagram is plotted in terms of the superconducting OPs Δ. The phase diagram for this set of parameters has areas of both odd and even winding numbers, and can either be trivial (0) or topological (1 and 2 MBSs). As the figure shows, when the magnetisation axis points considerably in the y-direction, the areas with odd winding numbers inside the visible region disappears, somewhere between $\theta = \pi/5$ and $\theta = 3\pi/10$. In the first figure, when the magnetisation axis is parallel with the z-axis, the topological phase boundaries are straight lines, and there are two areas of trivial topology in the first and third quadrant. However, in this case with no h_y component, the system has an additional unitary symmetry:

$$\sigma_z\tau_z : h_k \to h_k.$$

This has the consequence that although the winding number is trivial in the basis as used here, if the additional symmetry is used to block diagonalise the Hamiltonian

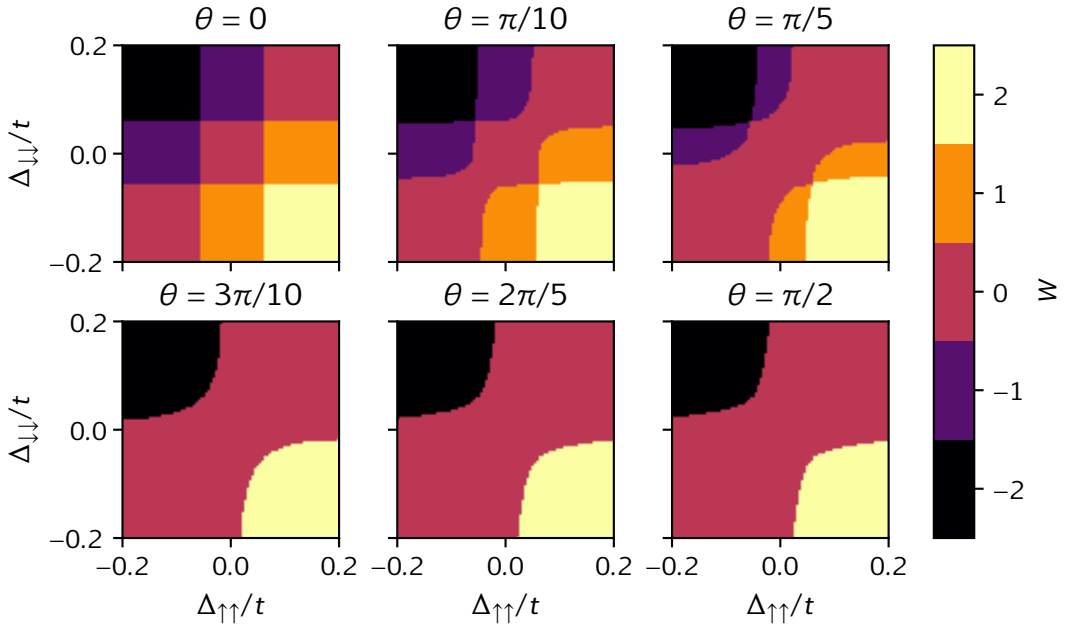

Figure 3.8: The topological phase diagram for $|M| = 0.15t$, $\mu = 0.1t$.

each block may have a topological invariant, but when they are considered together as here, they appear trivial. This is a general consideration in topological analysis, as a symmetrie can change the AZ class. But we do not analyse this case further in this thesis, as it is not relevant for the main points.

3.2.2 Marginal topological behaviour

Again, we look for the case when the imaginary part of the determinant of the off-diagonal part of the Hamiltonian, $\mathrm{Im}|A_k|$, is 0 for all values of k. The imaginary part is

$$8t\sin(2k)\Big[\mathrm{Im}(d_x)\Big(-\boldsymbol{h}^2+\boldsymbol{M}^2-\mu^2+4\sin^2(k)(d_y^2-\mathrm{Im}(d_x)^2)+4t^2\cos^2(k)\Big)-2h_z\mu d_y\Big] \tag{3.21}$$

A simple way to make this zero for all k is by having $d_x = 0$ and $h_z = 0$.

The first case we investigate is when there is only an antiferromagnetic exchange field. First we look at the determinant at $k = 0$ and $k = \pi/2$ with $d_x = h_z = 0$. At these points the real part of the determinant is

$$-(M_y^2+M_z^2-\mu^2+4)^2 \le 0, \qquad k = 0, \text{ and} \tag{3.22}$$

$$-\left|M_y^2+4iM_yd_y+M_z^2-\mu^2-4d_y^2\right|^2 \le 0, \qquad k = \pi/2. \tag{3.23}$$

Both of the points are located on the negative side of the real axis, except when the chemical potential is fine-tuned to the antiferromagnetic order parameter and the superconducting order parameter. As a consequence, the winding number can only be even. We were not able to find combinations of the parameters where the system was marginal topological in this configuration, yet we can not conclude that there is no marginal region in the pure antiferromagnetic system.

When a ferromagnetic field is present in the system in addition to the antiferromagnetic field, the exchange field is either ferrimagnetic when they are parallel or a SDW.

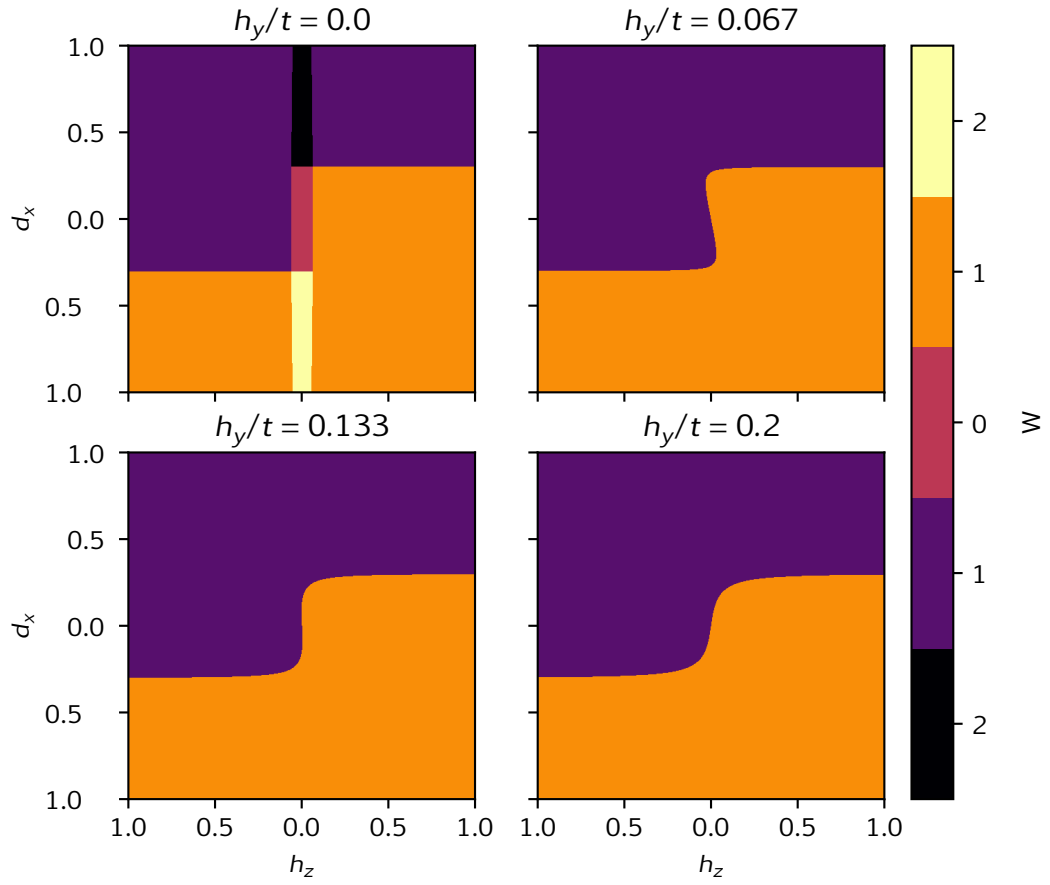

tbh

Figure 3.9: Phase diagram in $d_x h_z$-space varying h_y. The parameters were $\mu = -2t$, $d_y = 0.3t$ and $\boldsymbol{M} = 0.5t\hat{\boldsymbol{z}}$

In this case there are regions in the phase diagram which are marginal in the superconducting order parameter and in the z-component of the ferromagnetic exchange field. This should be no surprise, as in the limit of a zero antiferromagnetic order parameter we are back to the normal ferromagnetic case which was considered in the previous section, so we expect there to be intermediate regions between the fully antiferromagnetic system and the fully ferromagnetic system. Figure 3.9 shows the phase diagram around the origin in $h_z d_x$-space for various values of h_y. At zero ferromagnetic field (upper left) the origin is inside an area of trivial topology, so infinitesimal perturbations around this point will not bring the system into a topological phase. However, when the ferromagnetic order parameter is large enough, the area of trivial topology is suppressed and the system is a marginal topological superconductor for $h_z = d_x = 0$, surrounded by winding numbers with absolute value of 1. An interesting effect of increasing the h_y strength is that the sign of the winding number as a function of h_z switches as the boundary between the +1 and −1 phase rotates close to the origin.

Although an intrinsic p-wave superconductor proximised to an antiferromagnet can not be a marginal topological superconductor, it may open up paths to realise such systems, as external exchange fields can be used to push the system into a gapless region and can be easily used to control the topological invariant of the system by rotating the exchange field which quickly localises the MBSs.

3.3 s-wave superconductor in an inhomogeneous magnetic field

When a s-wave superconductor is combined with a semiconductor having SOC in a Zeeman field, the Hamiltonian can for some ranges of the parameters be modelled as an effective p-wave or p-wave like superconductor (Sato, Takahashi & Fujimoto, 2010), which can exhibit MBS (Alicea et al., 2011; Lutchyn et al., 2010), and have also been measured experimentally (Deng et al., 2012; E. J. H. Lee et al., 2014; Mourik et al., 2012). Alternatively, MBS can be obtained in systems consisting of an inhomogeneous Zeeman field impinged on a superconductor (Chen & Schnyder, 2015; Choy, Edge, Akhmerov & Beenakker, 2011; Klinovaja & Loss, 2013; Klinovaja, Stano & Loss, 2012; Marra & Cuoco, 2017; Nadj-Perge et al., 2013; Sedlmayr et al., 2015).

In this section we analyse the topological phase diagram of a s-wave superconductor in an inhomogeneous and noncollinear exchange field with a focus on marginal topology. Since s-wave superconductors are more abundant than the intrinsic p-wave superconductors, the results from this section can potentially lead to yet another path to marginal topology which is easier to design in experiments.

An extensively researched example of noncollinear exchange fields in s-wave superconductors is that of the helical exchange field, which is equivalent to a semiconductor with Rashba SOC in a ferromagnetic field. These systems can be unitarily transformed to each other by doing local spin-rotations. The first type of system is an effective way of obtaining strong SOC fields which can be comparable to the energy bandwidth. We chose to look at systems with translational symmetry, consisting of unit cells of a general number of lattice sites. The exchange field vectors in the unit cell are in general independent of each other and lie in the same plane, thus not breaking the chiral symmetry. Again, we do not solve the superconducting order parameter self-consistently and do not look at the free energy to compare the stability of the superconducting phase against the normal phase. This work has been done by for example Nadj-Perge et al. (2013), who showed that these types of system can be self consistent. However, self consistency is a natural next step to the analysis in this section.

3.3.1 Model

The general model we consider in this chapter is given by the tight binding Hamiltonian

$$\begin{aligned}\hat{H} = &- t \sum_{\langle ij\rangle\sigma} c^\dagger_{i\sigma} c_{j\sigma} - \mu \sum_{i\sigma} c^\dagger_{i\sigma} c_{i\sigma} \\ &- \sum_{iss'} c^\dagger_{is} \left(\boldsymbol{h}_i \cdot \boldsymbol{\sigma}_{ss'}\right) c_{is'} + \sum_i \left(\Delta_0 c^\dagger_{i\uparrow} c^\dagger_{i\downarrow} + \text{h.c.}\right).\end{aligned} \tag{3.24}$$

This Hamiltonian describes a superconductor at chemical potential μ with nearest neighbour hopping strength t, a varying Zeeman field h_i at lattice site i, and s-wave superconducting OP, $\Delta_0 \equiv \Delta_{\uparrow\downarrow}$, which is assumed to be a constant exogenous variable in the model. For now, we only impose the requirement on h_i that it lies in the xy-plane, in which case the model has a global chiral symmetry. This plane is arbitrarily chosen, so the results apply to any plane. Since the model is superconducting, it also has particle-hole symmetry, which means that it also must have TR symmetry. The symmetry operators are given by

$$\mathcal{T} = \tau_z \sigma_x K \qquad \mathcal{C} = \tau_x K \qquad \mathcal{S} = \tau_y \sigma_x. \tag{3.25}$$

These operators are only valid as long as the superconducting OP is real, which always can be achieved by a global $U(1)$ gauge transformation. All the symmetry operators in

eq. (3.25) square to one. Comparing this to table 2.1, we see that the system in question belongs to the topology class BDI, which can have a $\mathbb{Z}$ topological invariant.

3.3.2 Local spin rotation of the Hamiltonian

The Hamiltonian as given in eq. (3.24) can be transformed to a model with a collinear magnetic field. We can do a local spin rotation around the z-axis to align all the spins along one axis – in our case we choose the x-axis. If we define the angle the Zeeman field at lattice site i makes in the xy-plane as λ_i, the local rotation at this lattice site is

$$R_i = \exp\left\{-\frac{i(\lambda_i)\sigma_z}{2}\right\}. \tag{3.26}$$

This transformation aligns all local Zeeman fields along the positive x-axis,

$$R_i^\dagger \boldsymbol{h}_i \cdot \boldsymbol{\sigma} R_i = |h_i|\sigma_x.$$

Thus, in this new basis, the magnetic field is that of a SDW. An effect of the local rotations is that whenever to adjacent Zeeman fields are initially oriented in different directions (independent on the actual size of the fields), the previous 'normal' hopping parameter t between the to lattice sites is transformed to a combination of normal hopping and Rashba type SOC as follows,

$$t \to tR_j^\dagger R_i = t\Big(\cos\big(\delta\lambda_{j,i}/2\big)\sigma_0 + i\sin\big(\lambda_{j,i}/2\big)\sigma_z\Big)$$

Here the angle difference is $\delta\lambda_{j,i} = \lambda_j - \lambda_i$. The last two terms, the spin-independent chemical potential and the singlet OP transform trivially under this transformation. The resulting Hamiltonian is equivalent to that of a singlet s-wave superconductor in a collinear SDW field with a (modulated) Rashba spin-orbit coupling. We add a subscript, R, to the Hamiltonian to denote that the local transformation has been done,

$$\begin{aligned}\hat{H}_{\mathrm{R}} = &\sum_{\langle ij\rangle ss'} c_{js}^\dagger \left(t(j,i)\sigma_0 + i\alpha_R(j,i)\sigma_z\right)_{ss'} c_{is'} - \mu\sum_{is} c_{is}^\dagger c_{is} \\ &- \sum_{iss'} c_{is}^\dagger h_i(\sigma_x)_{ss'} c_{is'} + \sum_i \left(\Delta c_{i\uparrow}^\dagger c_{i\downarrow}^\dagger + \mathrm{h.c.}\right)\end{aligned} \tag{3.27}$$

3.3.3 Helical magnetic field

An important special case of the the model is when the local magnetic field is helical along the 1D wire, that is that the fields lie on a circle with a constant angle difference between the adjacent sites. Thus, the rotated Hamiltonian describes a superconductor with ferromagnetic field of strength h with hopping parameter $\tilde{t}\cos(\delta\lambda/2)$ and Rashba SOC strength $\alpha = t\sin(\delta\lambda/2)$. This system has been solved multiple times before by other authors (Alicea et al., 2011; Oreg, Refael & von Oppen, 2010; Sato et al., 2010), but in this context it is important to establish the connection between inhomogeneous magnetic fields and the collinear model with Rashba SOC. Furthermore, the results presented in this section will serve as a baseline for the other sections of this chapter.

The rotated system is translationally invariant, which implies that the momentum is a good quantum number and thus we do a Fourier transformation. The Fourier transformed Hamiltonian is then

$$H(k) = \begin{pmatrix} \epsilon_k\sigma_0 + \alpha_k\sigma_z - h\sigma_x & i|\Delta|\sigma_y \\ -i|\Delta|\sigma_y & -\epsilon_k\sigma_0 + \alpha_k\sigma_z + h\sigma_x \end{pmatrix}, \tag{3.28}$$

where $\epsilon_k = -2\tilde{t}\cos k - \mu$ and $\alpha_k = -2\alpha\sin(k)$. The basis is the regular Nambu spinors. Since the Hamiltonian has a chiral symmetry given by eq. (3.25), we can block off-diagonalise the matrix by rotating it into the basis in which the chiral operator is diag$(-1,-1,1,1)$. In this basis the Hamiltonian is

$$H(k) = \begin{pmatrix} 0 & A_k \\ A_k^\dagger & 0 \end{pmatrix}, \tag{3.29}$$

with

$$A_k = \begin{pmatrix} \alpha_k + i|\Delta| - \epsilon_k & h \\ h & -\alpha_k - i\Delta - \epsilon_k \end{pmatrix}. \tag{3.30}$$

The determinant of A_k is in general complex, and is thus a mapping from the torus T_1 to the circle S_1. As a consequence, we can define a winding number of this mapping as

$$n_W = \frac{1}{2\pi i}\int_k \frac{\mathrm{d}\,|A_k|}{|A_k|}. \tag{3.31}$$

This integral is only non-zero when the path that the determinant takes in the complex plane winds around the origin. Computing the determinant, we get

$$|A_k| = \epsilon_k^2 - h^2 - \alpha_k^2 + \Delta^2 - 2i\alpha_k\Delta. \tag{3.32}$$

The imaginary part can only be zero at $k = 0$ and $k = \pi$. Thus the path in the complex plane can only touch the origin at the point given by $k = 0$ or $k = \pi$. Followingly, only the real part is necessary to determine when the winding number is non-trivial. Inserting for $k = 0$ and $k = \pi$, we get the following two independent equations for when the gap is allowed to close

$$(2\tilde{t} + \mu)^2 + \Delta^2 = h^2 \quad \text{(gap closes at } k = 0) \tag{3.33}$$

$$(2\tilde{t} - \mu)^2 + \Delta^2 = h^2 \quad \text{(gap closes at } k = \pi) \tag{3.34}$$

What is interesting to note is that the topological phase diagram does not depend on the size of the Rashba SOC parameter at all, only on the Zeeman field strength, the band width and the superconducting gap parameter. However, the size of the spin orbit coupling affects the size of the bulk band gap which again affects the robustness of the MBSs against perturbations. This can be seen from the fact that the modulus of the determinant of A_k is the square root of the product of the eigenenergies of the Hamiltonian. Take for example a superconductor which is in the topologically nontrivial regime and let the SOC strength go towards 0. When the real part of the determinant is zero (which it must be at some point since the path winds around the origin), the modulus of the determinant is fully given by the size of the imaginary part at this point. Followingly, the smaller the SOC strength is, the smaller the bulk band gap is. Some of the same arguments applies to the size of the superconducting OP Δ. Although the phase diagram is dependent on Δ, it also affects the bulk band gap similar to SOC. The chemical potential decides where the band gap closes first as a function of the Zeeman field strength. If μ is negative then the bulk gap closes first at $k = 0$, and at $k = \pi$ when the chemical potential is positive. The interval of the topologically non-trivial regime is given by $\sqrt{(2|\tilde{t}| - |\mu|)^2 + \Delta^2} < h < \sqrt{2|\tilde{t}| + |\mu|)^2 + \Delta^2}$. We note that when the chemical potential is zero, the boundaries of the interval are equal and a topologically nontrival system is not possible.

We note that when the Rashba SOC strength is zero, the determinant of A_k is

$$\epsilon_k^2 - h^2 + \Delta_0^2.$$

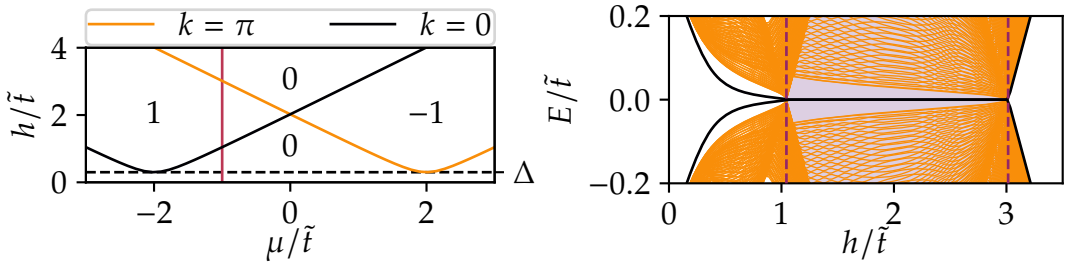

(a) Topological phase diagram for the helical case.

(b) Energy bands for the open boundary system as a function of h.

Figure 3.10: The topological phase diagram and the energy bands for an open boundary system are shown for the helical system. **(a)** The numbers in the figure denote the winding number, where 0 is a topologically trivial winding number. The lines were computed with eqs. (3.33) and (3.34). The phase diagram does not depend on α except for the case when $\alpha = 0$, in which case the system is trivial. **(b)** The energy bands for the open boundary system of 400 lattice sites as a function of the exchange field. The h-axis can be seen as following the red line in (a), with $\mu = -1\tilde{t}$ and $\Delta = 0.3\tilde{t}$.

From this we see that the smallest value of h which closes the gap is obtained when $\epsilon_k = 0$. When $-2|\tilde{t}| < \mu < 2|\tilde{t}|$, the smallest value is given by $|h_c| = |\Delta_0|$. This is of importance in chapter 4 when the chiral symmetry is broken.

3.3.4 Marginal topological superconductivity

In section 3.3.3 we explained that a superconductor in a ferromagnetic field has a band gap depending on the strength of the SOC. A non-zero SOC in the rotated Hamiltonian, which indicates inversion symmetry breaking, is equivalent to a non-collinear magnetic field in the original Hamiltonian. However, one question which arises is if a inversion symmetry breaking collinear field is enough to achieve a topological non-trivial phase. Since such a system has chiral symmetry, the winding number is a good topological number to classify the system by. We obtain a winding whenever the determinant of the off-diagonal matrix A_k winds around the origin. To do so, both the imaginary and real parts must be non-zero for at least some values of k and have positive and negative values as k goes from 0 to 2π. If either the real part or the imaginary part is constant zero in the reduced first Brillouin zone, the system can potentially be a marginal topological superconductor if it is gapless. Thus one way to analyse the system is to inspect the imaginary component of the determinant. The form the imaginary part takes depends on the size of the unit cell, and is increasingly complicated when the size of the unit cell increases. We therefore compute it for the first four unit cell sizes. We define the Hamiltonian as in eq. (3.24) where the spins have not been locally rotated, and where the magnetic field repeats it self after N_{Basis}. That means that the system is completely defined by the parameters μ, t, Δ and $\boldsymbol{h}_1, \ldots, \boldsymbol{h}_{N_{\text{Basis}}}$. The resulting expressions

for the imaginary part of the off-diagonal determinants are

$$\mathrm{Im}|A_k| = 0, \qquad N_{\mathrm{Basis}} = 1, \tag{3.35}$$

$$\mathrm{Im}|A_k| = 0, \qquad N_{\mathrm{Basis}} = 2, \tag{3.36}$$

$$\mathrm{Im}|A_k| = -4\Delta t^3 \sin(3k)|\boldsymbol{h}_1 \times \boldsymbol{h}_2 + \boldsymbol{h}_2 \times \boldsymbol{h}_3 + \boldsymbol{h}_3 \times \boldsymbol{h}_1|, \qquad N_{\mathrm{Basis}} = 3, \tag{3.37}$$

$$\mathrm{Im}|A_k| = 8\Delta\mu t^4 \sin(4k)|\boldsymbol{h}_1 \times \boldsymbol{h}_2 + \boldsymbol{h}_2 \times \boldsymbol{h}_3 + \boldsymbol{h}_3 \times \boldsymbol{h}_4 + \boldsymbol{h}_4 \times \boldsymbol{h}_1|, \qquad N_{\mathrm{Basis}} = 4. \tag{3.38}$$

After that, when the unit cell size increased the expression becomes even more complicated, where in addition to the cross products, terms like $h_i^x h_l^x h_k^x h_l^y$ appear. Thus analytically solving for the imaginary part becomes increasingly hard and gives little insight. We see from eqs. (3.35) and (3.36) that systems with a unit cells of at most two lattice sites can never be topologically non-trivial since they are not able to have a non-zero winding number. Thus ferromagnetic and antiferromagnetic systems are always topologically trivial. In the ferromagnetic case for example (unit cell of one lattice site), the gap is allowed to close when the magnetic field reaches $\sqrt{\Delta^2 + (2|t| - \mu)^2}$, as can be seen from eqs. (3.33) and (3.34) which are still valid in the ferromagnetic case (but with zero SOC in the rotated Hamiltonian). In contrast to the helical case as discussed in the previous section, the gap will not open again after it first closes when h is further increased. Instead, the Fermi points will move between $k = 0$ and $k = \pi$, before it gaps out when it reaches a time reversal invariant momentum again.

Looking at eqs. (3.37) and (3.38), we note that the imaginary part of $|A_k|$ is proportional to the area between the origin and the line segments connecting neighbouring magnetic fields (this does not generalise past $N_{\mathrm{UC}} = 4$). A consequence of this is that whenever the field vectors h lie on any line in the xy-plane, the total area is zero, and the system does not wind. Based on these observations, we wondered if this could be generalised to bigger unit cells. Thus we numerically computed the curves in the complex plane made by $|A_k|$ as k traversed the 1BZ when the magnetic field vectors were randomly placed on common lines, and repeated this procedure for different number of unit cell sizes. The result was that, infact, the imaginary part was always zero. Thus we propose the first observations on s-wave superconductors in a inhomogeneous magnetic field: s-wave superconductors with magnetic field vectors $\boldsymbol{h}_i$ which lie on a line in $h_x h_y h_z$-space will always be topologically trivial. A special case of this pattern is the class of collinear magnetic fields.

The second empirical observation we make is that the dependence of the imaginary part of $|A_k|$ on the field vectors is at most a first order polynomial in each component. That is, terms proporitonal to e.g. $h_1 h_2 h_3$ are allowed, but terms proportional to $h_1 h_2^2$ are not allowed. This means that any time the imaginary part is purely zero, the winding number is an odd function in each perturbation of a field vector in close proximity. However, for larger perturbations, the real part of the determinant must also be considered, which may close the gap in time reversal invariant momenta unsymmetrically in the perturbation.

We will now consider different examples of magnetic textures which all have gapless Hamiltonians and may or may not be topological.

Example 1: Collinear field in a unit cell of three sites

As an example we will consider a system with a unit cell of three lattice sites where the first lattice site has an exchange field of $\boldsymbol{h}_1 = h_1 \hat{\boldsymbol{x}}$, while the two other sites have zero exchange field, $h_{2,3} = 0$. Such systems can be realised by for example having different chemical elements in the basis. We now investigate how the system behaves when a

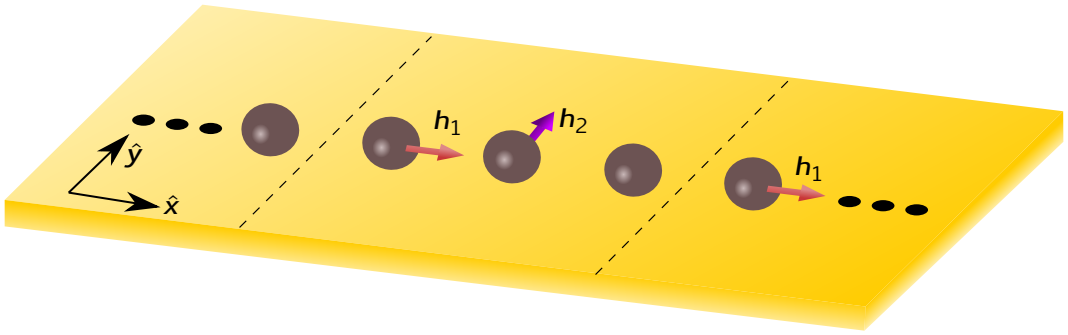

Figure 3.11: Schematic drawing of the case considered in example 1. The arrows show the direction of the local magnetic fields, and the dashed lines indicate the limits of the unit cell, showing one lattice site from each neighbouring unit cell.

magnetic field is added on the second lattice. We let the magnetic field at this site be given by $\boldsymbol{h}_2 = h_2\hat{\boldsymbol{y}}$. Looking at eq. (3.37), we deduce that when $h_2 = 0$, the imaginary part of the determinant $|A_k|$ is zero, thus the system is either gapless or gapful and topologically trivial as h_1 varies. However, for non-zero h_2 the three points projected by $\boldsymbol{h}_1$, $\boldsymbol{h}_2$ and $\boldsymbol{h}_3$ create a triangle which has an area, and thus the imaginary part is non-zero. In fact, the imaginary part is $-4\Delta_0 h_1 h_2 t^3 sin(3k)$ and is bilinear in h_1 and h_2. Keeping h_1 constant, we plot the energy bands for an *open boundary* system as h_2 is varied in fig. 3.12a. The figure shows that our predictions about the behaviour of the system bulk matches with the open boundary system. When the perturbation, h_2, is zero, the bulk band gap is closed except a small contribution from the finite size effect, which is expected to diminish as the length of the wire is increased. As h_2 is increased (or decreased) from 0, the gap opens but the lowest lying energy state remains at 0 energy and is protected by a topological winding number of ± 1 – thus being a MBS.

We computed the local density of the lowest energy state for three values of h_2 as it was increased from 0 to show how the MBS candidate localises at the edge of the system as the gap is opened. This is shown in fig. 3.12b. The figure shows that when the magnetic field is collinear and the gap is closed, the Majorana fermion extends through the whole superconductor, which allows the two Majorana fermions to interact and thus aquiring energy. It further shows that a magnetic field strength of only $h_2 = 0.05t$ (purple line), which is small compared to Δ ($h_2/\Delta \approx 0.17$) and even smaller compared to the magnetic field at the first site ($h_2/h_1 \approx 0.04$), is enough to considerably localise the Majorana fermion at the edge in a 200 unit cell system. As h_2 is increased further the MBS is even more localised at the edge (orange line).

In fig. 3.12c we show the winding curves for different values of h_2, showing how the imaginary part of the curve is considerably affected for small values, whereas the real part is only slightly affected.

The last figure, fig. 3.12d, shows how the band gap (scanned over the whole 1BZ) various as h_2 varies. The lines are generated for different values of h_1, where the smallest and largest values are in the topological trivial regime, while the three middle values are in the marginal topological regime. As the figure also shows, when $h_2 = 0$, the gap stays closed for an extended range of h_1, before it reopens to a topological trivial phase. The last observation we make from the figure is that the speed at which the gap opens as a function of $|h_2|$ is sensitive to the size of h_1, as can be seen by the change of the slope of the lines.

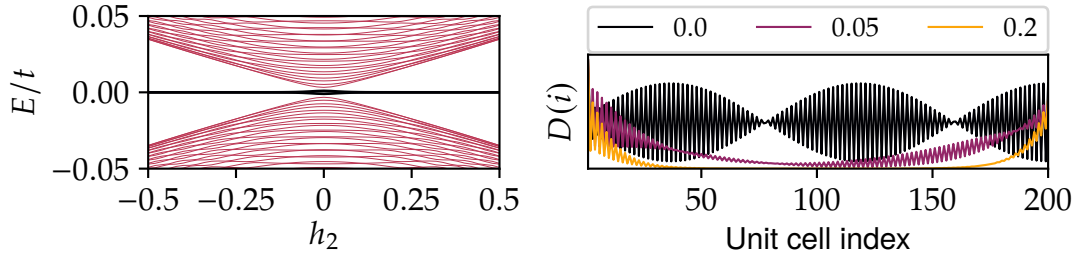

(a) Energies for an open boundary system as the perturbation h_2 is varied.

(b) Probability density (scaled) of the wave function corresponding to the lowest lying energy. The values in the legend are values of h_2.

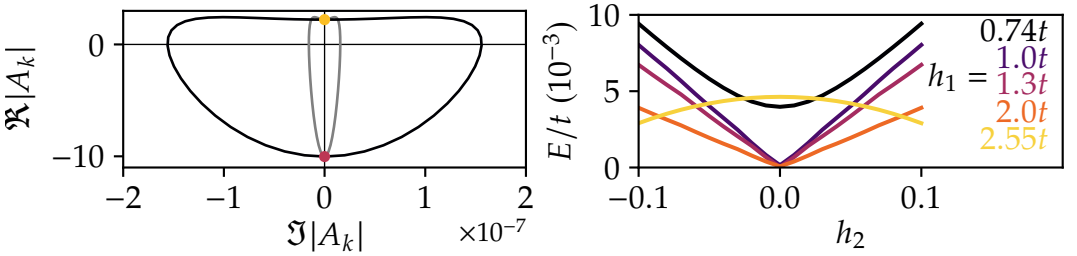

(c) The curve made by $|A_k|$ for $h_2 = 1e-8t$ (gray) and $h_2 = 1e-7t$ (black).

(d) Bulk band gap as a function of h' for various values of h.

Figure 3.12: Marginally perturbing a gapless system into a topological phase. A gapless superconductor in a collinear magnetic field can easily be brought into a topological non-trivial phase by adding a perpendicular magnetic field at one of the lattice sites in the unit cell. **(a)** The energy bands are shown in light (red) for the bulk bands, and black for the lowest lying energy. **(b)** The state with lowest energy extends through the whole system when it is gapless (light, orange). As the gap is opened, the state becomes more localised at the edges (dark, purple). The parameters for the plots were $\mu = -1.5t$, $\Delta = 0.3t$, $h_1 = 1.3t$ and $\boldsymbol{h}_2 = h_2\hat{\boldsymbol{y}}$, except for the panels that state otherwise.

As was defined earlier, a marginal topological phase is described as a collection of points in parameter space where the Hamiltonian is gapless and any perturbation of the system is likely to bring it into a topological phase. The case considered in this subsection is no different. All of the parameters as given in fig. 3.12 were perturbed, including h_2, and the resulting phase diagram is shown in fig. 3.13. As the figure shows, the phase diagram is antisymmetric in h_2, with a clear line dividing to topological phases with different winding number n_W. This line in h_2h_1-space is stable against perturbations in the other parameters and is embedded inbetween topological phases. That is, any system lying on the line will become topological when perturbed, provided that h_2 is non-zero. As we have experiences, marginal topological systems may have an imaginary part which depends on only a small number of parameters. Here that parameter is h_2.

Example 2: Gaplessness is not a sufficient criterion for marginal topology

We just demonstrated that certain gapless systems can easily be driven into a topological phase by perturbing the magnetic field at one site in the unit cell, thereby opening

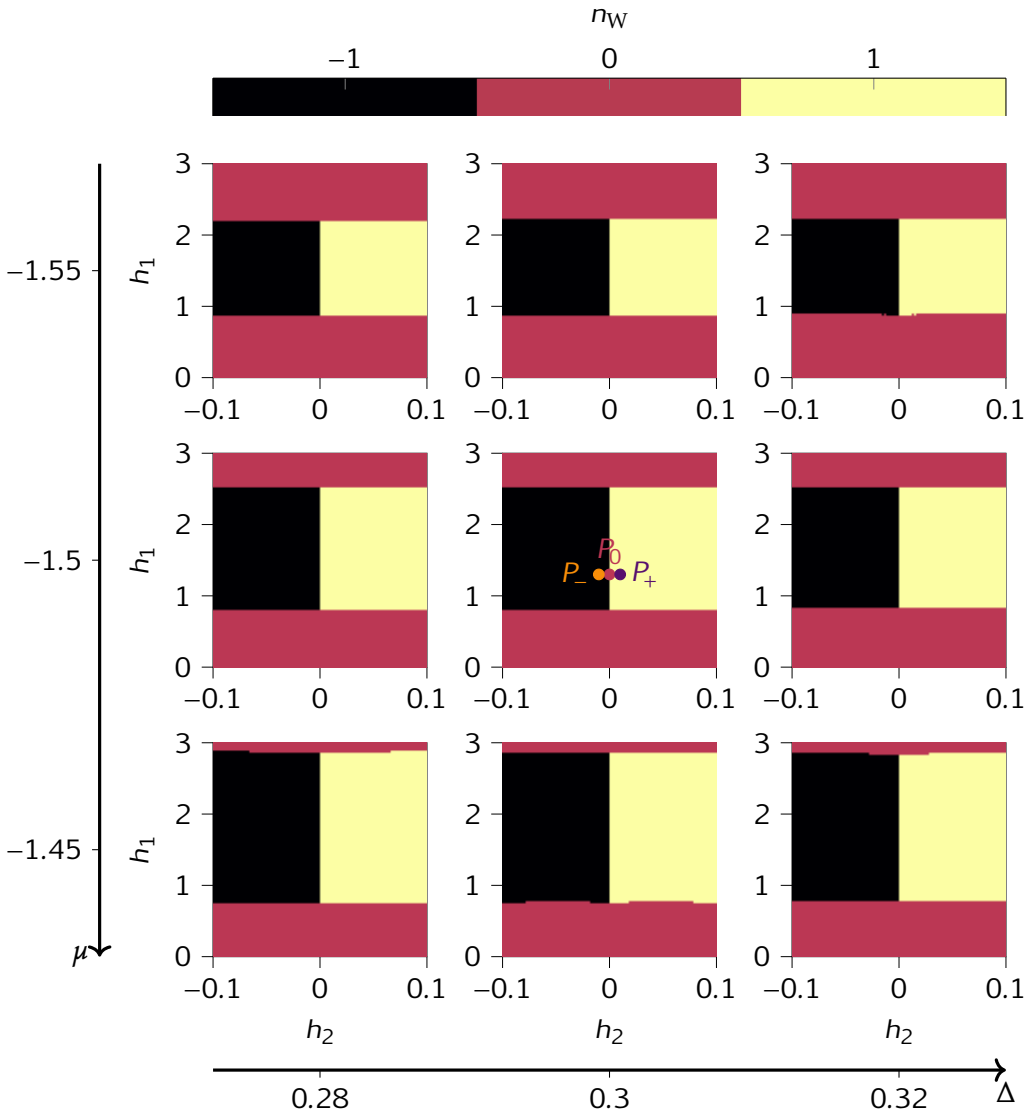

Figure 3.13: Phasediagram for the three-atom-basis SDW system. The system with three atoms in the basis can be a marginal topological superconductor. If the system lies at a point in parameter space in between the black and yellow areas, any perturbation will bring the system into a topological phase, with the sign of the perturbation h_2 deciding the sign of the winding number. At the boundary between $n_W = -1$ and $n_W = +1$, the imaginary part of the determinant $|A_k|$ is zero for all k, with the Hamiltonian having two nodes at $k \neq -k$ points. The figure consists of nine plots showing the phase diagram in h_2-h_1-space. These nine plots are then aranged on a 3-by-3 grid, where the columns are 'parameterised' by the SC OP, Δ and the rows are parameterised by the chemical potential, μ. Thus the figure is a 4-dimensional representation of the phase diagram.

the gap. However, we propose a further requirement for when the system is a marginal topological superconductor and when it is a trivial gapless system. We believe that the specific class of systems considered in this chapter will always have a imaginary part of $|A_k|$ which is proportional to $\sin qk$. In other words, as k traverses the (reduced)

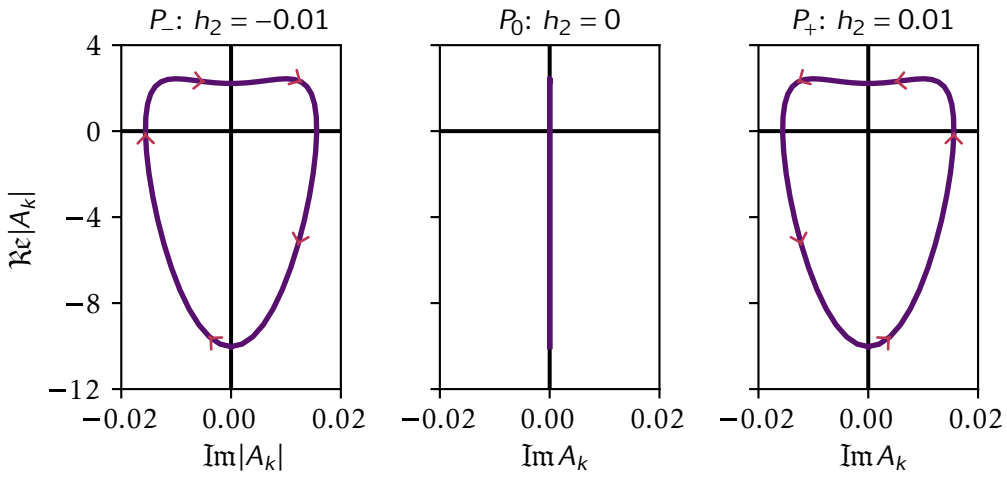

Figure 3.14: Winding curves for different values of the parameter h_2 shown as the points P_-, P_0 and P_+ in fig. 3.13.

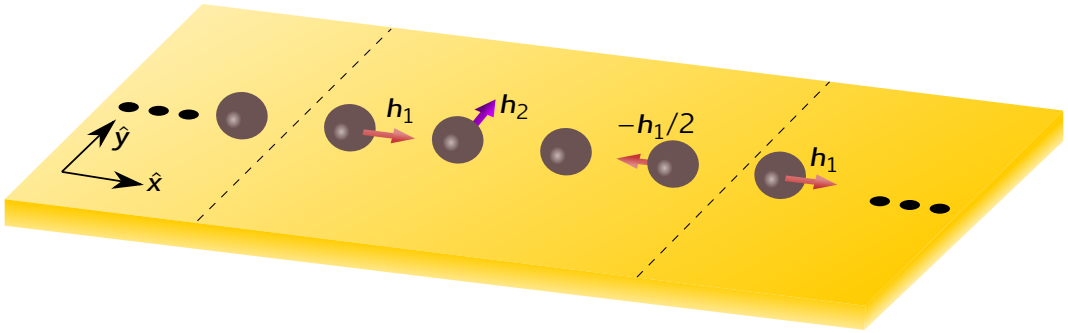

Figure 3.15: Schematic drawing of the case considered in example 2. The arrows show the direction of the local magnetic fields, and the dashed lines indicate the limits of the unit cell, showing one lattice site from each neighbouring unit cell.

Brillouin zone, the imaginary part oscillates once. From this empirical observation, the curve winds *if and only if* the number

$$\mathcal{M} = \operatorname{sign} \mathfrak{Re}|A_0| \cdot \mathfrak{Re}|A_{\pi/q}| \tag{3.39}$$

is -1, i.e. the real part has opposite sign at $k = 0$ and $qk = \pi$. The system described in the previous example satisfies this criterion. To demonstrate the opposite case, in which $\mathcal{M} = +1$, we consider a system with a unit cell consisting of four lattice sites, and where the exchange field is given by $\boldsymbol{h}_1 = h_1\hat{\boldsymbol{x}}$, $\boldsymbol{h}_2 = h_2\hat{\boldsymbol{y}}$, $\boldsymbol{h}_3 = -h_1\hat{\boldsymbol{x}}/2$ and $\boldsymbol{h}_1 = 0$. This system is depicted in fig. 3.15. The curve that $|A_k|$ takes in the complex plane (for a very negative h_2) is shown in fig. 3.16b. As can be seen, the real part of $|A_k|$ at $k = 0$ (red point) and $qk = \pi$ (yellow point) have the same sign. This leads to the curve not enclosing the origin, which means that the system is *not* a marginal topological superconductor. Thus, if the system is perturbed in a way that opens the gap, there will not be any Majorana fermions at the boundaries. As fig. 3.16c shows, there are two excited states that localises at the edges when the gap is opened, but as fig. 3.16a shows, these states have non-zero energies, meaning that they are not Majorana fermions. This is in

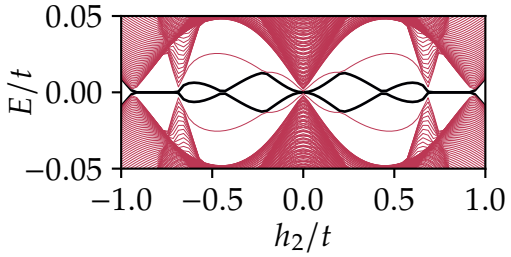

(a) Energy bands for a topologically trivial open system as the perturbation h_2 is varied.

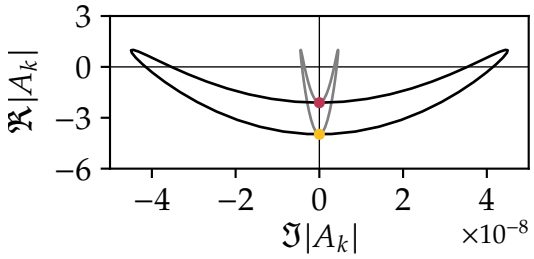

(b) Winding curve for the case considered in the text for $h_2 = 1 \times 10^{-8}\,t$ (gray) and $h_2 = 1 \times 10^{-7}\,t$ (black).

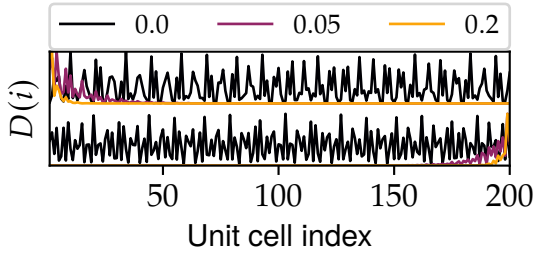

(c) Local density of states (LDoS) for first (bottom pane) and second (top pane) excited states. The system has two edge states for $h_2 \neq 0$, both of which have finite energy and are thus not Majorana fermions.

Figure 3.16: A system consisting of unit cells with a four lattice sites which is gapless, yet not marginally topological, as explained in example 2. The parameters used where $\mu = -0.5t$, $\Delta = 0.3t$, $h_1 = 2.5t$ and $N_{\mathrm{UC}} = 200$. **(a)** The energy bands for an open system are computed as a function of h_2, and shows that as the gap is initially opened, the lowest lying energies have non-zero energy. When $h_2/2$ reaches ≈ 0.65, the gap closes again, this time at a time reversal invariant momenum, thus leading to a non-trivial winding number. **(b)** The winding curve is drawn for $h_2/t = 0.005$ (gray curve) and $h_2/t = 0.05$ (black curve) demonstrating how the banana shape curve does not enclose the origin. The two dots indicate the point on the black curve where $k = 0$ (red) and $qk = \pi$ (yellow, light), and show how they are located on the same side on the real axis, giving $\mathcal{M} = +1$. **(c)** The density of the first excited (bottom pane) and second excited (top pane) states are drawn for different values of the perturbation, $h_2/2$.

contrast to the topological phase where there are two Majorana fermion edge states.

As a side note, as the perturbation h_2 is further increased to around $h_2 = 0.65t$, the system does close the gap at a time reversal invariant momentum, which brings the system into a topological phase. This can be seen as the regions in fig. 3.16a where the black band is flat. In these regions, the winding number is ± 1. However, this is not considered as a marginal topological region.

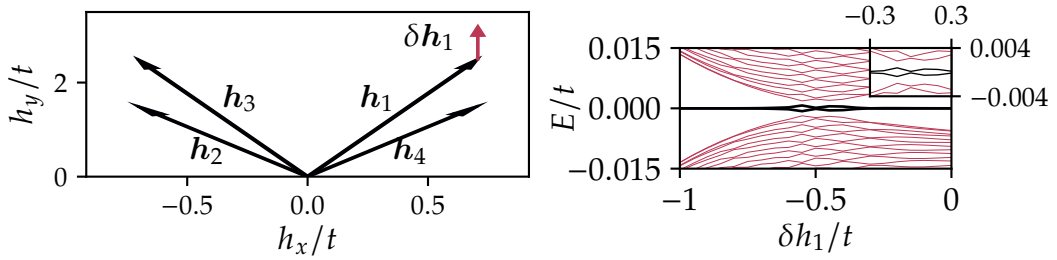

(a) Schematic representation of the magnetic pattern in example 3. The red arrow is the perturbation applied to the system in **(b)**.

(b) The energy bands as functions of the perturbation $\delta \boldsymbol{h}_1$. The lowest lying energy is shown in black, while the bulk energy bands are shown in red. The inset shows the same case, but zoomed in.

Figure 3.17: A marginally topological superconductor consisting of unit cells with four lattice sites in the basis, as described in example 3. The parameters used where $\mu = -1.5t$, $\Delta = 0.3t$ and $N_{\text{UC}} = 400$. Since the interaction between Majorana fermions at opposite edges decrease exponentially with system size (Kitaev, 2001), the system size was increased to 400 unit cells to show the effects more clearly. **(b)** The bulk energy bands arNote also that the energy bands are not symmetric with respect to the perturbation. This is a general fact, where the two previous figures are special cases that are symmetric due to the geometry of the patterns.

Example 3: Non-collinear marginal superconductor

In the last example of this section, we demonstrate that there exist other patterns than collinear patterns that are also marginally topological. The case we consider has a magnetic texture given in fig. 3.17a. This pattern is parameterised by $h_i/t = \cos(i\pi/2 - \pi/4)\hat{\boldsymbol{x}} + (0.5\sin(i\pi/2 - \pi/4) + 2)\hat{\boldsymbol{y}}$, and is part of a general pattern creating a horizontal number 8 shape shifted along the h_y-axis. One of the points is perturbed, as shown by the red arrow. The energy bands for the open boundary system are shown in fig. 3.17b, and the flat black band indicates that there is a Majorana fermion present at the boundaries when the first lattice site in the unit cell is perturbed along the direction of the red arrow. In this system, the band gap opened slower than the previous cases, hence we had to increase the size of the finite system to 400 unit cells due to finite size effects. As the inset in fig. 3.17b shows, when the band gap is only slightly opened, the Majorana fermions at the ends are still interacting considerably, which leads to them gaining energy at first. As the energy gap is opened further by the perturbation, the interaction between the Majorana fermions at the boundaries diminishes due to the increased inability of the Majorana fermions to propagate through the bulk. Thus as the gap increases, the energy of the Majorana fermions approach zero. Although this system can easily be brought into a topological phase by a very small perturbation, we would still argue that it is not a marginal superconductor based on our definition of such systems. This is because the magnetic texture in this example is one which is highly fine-tuned and thus not easy to obtain experimentally.

Dependency on the perturbation

In the examples considered here, the functional form of the imaginary part of $|A_k|$ has been odd in the perturbation. As a result, when the perturbation is applied with a

negative sign, one obtains a topologically different phase. Both phases have the same amplitude of the winding number, but have opposite signs. The implications of this is that the compatibility of two domains with the same type of perturbation depends on the direction of the perturbation. If we for example take the case considered in example 1 above, and set the perturbation to $h_2\hat{\boldsymbol{y}}$ in the first domain, and couple this domain to a second domain with the perturbation $-h_2\hat{\boldsymbol{y}}$, two MBSs will appear at the domain wall between them. This is a result of the bulk-boundary condition, which says that the topology of two bulks with different topological number can not be continuously transformed into each other without closing the gap – a clock wise oriented curve can not be transformed into a anti-clockwise oriented curve without first squashing it and intersecting itself, thereby forcing the gap to be closed somewhere. This can potentially be a path to easy control and transportation of MBSs in practical systems as only small perturbations are needed to change the topology of regions of the device. However, the smaller the device is, the larger the perturbation needs to be since small gaps means that the MBS extends far into the bulk and will interact increasingly with small device sizes.

In terms of a general gapless Hamiltonian, we wonder if there may exist cases or perturbations where the imaginary part of the determinant is even in the perturbation. Such a system would be less sensitive to domain specific differences in the gap opening perturbation, which again would limit the tendency of the MBSs to condence at the boundary between the domains.

3.4 Conclusion

We analysed three different types of superconducting systems with a focus on marginal superconductivity. The criteria in the parameters of the models which give rise to marginal topology were easily found by searching for the cases when the curve given by the off-diagonal determinant was purely real. The realness-criteria of the winding curves were seen to rely on just a small number of the parameters in the model, and in such a way that the the realness was satisfied by them being zero. Obtaining a value of 0 is in general an easily obtainable value for many parameters, thus making the marginal topological phase easily realisable in the laboratory. In the p-wave systems the realness criteria relied on the d_x OP and the h_z component of the ferromagnetic field. The marginal topology of the system with antiferromagnetic order did not rely on the the value of the antiferromagnetic order parameter, $\boldsymbol{M}$. We do not speculate in how a value of $d_x = 0$ is to be obtained experimentally, but we speculate in if using this parameter as a driving parameter in a marginal topological superconductor is hard to do without using strong magnetic fields and/or electric fields, and even so, is hard to control with these tools. Thus we assume that experimentally driving the marginal topological phase of p-wave superconductors is most easily done by controlling the h_z component of the exchange field, which in the case of an external field is as easy as rotating either the source of the magnetic field around the specimen or rotating the specimen itself.

The s-wave superconductor in a noncollinear magnetic field does only depend on one superconducting order parameter which is easier to control in contrast to the p-wave order parameter. Thus to realise a marginal topological phase in such systems one need only look for magnetic materials with a smallest unit cell of three or more atoms in the basis which satisfy the equations given in the last section or equivalent equations for unit cells of five or more atoms. If the unit cell consists of different atoms for example, we speculate that one can use short laser pulses to change the magnetic

moment at each lattice site individually by tuning the laser pulse frequency accordingly. Kirilyuk, Kimel and Rasing (2010) review different methods and experiments to control the magnetic order of materials, which may be heat effects or polarised light pulses interacting with the electrons and the lattice.

As we saw in fig. 3.16, gaplessness is not a sufficient requirement alone to have a marginal topological state. In the case where only nearest neighbour hopping is significant and the winding number can only be -1, 0 or $+1$, the number of nodes in the Brillouin zone are important. If the number of nodes in each half is even, the system is trivial. On the other hand, if it is odd, the system is guaranteed to be marginal topological. In fact, this applies to all 1D systems with a winding number, since the sign difference means that the winding number can only be odd, which excludes the trivial value of 0. We also showed that the system can be marginal topological with an even number of nodes in each half of the Brillouin zone if there are next nearest and third nearest neighbour hopping in the system as in section 3.1. Thus when the gap is opened multiple MBSs appear on the edges.

4 | Elliptical magnetic chain on a s-wave superconductor

In section 3.3 we reviewed s-wave systems with easy-plane magnetic fields with no further requirements. In this chapter we analyse a more specific case, namely s-wave superconductors with elliptical magnetic fields or elliptical conical magnetic fields. Indeed, such textures may be found in nature in the form of for example some perovskites (Quezel, Tcheou, Rossat-Mignod, Quezel & Roudaut, 1977; Yamasaki et al., 2007). In addition, there may be methods to modify the characteristics of such systems that are easily available experimentally. Such modifications may include

- increasing or decreasing the amplitude of the elliptical field,
- changing the global offset of the elliptical motion,
- changing the offset of the field at isolated points,
- shifting the whole ellipse via external homogeneous fields.

For instance, the helicity of $TbMnO_3$ can be controlled by applying an electrical field during cooling (Yamasaki et al., 2007) or by external magnetic fields (Kimura & Tokura, 2008), or the cycloidal nature in the material $Gd_{1-x}Tb_xMnO_3$ can be controlled by applying an external magnetic field (Yamasaki et al., 2008). Other examples are helicity control in $Eu_{0.55}Y_{0.45}MnO_3$ (Murakawa et al., 2008, 19).

The topological nature of such systems, especially helical and conical structures, have already been investigated by Braunecker and Simon (2013), Chen and Schnyder (2015), Choy et al. (2011), Marra and Cuoco (2017), Nadj-Perge et al. (2013). As we already showed, *helical* magnetic field can be transformed into ferromagnetism with strong Rashba SOC, which allows MBS. By applying elliptical magnetic fields instead

Table 4.1: Unitarily connected models. The models in the same row can be unitarily transformed to each other by spin-rotations, which means that the energies are the same except spin-dependent observables.

Model 1	**Model 2**
Helical, uniform angles	FM + SOC
Helical, arbitrary angles	FM + nonuniform SOC
Elliptical, uniform angles	SDW + SOC
Elliptical, arbitrary angles	SDW + nonuniform SOC
Elliptical conical, uniform angles	SDW + SOC (nonperpendicular)
Elliptical conical, nonuniform angles	SDW + nonuniform SOC (nonperpendicular)

of helical magnetic fields in the model, the system is parameterised by two additional parameters: the eccentricity of the ellipse and the offset. A circle has a continuous translation symmetry in the angle, whereas an ellipse has a discrete translation symmetry with a period of π. Thus, in contrast to the helical case, the offset is of importance and can not be gauged away by a global transformation. Such a model is unitarily connected to systems with SDW and uniform (nonuniform) SOC when the angle differences between the exchange fields are uniform (nonuniform) (cf. table 4.1).

One of the focus point in the investigation into these elliptical systems is the additional symmetries that appear when we consider the ellipse parameters as synthetic momenta. The eccentricity and offset of the exchange field vectors in the ellipse give an additional two dimensions, and followingly change the topology of the system in the expanded space. By treating these parameters as synthetic momenta we can understand the topology in the real 1D system more clearly by the topology in 2D or 3D. Other questions we consider is the importance of time-reversal breaking and inversion breaking in this system. The goals of this chapter is to evaluate the phase diagram of the elliptical (elliptical conical) model, and assess the topological nature of it in light of the symmetries. We also want to analyse the effects of breaking chirality. The model is then later analysed with time-dependent parameters in chapter 5.

4.1 Model

The model we use in this chapter is derived from the one given in section 2.6. We consider a magnetic chain on top of a 2D slab of a s-wave superconductor. There is no spin-dependent hopping in this system, only normal hopping proportional to t. The local magnetic field at each site is parameterized on the elliptical cone given by

$$\boldsymbol{h}_i = h_i\left[\cos(\lambda_i+\phi)\hat{\boldsymbol{x}} + \sin(\lambda_i+\phi)\hat{\boldsymbol{y}}\right] + h_z\hat{\boldsymbol{z}}, \tag{4.1}$$

where the site dependent in-plane local amplitude, h_i, is given by the angle and minor and major axis,

$$h_i = \frac{hab}{\sqrt{b^2\cos^2(\lambda_i+\phi) + a^2\sin^2(\lambda_i+\phi)}}. \tag{4.2}$$

Here h modulates the overall amplitude and a and b controls the eccentricity of the ellipse. This parameterisation of the ellipse ensures that the angle $\lambda_i+\phi$ is the same as the angle of the exchange field vectors. The ellipse minor and major axis is modulated by the parameter θ as $a = \cos(\theta)$ and $b = \sin(\theta)$. When $\sin(\theta)$ is negative, the angle, λ_i is negated, and when $\cos(\theta)$ is negative, the angle transforms according to $\lambda_i+\phi \to \pi-\lambda_i-\phi$. These transformations can be understood by the fact that the axes flip when $\sin\theta$ or $\cos\theta$ change sign. This way to parameterise the field allows for the reversal of the elliptical motion, which is relevant in systems like the aforementioned perovskites which can be electrically or magnetically tuned.

We note that whether the elliptical (or elliptic cone) spin-texture is transverse or longitudinal is of little importance as the spins are independent of the momentum of the electrons (no SOC), which means that any spin-plane can be chosen as the easy plane in this model. Thus the results obtained here with the momentum along the x-axis and the elliptical motion in the xy-plane are easily generalised to any spin-plane and quantum wire orientation.

We now assume that the angle λ_i rotates uniformly with some offset ϕ, and that it is commensurate with the lattice, that is $\lambda_i = \frac{2\pi p}{q}i + \phi$, where p and q are coprimes.

Followingly, the Hamiltonian has a superlattice constant of qa, where a is the lattice constant between neighbouring lattice sites. In the following, we assume that the lattice constant is of unit size. Equivalently, the lattice consists of units cells of q lattice sites. The fermion operators are relabelled to include the unit cell index, i, and the intracell index, l, as

$$c_{i,l} = c_{q\cdot(i-1)+l}.$$

The spin index is implied. We also do a local spin rotation around the z-axis in this model to align the exchange field vectors along the x-axis (xz-plane when $h_z \neq 0$), given by eq. (3.26). We now assume periodic boundary conditions, and in this new labelling scheme, we define the Fourier transformed fermion operators by

$$c_{i,l} = \frac{1}{N_{\mathrm{UC}}} \sum_k e^{iqki} c_{k,l}. \tag{4.3}$$

The momentum, k, is now limited to $k \in (-\pi/q, \pi/q)$. In k space, the Hamiltonian becomes

$$\begin{aligned} \hat{H} = &-t \sum_{kss'} \sum_{\eta=\pm1} \sum_{l}^{q} c^\dagger_{k,l+\eta,s} \left[\cos\left(\delta\lambda_{l+\eta,l}/2\right)\sigma_0 + i \sin\left(\delta\lambda_{l+\eta,l}/2\right)\sigma_z \right]_{ss'} c_{k,l,s'} \beta(l,\eta) \\ &-\mu \sum_{kls} c^\dagger_{k,l,s} c_{k,l,s} - \sum_{klss'} c^\dagger_{kls} (h(l)\sigma_x + h_z\sigma_z)_{ss'} c_{kls'} + \sum_k \left(\Delta_0 c^\dagger_{kl\uparrow} c_{-kl\downarrow} + \text{h.c.} \right) \end{aligned} \tag{4.4}$$

where the basis index $l+\eta$ is taken modulus q. The intersite hopping phase factor

$$\beta(l,\eta) = \begin{cases} e^{-iqka} & l = q, \eta = +1 \\ e^{iqka} & l = 1, \eta = -1 \\ 1 & \text{otherwise} \end{cases}$$

was defined, which comes from the Fourier transformation when two sites lie in different unit cells. To write this Hamiltonian in the BdG formalism, we define the column vector

$$D_k = \left(c_{k,1,\uparrow},\ c_{k,1,\downarrow},\ \ldots,\ c_{k,q,\uparrow},\ c_{k,q,\downarrow},\ c^\dagger_{-k,1,\downarrow},\ -c^\dagger_{-k,1,\uparrow},\ \ldots,\ c^\dagger_{-k,q,\downarrow},\ -c^\dagger_{-k,q,\uparrow} \right)^{\mathrm{T}}.$$

The Hamiltonian can thus be written as

$$\hat{H} = \frac{1}{2} \sum_k D^\dagger_k H_k D_k \tag{4.5}$$

where the Hamiltonian matrix is

$$H_k = \begin{pmatrix} h_{k-} & \hat{\Delta} \\ \hat{\Delta} & h_{k+} \end{pmatrix}, \tag{4.6}$$

with

$$h_{k\pm} = \begin{pmatrix} \pm\mu - h(1)\sigma_x & \pm W_{12} & 0 & \ldots & \pm W_{1q} e^{-iqka} \\ \pm W^*_{12} & \pm\mu - h(2)\sigma_x & \pm W_{23} & \ldots & 0 \\ 0 & \pm W^*_{23} & \pm\mu - h(3)\sigma_x & \ldots & 0 \\ \vdots & \vdots & \vdots & \ddots & \vdots \\ \pm W^*_{1q} e^{iqka} & 0 & 0 & \ldots & \pm\mu - h(q)\sigma_x \end{pmatrix} \tag{4.7}$$

and

$$\hat{\Delta} = \Delta_0 \mathbb{1}_q \sigma_0.$$

Here the site and spin dependent hopping term, W_{ij}, was defined as $W_{ij} = t\cos\left(\delta\lambda_{ij}/2\right)\sigma_0 + it\sin\left(\delta\lambda_{ij}/2\right)\sigma_z$.

4.2 Symmetries

4.2.1 AZ symmetries

The next step is to consider which symmetries are present in the system. We already know that the system has particle-hole symmetry because of the superconductivity. This symmetry is given by $\mathcal{C} = \tau_y\sigma_y K$ instead of just τ_x because of the spin rotated hole sector. To find the time reversal symmetry operator in k-space, we first complex conjugate the Hamiltonian followed by reversing the momentum. The superconducting sector is not affected by this transformation. The only affected part of the matrix given in eq. (4.7) is the submatrices W_{ij} which are complex conjugated, which flips the sign in front of the spin-operator σ_z. Since this is the only term in the matrix which is proportional to σ_z, finding the TR operator is trivial: We need only find the matrix which anticommutes with σ_z and commutes with the rest, which are σ_0 and σ_x. Thus, the TR operator is σ_x, and does not mix particles and holes. Followingly, we find the chiral symmetry operator by multiplying the two, upon which we arrive at $\mathcal{S} = \tau_y\sigma_z$. Of course, a unit matrix in lattice space is implied for the operators. Thus, in the space spanned by k, the special symmetry operators are

$$\mathcal{T} = \sigma_x K \qquad \mathcal{C} = \tau_y\sigma_y K \qquad \mathcal{S} = \tau_y\sigma_z, \tag{4.8}$$

$$\mathcal{T}^2 = +1 \qquad \mathcal{C}^2 = +1 \tag{4.9}$$

Note that the TR operator given here is the only TR operator available in this model. A consequence of this is that an exchange field proportional to σ_z, which is not affected by complex conjugation, will anti-commute with the TR operator. Followingly, TR and by extension chiral symmetry is broken when the field is conical. This means that the winding number is not defined for systems with conical exchange fields, and we must rely on the Pfaffian to characterise the topological phases in those cases.

We want to evaluate the topological objects in this model in terms of the space extended by the real momentum k, and the synthetic momenta θ and ϕ. We remind the reader that the chiral operator is local in momentum space. This means that in this extended space, the chiral operator is always present as long as the exchange field is elliptical. We begin by trying to find the symmetries which flip the direction of either θ or ϕ. When θ is flipped, the direction of the elliptical (conical) motion is flipped by flipping the y-component of the spin. Intuitively, we expect that if an operator which flips θ back exists, it must flip the y-component of the spin. Possible candidates for this operation are the σ_x or σ_z matrices. The latter does not work, because it also flips the spin in the x-direction. So the only remaing option is σ_x. Again, by inspection, we see that eq. (4.7) changes only in the W_{ij} matrices the same way as previously. Thus, we reuse the previous arguments to conclude that indeed there exist a symmetry operation defined by

$$\sigma_x H(k,\theta,\phi)\sigma_x = H(k,-\theta,\phi). \tag{4.10}$$

If we combine this symmetry operator with the TR operator given in eq. (4.8), the result is a new TR symmetry in the plane spanned by θ and k, which is simply

$$KH(k,\theta,\phi)K = H(-k,-\theta,\phi). \tag{4.11}$$

We conclude that in this two dimensional space, the system is a two dimensional superconductor belonging to the AZ class of BDI. We do not write down the PH operator in this space, but emphasise that it can easily be found as the product of the chiral symmetry operator (same as before) and this new TR operator. Note that the TR operator

in this space is not broken by a non-zero out-of-plane field h_z. We then conclude that it is the PH operator which is broken by a non-zero h_z field in this synthetic 2D space. It then follows that when the chirality is broken by a non-zero h_z, the system belong to the real class AI.

To flip the synthetic momentum variable ϕ by a symmetry, more work is required. At first we note that the negation of ϕ is able to change the length of the local exchange field at each atom in the basis, except the last atom in the unit cell where the length is invariant but the y-component is negated. If we on the other hand do the transformation $\phi \to -\phi - \lambda$, followed by a spin rotation of π around the x-axis given by the operator σ_x, the exchange fields swap places as $h_i \to h_{q-i+1}$. That is, the unit cell is reflected internally. If we then proceed to multiply the Hamiltonian by the lattice operator which inverts the unit cell,

$$M = \overbrace{\begin{pmatrix} 0 & 0 & \dots & \sigma_0 \\ \vdots & \vdots & \iddots & \vdots \\ 0 & \sigma_0 & \dots & 0 \\ \sigma_0 & 0 & \dots & 0 \end{pmatrix}}^{N_{\text{Basis}}}, \tag{4.12}$$

we expect to obtain the original Hamiltonian with the momentum inverted. In summary, we can flip the ϕ around $-\lambda$ by the operator

$$M^{-1}\sigma_x H(k,\theta,\phi)\sigma_x M = H(-k,\theta,-\phi-\lambda) \tag{4.13}$$

There is also a similar antiunitary operator which does not flip the physical momentum given by

$$M^{-1}\, KH(k,\theta,\phi)\, KM = H(k,\theta,-\phi-\lambda). \tag{4.14}$$

However, none of these can combine with the TR operator in θ-k space given above to create a new 3D TR operator. It then follows that the system belongs to the complex AZ class AIII in the synthetic 3D space when $h_z = 0$ and to the complex class A when h_z is non-zero.

4.2.2 Nonsymmorphic symmetries and additional topological invariants

It is known that additional symmetries to the AZ symmetries can have implications for the topological characterisation of systems (Chiu & Schnyder, 2014; Chiu et al., 2016). An example of such symmetries are nonsymmorphic symmetries. In their paper, Shiozaki, Sato and Gomi (2016) show that the AZ table can be extended to include nonsymmorphic symmetries. A nonsymmorphic symmetry is a space group symmetry which combines a point group operation with a lattice non-primitive lattice translation. That is, the system is not translated by whole unit cells at the time. The resulting nonsymmorphic operator is k-dependent. The elliptical system does not have nonsymmorphic symmetries when the unit cell is odd (except at $\theta = \pi/4$), but when the unit cell is even, every local exchange field is matched in amplitude by the site which is half a unit cell away in the chain. The other exchange field vector then points in the opposite direction for any p/q, since we have assumed that they are coprime. Thus, if we rotate the magnetic pattern by π around the z-axis and translate by $q/2$ lattice sites, the Hamiltonian should be left invariant. However, when we translate the lattice sites by half a unit cell, exactly half of the sites will end up in the initial unit cell while the other half will end up in the next unit cell. When the Hamiltonian is subsequently Fourier transformed, there will be an additional k-dependent factor which has to be

compensated in the operator itself. The operator which translates the lattice sites by half a unit cell and wraps the overflowing sites back to the start is the matrix $\left(\begin{smallmatrix} 0 & \mathbb{1}_{q/2} \\ \mathbb{1}_{q/2} & 0 \end{smallmatrix}\right)$. Although the spins must be rotated around the z-axis in the original basis, in the basis where the spins have been rotated to be collinear, this is not needed. The k-dependent nonsymmorphic symmetry operator is then

$$U = \begin{pmatrix} 0 & -ie^{-iqk}\mathbb{1}_{q/2} \\ i\mathbb{1}_{q/2} & 0 \end{pmatrix}.$$

According the the approach given by Shiozaki et al. (2016), this is a order two nonsymmorphic group transformation, and it is important that it squares to $\mathbb{1}e^{-ik}$ in the following, which is the case. The nonsymmorphic operator transforms as follows under the AZ symmetry operations

$$\mathcal{T}U(k) = -U(-k)\mathcal{T} \qquad \mathcal{C}U(k) = -U(-k)\mathcal{C} \qquad \mathcal{S}U(k) = U(k)\mathcal{S}. \tag{4.15}$$

According to Shiozaki et al. (2016, tab. V), this extra symmetry allows for an extra $\mathbb{Z}_2$ symmetry in addition to the $\mathbb{Z}$ winding number. If the $\mathbb{Z}_2$ number is nontrivial, there will be a topological edge state at a boundary parallel to the k-axis. This means that if one were able to open up the θ-axis in a hypothetical position representation of the synthetic momentum variable θ, we would have an edge state. The topological number can be computed by block-diagonalising the Hamiltonian in eigensectors of the nonsymmorphic operator, and compute the integral

$$\nu_{\pm} = \frac{i}{\pi}\int_{-\pi}^{\pi} \mathrm{d}\theta\, \mathrm{Tr}\{\mathcal{A}_{\pm}(k,\theta)\},$$

where $\mathcal{A}_{\pm}$ is the Berry connection in the sector with eigenvalue ± 1 of the nonsymmorphic operator. These topological invariants were computed for different sets of parameters, but were not found to be nontrivial in the elliptical system for the combinations computed.

4.3 Phase diagram

One of the main results of this chapter is the phase diagram with unbroken chiral symmetry ($h_z = 0$), which we now present for an odd unit cell with a three atom basis in the θ-ϕ space for various sets of the amplitude of the elliptical field and for different values of the chemical potential. In the following, we set the superconducting order parameter to $\Delta_0 = 0.3t$. The phase diagram for a three-atom basis unit cell with $p/q = 1/3$ is shown in fig. 4.1 in the space spanned by θ and ϕ, and by varying the amplitude of the elliptical exchange field between the columns, and varying the chemical potential between rows. Initially, we note that the winding number for the parameters used are only taking values in the set $\{-1, 0, 1\}$. The diagram clearly shows that a zero exchange field (left column) gives a trivial topological phase everywhere in the space spanned by θ and ϕ. This is expected, since in that limiting case, the angles between the zero-length exchange fields are arbitrary, and the system is unitarily connected to a s-wave superconductor with spin-independent hopping, which we know is trivial. On the other hand, we see that when the amplitude of the ellipse is initially increased (moving east), an increasing number of disconnected areas of non-trivial topological phases appear in the phase diagram. This is due to an increasing number of energy bands crossing zero energy as the average exchange field amplitude is increased. In the **c5)** frame, notice

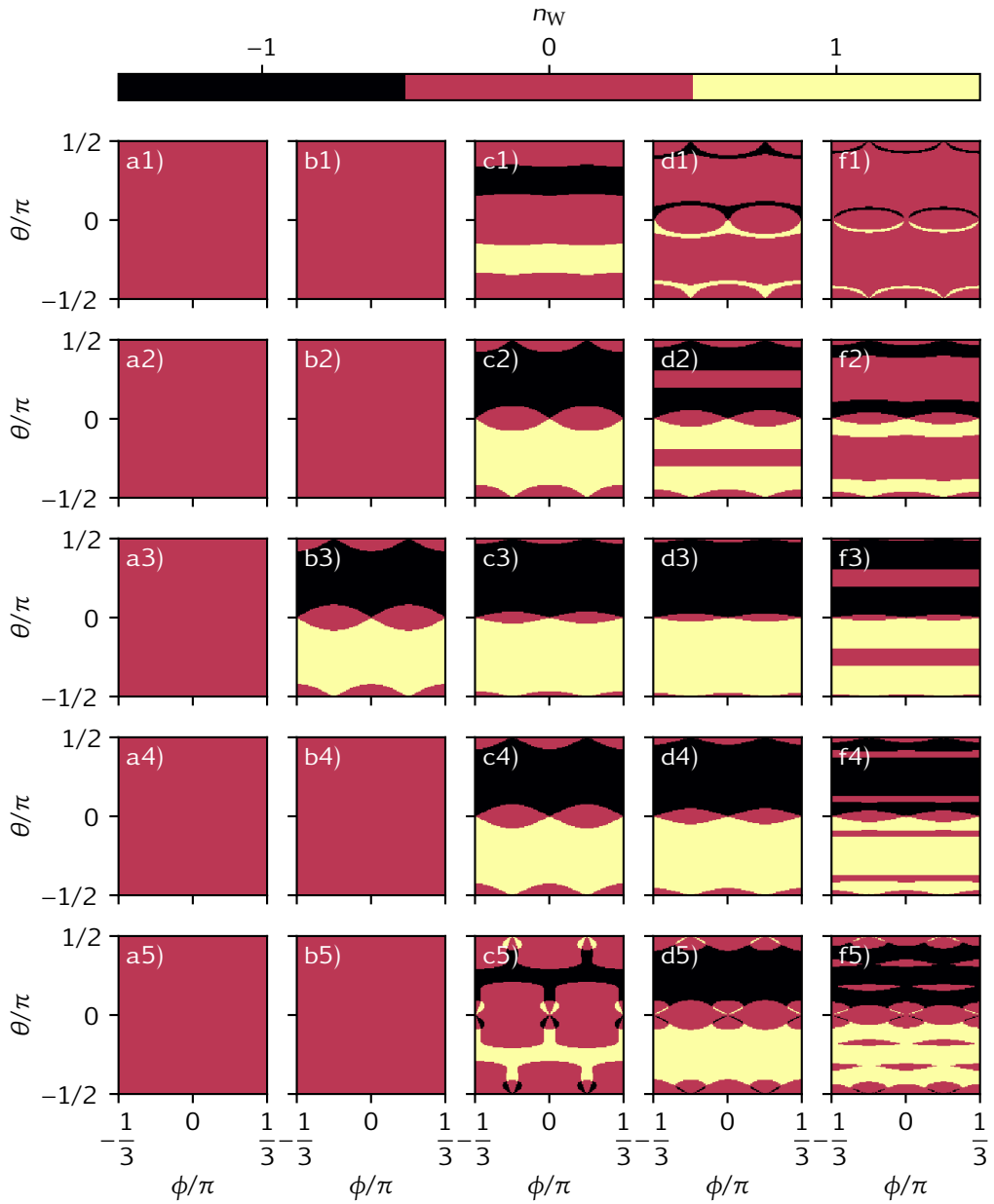

Figure 4.1: The phase diagram for a three-atom unit cell in θ-ϕ-space varying μ and h, computed on a 151×151 grid. The rows represents different values of μ, with the row numbers $(1, 2, 3, 4, 5)$ corresponding to $(-0.1, -1/2, -1, -3/2, -2)t$ for μ, while the columns represent different values of the ellipse amplitude, h, with the column letters (a, b, c, d, e) corresponding to $(0, 3/4, 3/2, 9/4, 3)t$ for h. The maximum winding number is $+1$, while the smallest is -1. The s-wave order parameter was not solved self consistently, but set to $0.3t$ in all frames.

that there are both negative and positive winding numbers on the same side of $\theta = 0$. This is an interesting effect in this model. Instead of flipping the direction of the elliptical spin, one can alter the shape and offset of the motion to change the winding number. The phase diagram is strongly dependent on the filling factor modelled by the

chemical potential, μ. In fact, the superconductor is topologically trivial at half-filling ($\mu = 0$) for any ellipse shape and size and any superconductor OP (not shown). This is similar to the helical model or the s-wave superconductor with Rashba SOC in a ferromagnetic field, which are related by unitary transformation. Indeed, at $\theta = \pi/4$, the magnetic order is exactly helical. In systems with a helical or conical exchange field, the minimum value of the in-plane field needed for achieving a topological phase is obtained when the chemical potential is matched to the spin-independent hopping in the transformed collinear SDW Hamiltonian, i.e. when $\mu = \pm 2\tilde{t}$ (Nadj-Perge et al., 2013), where $\tilde{t} = \cos(\lambda/2)t$. In the case considered here, we have $\tilde{t} = \cos(\pi/3)t = \frac{t}{2}$. This means that we expect that $\mu = \pm 1$ gives the smallest value of the exchange field at $\theta = \pi/4$. This is also supported by the phase diagram.

In fig. 4.2 we show the phase diagram for the even unit cell with four atoms in the unit cell. The phase diagram is produced from the same set of parameters as in the previous figure, except for the unit cell size parameter of course. Based on the results of the helical model (section 3.3.3), we might except that the line $\theta = \pi/4$ would be equal for the two unit cell sizes in all the panels, but the for instance **b4)** panel differs between the two unit cell sizes. However, note that it is not the pure hopping parameter t in eq. (4.4) which defines (together with μ and Δ_0) the gap closing and opening at $k = -k$, but the modified hopping strength $\tilde{t} = t\cos\lambda/2$. This means that in principle the period of the helical texture, parameterised by λ, can be used to drive a topological phase, although this might be harder to accomplish than e.g. changing the shape of the elliptical motion as in the perovskites like $TbMnO_3$. However, in instruments that employ nanomagnets ()

We expect that for values of θ close to $\pi/4$ it is the fraction p/q which is most defining for the phase diagram, since it is this number which modifies the effective spinless hopping in the model, $\tilde{t}$. Closer to $\theta = 0$ or $\theta = \pi/2$ at the high symmetry points of ϕ, we expect that the parity of the unit cell given by the number q to a larger extent affects the phase diagram. This is because at these edge case values of θ and ϕ, the unit cell obtains a finite magnetic moments in the odd case because one of the magnetic moments will dominate the others in size, whereas the even unit cell always has a zero magnetic moment when q is even.

4.4 Topology in 2D and 3D

In section 4.2 we showed that the system belongs to the AZ class BDI when in 1D spanned by k and 2D spanned by k and θ, because of the additional unitary symmetry which flips θ: $\theta \to -\theta$. We still assume that the out-of-plane exchange field h_z is zero. As we already know, the BDI class can be topologically nontrivial in one dimension, but looking at table 2.1, we see that the BDI class is topologically trivial in 2D and 3D. This is true when the codimension of defects is one, which is the case when the dimensionality of the boundary is one less than the bulk. Such boundaries are those that distinguishes the bulk from the surroundings: i.e. the 0D end of a chain, the 1D edges of a 2D object or the 2D surface of a 3D object. However, the two dimensional BDI system may have topologically protected nodes off high-symmetry points and the 3D AIII system may have topologically protected line nodes (Chiu & Schnyder, 2014). These nodes or lines are protected by a $\mathbb{Z}$ number which can be computed by surrounding the node by a small closed curve, $\mathcal{C}$, and computing the winding along this curve,

$$W = \frac{1}{2\pi i}\int_{\mathcal{C}} \frac{\mathrm{d}\det A_{k,\theta}}{\det A_{k,\theta}}. \tag{4.16}$$

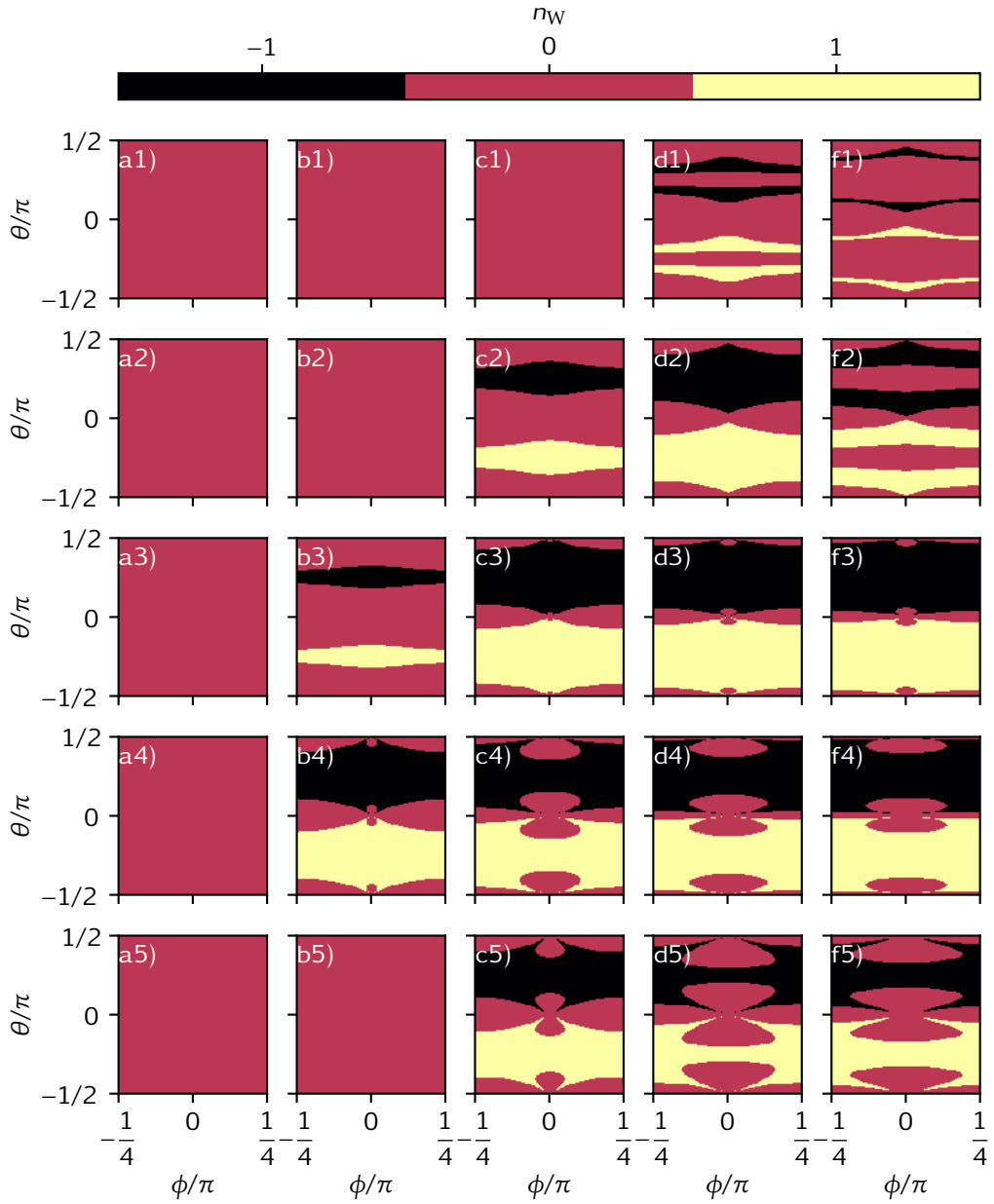

Figure 4.2: The phase diagram for a four-atom unit cell in θ-ϕ-space varying μ and h, computed on a 151×151 grid. The rows represents different values of μ, with the row numbers $(1, 2, 3, 4, 5)$ corresponding to $(-0.1, -1/2, -1, -3/2, -2)t$ for μ, while the columns represent different values of the ellipse amplitude, h, with the column letters (a, b, c, d, e) corresponding to $(0, 3/4, 3/2, 9/4, 3)t$ for h. The maximum winding number is $+1$, while the smallest is -1. The s-wave order parameter was not solved self consistently, but set to $\Delta_0 = 0.3t$ in all frames.

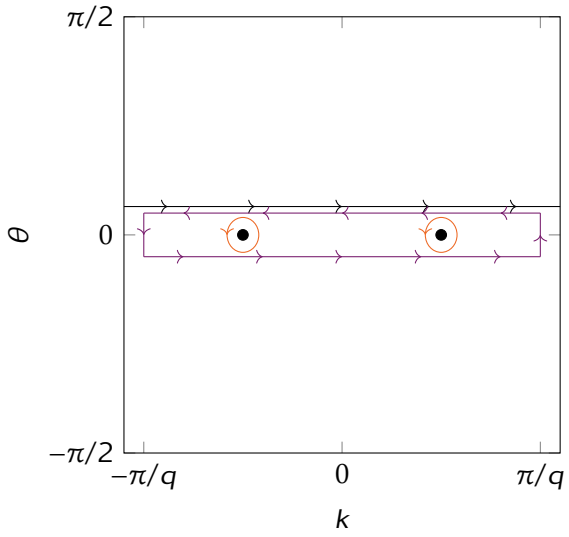

Figure 4.3: Examples of curves that a winding number can be computed on. The black curve is the curve that the regular winding number is computed along, going parallel to the k-axis, whereas the orange curves encloses Nodes in the Hamiltonian which may change the winding number. The purple curve is an counterclockwise curve which encloses the whole k-axis and thus gives a winding number which is the sum of the two orange curves.

This is depicted for the 2D case in fig. 4.3 as e.g. the orange curves, but other alternatives exist which wrap multiple nodes (purple) or traversed the 1BZ (black). The system is gapfull in θk-space when the exchange field amplitude is zero. Thus there does not exist any closed curve which gives a nonzero winding number. As long as the gap never closes on the curves considered, the winding number can not change by the same arguments as presented previously in this paper. From this argument, whenever the gap in the Hamiltonian closes at a point in the 2D Brillouin zone, the point must either be characterised by a zero winding number, or it must come in pairs of nodes with opposite winding numbers. This gives rise to a conservation law for the whole Brillouin zone: the sum of the winding numbers of the nodes must be zero for all parameters.

The physical system is extended by the momentum dimension k, which means that the topological phase of the physical system is defined by the winding number computed along curves that are constant in θ-ϕ-space and traverses the k Brillouin zone, such as the black curve in fig. 4.3 or the purple straigth curves in fig. 4.4. If we monitor these lines as we slowly turn on the exchange field amplitude, we will see that the physical system defined by such a line is trivial as long as the gap stays closed on the line, even when there appears nodes in the Hamiltonian in the 3D space. However, when the parameters of the model change, the nodes will move around. When a node with a nontrivial winding number crosses the 'integral'-lines parallel to k, the winding number changes from a trivial zero to a nonzero winding number. As an example of this, take the two straight lines in fig. 4.4 that we compute the winding along for different values of ϕ and θ. These lines are separated by a line node. If the circular line integral, eq. (4.16), around this line node is $n_{\mathrm{W},\mathcal{C}} \neq 0$, the two straight integral-lines must have a winding number difference of $n_{\mathrm{W},\mathcal{C}}$. Therefore at least one of the lines represents a system with MBS at the boundaries as both can not be zero. To say it another way, the line nodes in the 3D space are boundaries between regions with different topological

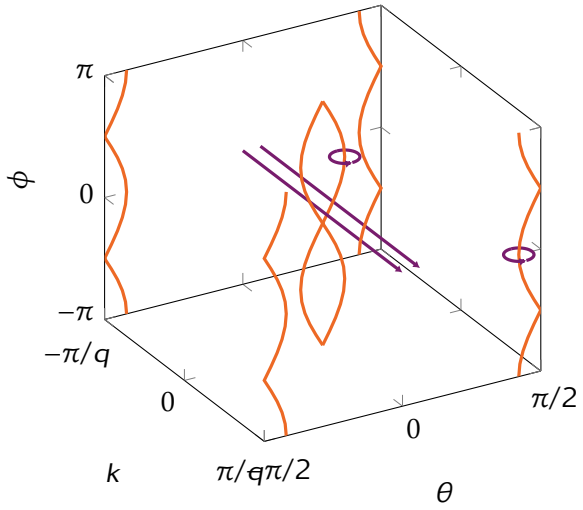

Figure 4.4: Examples of line nodes and line integrals in $k\theta\phi$-space. The orange lines schematically represent line nodes whereas the purple circles or lines (traversing the whole 1BZ) represents line integrals that may have a nontrivial winding number. All the purple curves are topologically different, meaning that they can not be continuously transformed to each other without closing the gap. The straigth lines are the lines that give the topological phase in the physical system extended by the k-dimension.

phases.

4.5 High symmetry points

Looking at the phase diagrams in figs. 4.1 and 4.2, the symmetries of the phase diagram clearly stands out. The winding number is antisymmetric with respect to $\theta = 0$. This is because the two systems obtained by θ and $-\theta$ are mirrored versions of each other. When the sign of θ is flipped, the y-component of the exchange field flips and the elliptical pattern changes direction. Thus, an eigensolution, u, to the Hamiltonian $H(\theta)$, with the y-spin flipped (cf. eq. (4.10)),

$$u \longrightarrow \sigma_x u$$

will be a solution to the θ-flipped Hamiltonian $H(-\theta)$. This can be seen by the following proof.

Proof. Assume that the eigensolution u satisfies the eigenvalue problem, $H(\theta)u = Eu$ and that the chiral symmetry is unbroken, that is, $h_z = 0$. Then the transformed eigensolution, $\sigma_x u$, is an eigensolution of the Hamiltonian $H(-\theta)$ with the same energy. That is $H(-\theta)\sigma_x u = E\sigma_x u$:

$$\begin{aligned} H(-\theta)\sigma_x u &\overset{(4.10)}{=} \sigma_x H(\theta)\sigma_x\sigma_x u \\ &= \sigma_x H(\theta)u \\ &= E\sigma_x u \end{aligned}$$

□

Alternatively, this transformation can be combined with the TR operator to give a momentum-reversed and y-spin-flipped solution given solely by the complex conjugation

$$u \to Ku. \tag{4.17}$$

which satisfies

$$H(k,\theta)u = Eu \implies H(-k,-\theta)Ku = EKu.$$

Because the energies and the eigensolutions for the two different Hamiltonians obtained with opposite signed θ are unitarily connected, it follows that they must both be topologically trivial or non-trivial at the same time. But it does not mean that they are compatible, as is seen in the difference in sign of the winding number. This is because the operator which transforms between them does not commute with the chiral symmetry operator.

In addition to the antisymmetry with respect to $\theta = 0$, the phase diagram is also symmetric to $\phi = 0$ (and similar points where the exchange field vectors are mirror symmetric). This is true for any combinations p/q, not just the two which were shown in the previous section. This symmetry in the phase diagram is related to the two symmetries given in eqs. (4.13) and (4.14), which exists around any ϕ point with mirror symmetry.

When θ, which controls the eccentricity of the ellipse, approaches $\pi m/2$, $m \in \mathbb{Z}$, the ellipse is flat along either the x or y axis. This means that all the exchange field vectors are collinear. We already know that collinear exchange fields gives rise to systems which are either in a topological trivial region or are marginal topological and between two topological phases with opposite winding numbers. With the exchange field parameterised by eq. (4.2), the system is always topological trivial for a general ϕ for these extreme values of θ except at the points

$$\phi = \begin{cases} \pi(n - \frac{2p}{q}m), & \text{when } \theta = \pi l \\ \pi(n + \frac{1}{2} - \frac{2p}{q}m), & \text{when } \theta = \pi/2 + \pi l \end{cases} \tag{4.18}$$

for any integers l, m and n. At all other values, the exchange field is uniformly zero. When all exchange fields are zero, the transformation which was done to make the exchange field vectors collinear (cf. eq. (3.26)) is then arbitrary and in principle independent of the angles between the zero-length exchange field vectors. The system is then equivalent to a normal s-wave superconductor. However, at the special points as given in eq. (4.18) when $\theta = m\pi/2$, the exchange field pattern has one (two) non-zero exchange field vector in the unit cell in the odd (even) case with same (opposite) direction, whereas the rest of the vectors are zero. It is a well known fact that s-wave superconductors in general are more compatible with AFM magnetic ordering than FM magnetic ordering, since the momentum of the electrons in the Cooper pairs are more compatible. Therefore, we expect that the Hamiltonians obtained in the case considered here is more able to close the gap in the odd unit cell than in the even unit cell, since the first has a net magnetic moment. Taking a closer look at the phase diagrams in the latter section, we see that there are qualitative differences between the two diagrams close to the $\theta = 0$, $\phi = 0$ point. In the first phase diagram where the unit cell is odd, this high symmetry point divides two different topological phases with opposite winding numbers provided that the exchange field is strong enough and the system is away from half-filling. That is, when we open the ellipse by changing θ, the system goes straight into a topological phase. This is no different than the marginal topological systems we discussed earlier. Interestingly enough, this is not always true in the odd

case. Take for instance the subfigure **c5)** of fig. 4.1 where the chemical potential is very low. Here we see that close to the $\theta = 0$, $\phi = 0$ point the system is trivial when θ is varied, whereas when θ is varied together with ϕ (at an angle in the phase diagram) a non-trivial phase can be achieved.

On the other hand, when the unit cell is even as shown in the second phase diagram (fig. 4.2), the system obtains a trivial phase when θ is varied from 0, as seen as the bubble-like shapes of trivial topology in the phase diagram close to these high symmetric points. When the ellipse is opened up significantly (θ approaching $\pi/4$) however, the system is again able to close the gap and go into a topologically non-trivial phase.

4.5.1 Marginal topological phases

When the exchange fields are mirror symmetric and collinear ($\theta = \phi = 0$), the system may lie between two topologically non-trivial phases with opposite winding number. This means that the winding number, which is a path integral along lines parallel to the k-axis in the space spanned by θk, changes at $\theta = 0$. We remind the reader that this winding number is computed from the determinant of the off diagonal part of the Hamiltonian in the chiral basis, $|A_k|$. This determinant is continuous in the θk-space, and followingly we may define closed loops other than the ones that run parallel to the k-axis. Indeed, if we define a curve similar to the purple curve drawn in fig. 4.3, which goes parallel to k for an infinitesimal value $\theta = 0^-$ and through the whole Brillouin zone, then goes from $\theta = 0^-$ to $\theta = 0^+$, then goes back along k and in the end closes the path, the winding number computed along this path must be exactly equal to the winding number difference of the winding number at $\theta = 0^-$ and the one at $\theta = 0^+$. Here we assume that the curve does not pass through nodes of the Hamiltonian where the integrand $\frac{\mathrm{d}\det A_k}{\det A_k}$ blows up and is undefined. The reason for this equivalence is that the short sides of this path are negligible when θ approaches zero. Also, the integral can only change whenever the path that we integrate along passes through a node in the Hamiltonian.

If the winding number along the purple curve is non-zero, we expect that there are at least one source of 'winding' at the $\theta = 0$ line. Such a source of winding can only be located at places where the Hamiltonian has nodes. Thus we expect that the Hamiltonian is gapless at the $\theta = 0$ line when the system is marginally topological. In fig. 4.3 we have schematically drawn to nodal points that each have a winding of $+1$ when we integrate along CCW curves that encloses them (orange). Thus a regular winding number n_W at $\theta = 0^+$ subtracted from the winding number at $\theta = 0^-$ is the sum of the winding numbers on the orange curves. If the nodal points of the Hamiltonian does not lie in the $\theta = 0$ line, the integral along the purple curve is zero, which means that the regular winding number close to $\theta = 0$ is zero and followingly the system is not in a marginally topological phase.

As an example, we consider the system with three atoms in the unit cell. When the exchange field amplitude is gradually turned on, the energy gap eventually closes at a non-zero k on the $\theta = 0$ line. This transition is shown in fig. 4.5. If we define a small curve that encloses this point and compute a winding number along it, it will be zero before the gap closes, because it can be continuously deformed into a small point without passing a gap. When eventually the gap closes inside this curve as we turn on the exchange field, the winding number must still be zero since the gap has not been closed *on* the curve yet, only inside it. However, when the amplitude is further increased, two nodes appear from this gap closing, as can be seen in the purple curve in fig. 4.5. If we wrap a curve around each of the nodes, we will see that they each have

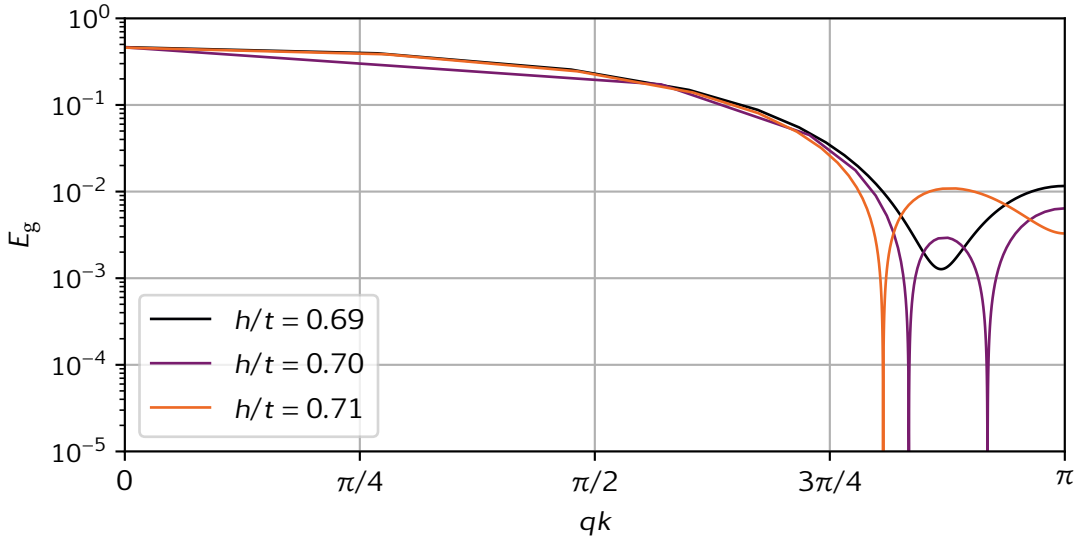

Figure 4.5: Energy gap at $\phi = 0$, $\theta = 0$ line varying h. The parameters are $\mu = -1.4t$, $\Delta = 0.3t$ and $p/q = 1/3$.

a non-zero winding number and since they must sum to zero, they have opposite signs. The determinant of the off-diagonal matrix A_k and the energy gap was computed for the parameters used in the purple curve in fig. 4.5 for a region in θk-space, which is shown in fig. 4.6. The arrows in this figure point in the direction of the determinant in the complex plane, while the contours represents the logarithm of the energy gap, with the darkest colours being the smallest gap. By following the arrows around each of the two nodes in this region, one can visually see how the winding takes place. Following a CCW path around the left node, one can see that it winds one time CCW, whereas the arrows turn one time clockwise (CW) when a CCW path around the right node is followed. The two nodes were initially created as a pair at the same point when the exchange field amplitude reached a certain threshold between $0.69t$ and $0.7t$. Initially, these nodes are created on the $\theta = 0$ line, both at some $k = k'$ and at $k = -k'$ due to TR and PH. When the exchange field amplitude is further increased, the nodes in each pair move independently of each other along the $\theta = 0$ line. Eventually, the nodes with the same winding number from each pair meets at a time reversal invariant momentum, and subsequently they are allowed to move along these fixed momentum along the θ-axis. This is shown in fig. 4.5, where the node pair is initially created close to $h = 0.7t$, and one node moves toward $k = 0$ and the other moves towards $qk = \pi$, and finally when h is large enough, the latter node disappears from the $\theta = 0$ line and moves into non-zero values of θ, as seen for the orange curve in fig. 4.5. As soon as one of the nodes moves into non-zero values of θ, the superconductor is marginally topological at $\theta = 0$: Two nodes with the same winding numbers are located at the $\theta = 0$ line, while the other two nodes with opposite winding numbers of the first two are located at $(qk, \theta) = (\pi, \pm\theta')$. Thus the line integrals along the k-axis at $\theta = \pm\delta\theta$ have different winding numbers. The sign change in the winding is due to a sign change in the imaginary part of the determinant, $|A_k|$ as explained in section 3.3.

The marginal topological phase at $\theta = 0$ also underlines another key point for topology in magnetism coupled to superconductivity. At this line, the system is inversion symmetric due to the lack of a h_y component in the spin-texture, but has broken conventional TR symmetry ($\mathcal{T}^2 = -1$ is broken, but we still have $\mathcal{T}^2 = +1$). As soon as inversion is broken by a nonzero θ value, the system becomes topological nontrivial. This

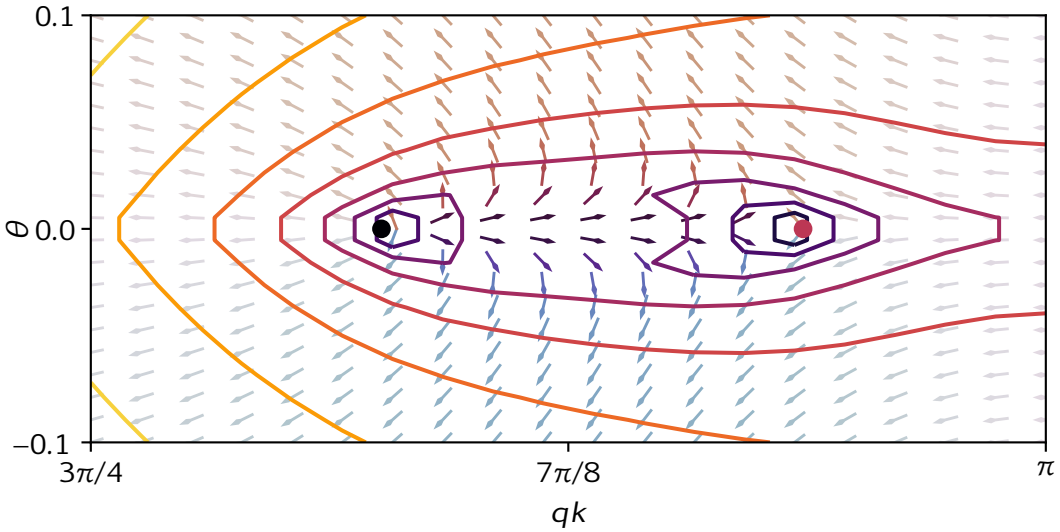

Figure 4.6: Energy contours and winding around nodes in the θ-k-plane. The contours go from dark (smallest) to light yellow (largest) energy gap measured by the logarithm of the smallest energy. The arrows point in the direction of the complex number $|A_{k\theta}|$ in the complex plane. The black and red dots are nodes in the Hamiltonian. As can be seen visually, the arrows around each node winds opposite of each other. By following a CCW curve around the left node, a winding of +1 will be obtained, while the right will have a winding of −1, thus summing up to 0.

underlines the importance of both conventional TR symmetry breaking and inversion symmetry breaking to achieve a topological phase. We also note that both symmetries need to be broken, as we can imagine a superconductor coupled to a semiconductor with a Rashba SOC. As we have already explained, when there is no TR symmetry breaking (no magnetism), such a Hamiltonian can be spin-rotated to reconstruct the inversion symmetry, where we end up with a pure conventional superconductor. However, when the conventional TR is broken by a magnetic field, the inversion symmetry can in general not be reconstructed since the exchange field vectors will interfere.

4.6 Chiral symmetry breaking

As long as the h_z component 0 the Hamiltonian has both TR symmetry and PH symmetry, and thus also chiral symmetry, but when the out-of-plane component of the exchange field is nonzero, the TR symmetry and consequently chiral symmetry is broken. As a result, we can no longer define a winding number on the Hamiltonian. Instead we can use the PH symmetry to compute the Pfaffian at the time reversal invariant momenta as in the Kitaev model (Chen & Schnyder, 2015). Tewari and Sau (2012) showed that the Pfaffian computed on the topological nanowires as the ones considered here gives the parity of the winding number. Since the system only has nearest neighbour hopping and simple s-wave superconductivity, the Pfaffian and the winding number will always give the same topological phase. If the absolute value of the winding number were able to be larger than 1, the Pfaffian would be trivial when the winding number were ±2. As long as the chiral symmetry is conserved, the winding number would give the correct number of MBSs at each boundary. If the chiral symmetry is broken,

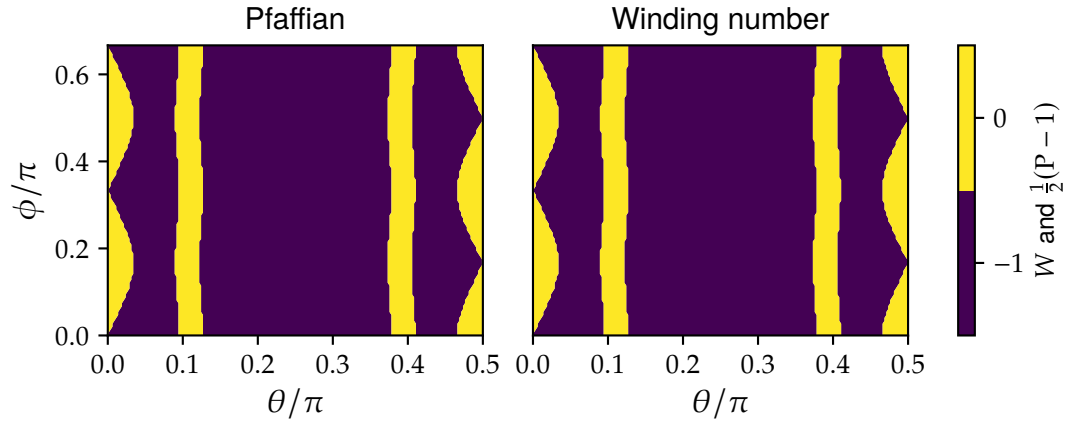

Figure 4.7: Comparison of phase diagram computed with the Pfaffian or winding number when the chiral symmetry is unbroken. The parameters were $p = 1$, $q = 3$, $h = 2.76t$, $\Delta_0 = 0.3t$ and $\mu = -1.41t$.

the MBSs can in general interact and as a consequence pair up and gap out. If there are an odd number of MBSs, there will always be one MBS left after such an interaction, whereas if there are an even number of MBSs, there is no such guarantee. This explain how the Pfaffian is connected to the winding number even in systems with larger values of the winding.

The Pfaffian can not change without the gap closing at a time reversal invariant momentum, and thus we expect that the nodal points (lines) in the two (three) dimensional space spanned by $k\theta$ ($k\theta\phi$) are not only protected by the topological winding number around these objects, but also by PH. The out-of-plane exchange field may move the nodes, but it may only do so in a continuous manner. From this we expect the topological phases in the chiral model to continuously develop as the chiral symmetry is increasingly broken. In other words, if a given Hamiltonian is located deep inside a topological area in the phase diagram and therefore has MBS at the boundaries, we expect that the addition of an out-of-plane field will not remove the MBSs, but may only do so by closing the bulk energy gap first. A comparison of the Pfaffian and the winding number is shown in fig. 4.7 in a case which has the chiral symmetry intact, since this is the only case where the winding number can be computed for the comparison. As the figure makes clear, whenever the Pfaffian topological invariant is nontrivial ($\operatorname{sign}\operatorname{Pf} H = -1$), the winding number is also nontrivial. However, the Pfaffian being a $\mathbb{Z}_2$ number and the winding number being a $\mathbb{Z}$ number, the Pfaffian can not give us the sign of the winding number.

When the chiral breaking term h_z is introduced in the model, the phase diagram is modified as shown for the specific case of an odd unit cell of three atoms in fig. 4.8. We note a few interesting behaviours as seen in this figure. First, the phase diagram as shown in **a)** changes most close to $h_z = \Delta_0$. This is close to the point where the s-wave energy gap is closed in a ferromagnetic field. Close to this field strength, new nodal points are created in pairs at TR symmetric momenta k on the θ line which subsequently move around and may merge again with the initial nodes to gap them out. That is, one pair is created, call the nodes A and B. A can then merge with an initial node C and gap out, while B can merge with an initial node D and gap out. The result is that two nodes are removed in total. Second, when $h_z = \Delta_0$, the nodal points in $k\theta$-space extend into line nodes instead, as shown in fig. 4.9. These line nodes may

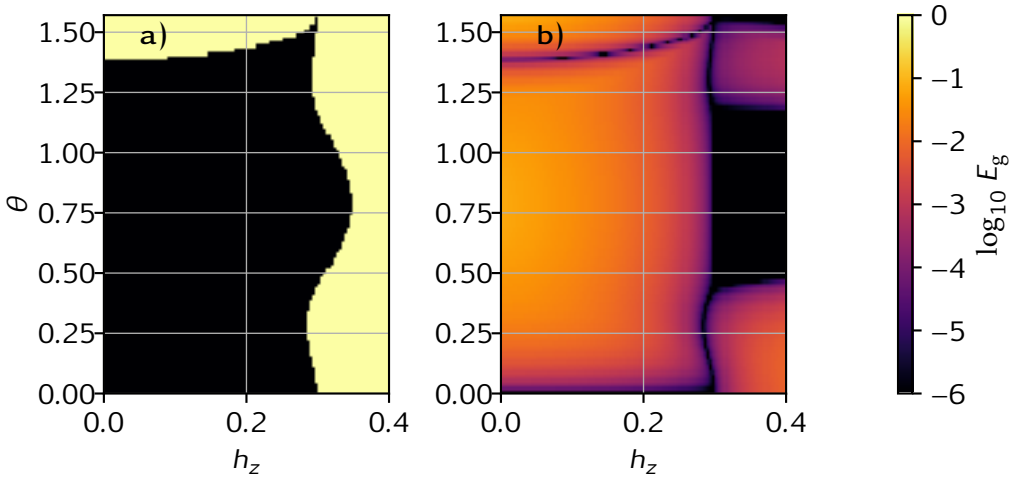

Figure 4.8: Phase diagram in θ-h_z space and the energy gap. When h_z is close to the superconducting order parameter in size, Δ_0, the phase diagram changes significantly. But for $h_z > \Delta_0$ the phase diagram still has nontrivial areas. However, these regions are gapless and can thus not support MBSs. The parameters were $\mu = -t$, $h = t$, $\Delta_0 = 0.3t$, $\phi = 0$ and $p/q = 1/3$.

extend into non time reversal symmetric k and at values of θ where the Hamiltonian has a nontrivial topological invariant. Thus at these points the Hamiltonian becomes gapless, and the sign of the Pfaffian of the Hamiltonian is undefined. Although the sign of the Pfaffian as computed at $k = 0$ and $qk = \pi$ is still defined, the sign of the Pfaffian for the Hamiltonian as a whole is not defined because of the nodes. In addition, presence of nodes in the bulk Hamiltonian means that the MBS at the edges can interact through the bulk and thus gap out. Thus we conclude that whenever the gap is closed, but the Pfaffian at the TR invariant k is nontrivial, the system is in a trivial phase. This is of importance later, when we investigate the effects of sudden quenches in the out-of-plane field, h_z both to subcritical values below Δ_0, and supercritical ones.

4.7 Conclusion

The s-wave superconductor with an elliptical magnetic texture belongs to the class BDI and has a winding number topological invariant. In addition, depending on the number of lattice sites in the unit cell, the system may have an additional nonsymmorphic symmetry in 1D. This symmetry in principle allows an extra $\mathbb{Z}_2$ number in addition to the winding number. However, we did not find combinations of the parameters where this number was nontrivial.

When the exchange field is helical, we already know analytically that the lowest exchange field which puts the system in the topological phase is obtained when the chemical potential is at the top or bottom of the energy bands when no field is applied. That is, the system is either full or empty. The phase diagram indicates that the same applies to the elliptical systems in general for other values of θ than just $\pi/4$. The phase diagram was also different for even and odd unit cells, where the odd unit cell could be marginal topological at $\theta = \phi = 0$ and equivalent points, whereas the even unit cell has a trivial phase close to these points. This is likely due to the difference between

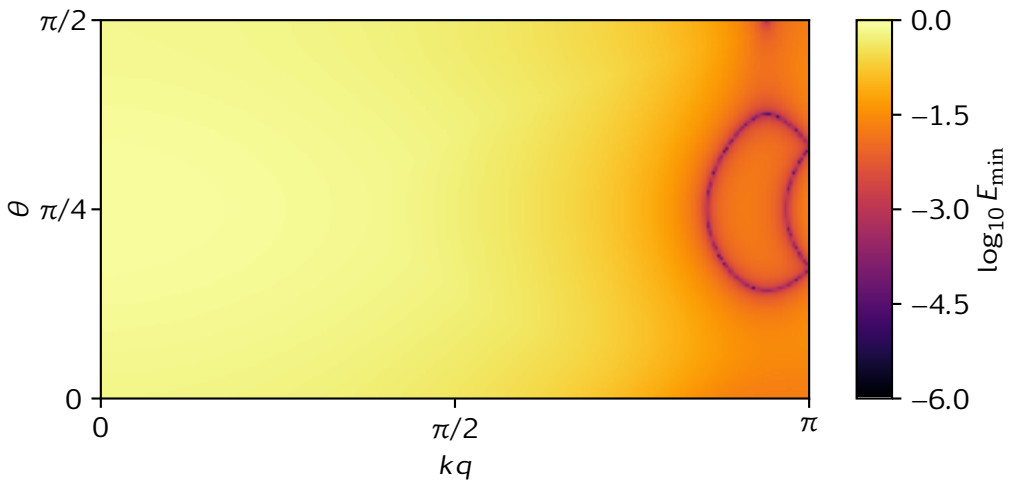

Figure 4.9: Energy gap in the $k\theta$-plane for a system with broken chirality. The nodal points are turned into nodal lines when $h_z \geq \Delta_0$. The parameters are $h = -\mu = t$, $h_z = 0.32t$, $\Delta_0 = 0.3t$, $\phi = 0$ and $p/q = 1/3$.

the qualitative exchange field close to these points. In the even case, the net magnetic moment in the unit cell is always zero, whereas it is nonzero for odd unit cells close to this point.

In the space spanned by k and θ the system still belongs to the AZ class BDI, which is a trivial class. But, it meant that it had symmetry protected nodes, and in the case of the third dimension ϕ, there were symmetry protected lines. These nodal points (lines) are protected by a well defined winding number due to the chiral symmetry. Thus, these nodes generate nontrivial winding when we look along lines parallel to the k-axis, which is the winding number which gives rise to MBSs in the 1D finite system. Since the nodes had winding numbers, this meant that equal winding number nodes would not interact, but opposite nodes could interact and gap out.

When the chiral symmetry breaking out-of-plane exchange field, h_z, was turned on, the nodal points did not gap out, which indicates that they are also protected by the PH symmetry. It was also seen that the previous nontrivial winding number was connected to a nontrivial Pfaffian invariant. As a consequence, the MBS in the chiral case do not gap out when the chiral symmetry is broken, and still require the bulk energy gap to close to disappear. When the h_z component reached a critical value, equal to the superconducting order parameter Δ_0, the point nodes in the $k\theta$-plane turned into connected line nodes. These line nodes extended into the Brillouin zone, and leads to the gap closing for ranges of θ-values. Since the line nodes in general were not located at the time reversal invariant momenta, a Pfaffian invariant was still possible to compute. However, since the gap closed at non-time reversal invariant momenta, this meant that the Pfaffian invariant was meaningless, and no MBSs were present at the edges.

5 | Time-dependent driving

Until now we have only considered static Hamiltonians, or by extension, adiabatic changes in the Hamiltonian. We will now consider time-dependent Hamiltonians where the characteristic time-scale is short enough to excite states and affect the time-evolution of the Hamiltonian. Knowledge about the dynamical properties of topological systems is important in practical use cases as for example in quantum computers, since the MBSs will be quickly turned on and off and moved around in such setups. For instance, there are suggestions of systems with quantum gates which can be turned on and off to braid the Majorana states which rely on the behaviour during fast driving (Alicea et al., 2011; Amorim, Ebihara, Yamakage, Tanaka & Sato, 2015; Scheurer & Shnirman, 2013). Examples of important characteristics are the robustness of the MBSs, the oscillations of them after a quench or the ability to destroy them effectively by altering the parameters.

In particular, we will consider quenches in the Hamiltonian of the elliptical model presented in chapter 4, either within the same topological phase, to a phase boundary or across a phase transition. This is a general problem in quantum mechanics and in the framework of topological quantum systems has been faced by many authors (Bermudez, Patanè, Amico & Martin-Delgado, 2009; Bonnes, Essler & Läuchli, 2014; Pyka et al., 2013; Sacramento, 2016, 2014). During a sudden quench of parameters within a finite size system, the fate of the edge states depends on whether the initial and final state are both topological or if the final phase is trivial. In the first case, if the topological invariant is the same before and after the transition the probability of finding MBSs will in general decay to a finite nonzero and non-unity value. In the latter case, when the system is quenched to a topologically trivial phase, the survival probability will either oscillate as the edge state moves between the boundaries of the finite system (Perfetto, 2013; Sacramento, 2016) or it can quickly decay to zero with minor erratic peaks.

In general, we want to solve the time-evolution of single particle states given a Hamiltonian that is time-dependent, $H(\tau)$. We choose to denote the time variable by τ to discern it from the hopping strength parameter t. The characteristic equation we need to solve is then the time-dependent Schrödinger equation,

$$i\hbar\frac{\partial}{\partial\tau}\left|\psi(t)\right\rangle = \hat{H}(t)\left|\psi(t)\right\rangle. \tag{5.1}$$

We set $\hbar$ to unity in the following, which effectively sets the time scale to $\hbar/t$ (t has the unit J and defines the energy scale, whereas $\hbar$ has the unit Js). The time-evolution operator is the operator that transforms the eigenstates from an initial time τ_0 to a later time τ, and is

$$U(\tau,\tau_0) = e^{-i\int_{\tau_0}^{t}\mathrm{d}\tau'\hat{H}(\tau')}, \tag{5.2}$$

assuming the Hamiltonians at different times commute. The Schrödinger equation can then be rewritten as

$$i\frac{\partial}{\partial\tau}U(\tau,\tau_0)\left|\psi(\tau_0)\right\rangle = \hat{H}(\tau)U(\tau,\tau_0)\left|\psi(\tau_0)\right\rangle. \tag{5.3}$$

The initial state can be decomposed in the eigenenergy states

$$\left|\psi(\tau_0)\right\rangle = \sum_n c_n(\tau_0)\left|\psi_n(\tau_0)\right\rangle \qquad \text{with } \sum_n |c_n|^2 = 1 \tag{5.4}$$

$$\hat{H}(\tau_0)\left|\psi_n(\tau_0)\right\rangle = E_n(\tau_0)\left|\psi_n(\tau_0)\right\rangle \tag{5.5}$$

We write the Hamiltonian as

$$\hat{H}(\tau) = \sum_n E_n(\tau)\left|\psi_n(\tau)\right\rangle\left\langle\psi_n(\tau)\right|. \tag{5.6}$$

We will only consider states of the systems in question that are given by the ground-state plus one excitation, and assume that the system stays in the one excitation subspace. Thus we only need to follow the dynamics of the the excited state through the time evolution of the Hamiltonian.

5.1 Quenching

Quenching of the Hamiltonian, also referred to as the sudden approximation, is when the changes in the Hamiltonian happen over a time interval which is significantly shorter than the inverse energy differences over the transition, $\hbar/|E_n^f - E_l^i|$, where E_n^f are the energies in the final Hamiltonian and E_l^i are the energies in the intermediate Hamiltonian (Jacob Linder, 2017). Thus, before such a sudden change occurs in the Hamiltonian, the systems time-evolution is given by an initial Hamiltonian, whereas after the change the time-evolution is given by a different Hamiltonian with in general different energies and eigenvectors. Imagine that the Hamiltonian is given by $\hat{H}_0 = \hat{H}(\xi_0), \tau < \tau_0 = 0$ for an initial set of parameters ξ_0, and $\hat{H}_i = \hat{H}(\xi_i), \tau_{i-1} < \tau < \tau_i$ at different times for other sets of parameters, where τ_i satisfies $\tau_i > \tau_{i-1}$. In each time interval the eigenstates of the Hamiltonian are $\hat{H}(\xi_i)\left|\psi_n(\xi_i)\right\rangle = E_n(\xi_i)\left|\psi_n(\xi_i)\right\rangle$. Thus, before the first quench the system has the eigenstates $\left|\psi_n(\xi_0)\right\rangle$. Inside each time interval where the Hamiltonian is constant, the time evolution operator is

$$U_{\xi_i}(\tau,\tau_{i-1}) = \sum_n e^{-iE_n(\xi_i)(\tau-\tau_{i-1})}\left|\psi_n(\xi_i)\right\rangle\left\langle\psi_n(\xi_i)\right|. \tag{5.7}$$

Since we are working in the sudden approximation, and the Schrödinger equation is a linear and continuous equation, the time-evolution operator must also be continuous on the whole time-line. Thus, the total time evolution operator is simply the time-evolution operators 'glued' together at the intersecting times. For the times $\tau_{j-1} < \tau < \tau_j$ the time evolution operator is

$$U(\tau,\tau_0) = U_{\xi_j}(\tau,\tau_{j-1})U_{\xi_{j-1}}(\tau_{j-1},\tau_{j-2})\cdots U_{\xi_1}(\tau_1,\tau_0). \tag{5.8}$$

Written out, the time-evolution operator is

$$U(\tau) = \begin{cases} \sum_{m_0} e^{-iE_{m_0}(\xi_0)\tau} \left|\psi_{m_0}(\xi_0)\right\rangle\left\langle\psi_{m_0}(\xi_0)\right|, & \tau \le 0 \\ \sum_{m_1} e^{-iE_{m_1}(\xi_1)\tau} \left|\psi_{m_1}(\xi_1)\right\rangle\left\langle\psi_{n_1}(\xi_1)\right|, & 0 \le \tau \le \tau_1 \\ \sum_{m_2 m_1} e^{-iE_{m_2}(\xi_2)(\tau-\tau_1)} e^{-iE_{m_1}(\xi_1)\tau_1} & \\ \qquad \left|\psi_{m_2}(\xi_2)\right\rangle\left\langle\psi_{m_2}(\xi_2)\middle|\psi_{m_1}(\xi_1)\right\rangle\left\langle\psi_{m_1}(\xi_1)\right|, & \tau_1 \le \tau \le \tau_2 \\ \ldots, & \ldots \end{cases}. \tag{5.9}$$

Here it can be seen that each time evolution operator projects the old states at the end of the previous time interval onto its own states, which is then time-evolved according to the new energies. When the time, τ, is in the beginning of an interval, say $\tau = \tau_i$, we see from eq. (5.7) that $U(\tau = \tau_i, \tau_i) = \mathbb{1}$ due to the completeness relation, meaning that the transition from one set of parameters to another is a continuous one.

We now consider the case where we have an initial state which is an eigenenergy state of the Hamiltonian for times $\tau < \tau_0$. We denote this state $\left|\psi_{m_0}(\xi_0)\right\rangle$, where the subscript 0 in m_0 means that it is the m_0 eigenstate of the Hamiltonian with parameters ξ_0. We wish to inspect the probability that we observe an eigenstate, $\left|\psi_{n_0}(\xi_0)\right\rangle$ of the initial Hamiltonian at a later time τ after the system has evolved according to the quenches that have been applied. Thus at time $\tau > \tau_0 = 0$, the system is in the state

$$\left|\psi(\tau)\right\rangle = U(\tau, \tau_0)\left|\psi_{m_0}(\xi_0)\right\rangle. \tag{5.10}$$

The probability to find the initial state at time t is then the overlap of the two states squared:

$$P_{n_0,m_0}(\tau) = \left|\left\langle\psi_{n_0}(\xi_0)\right| U(\tau, \tau_0)\left|\psi_{m_0}(\xi_0)\right\rangle\right|^2. \tag{5.11}$$

Let for example $0 < \tau < \tau_1$, then the probability to find the eigenstate labelled n_0 is

$$P_{n_0,m_0}(\tau) = \left|\left\langle\psi_{n_0}(\xi_0)\right|\left(\sum_{m_1} e^{-iE_{m_1}(\xi_1)\tau}\left|\psi_{m_1}(\xi_1)\right\rangle\left\langle\psi_{m_1}(\xi_1)\right|\right)\left|\psi_{m_0}(\xi_0)\right\rangle\right|^2 \tag{5.12}$$

$$= \left|\sum_{m_1} e^{-iE_{m_1}(\xi_1)\tau}\left\langle\psi_{n_0}(\xi_0)\middle|\psi_{m_1}(\xi_1)\right\rangle\left\langle\psi_{m_1}(\xi_1)\middle|\psi_{m_0}(\xi_0)\right\rangle\right|^2. \tag{5.13}$$

5.1.1 Numerical method

To proceed numerically, we choose a common basis to compute all the eigensolutions in. The position basis is a natural choice when we are dealing with systems with finite size. Thus, for each set of parameters and accompanying Hamiltonian, we compute the set of eigenvectors that solve the BdG-equation (eq. (2.28)). As a reminder, the result of such an equation is an array of energies, $(E_1(\xi_i), E_2(\xi_i), \ldots)$, and a matrix, V_{mn}, where the columns are the eigenvectors of the BdG matrix. For a given constant Hamiltonian the time-evolution operator, which is now a matrix, is

$$U_{ij}(\tau) = \sum_n e^{-iE_n(\xi_i)\tau} V_{in}(\xi_i)(V(\xi_i)^\dagger)_{nj}. \tag{5.14}$$

The matrix product of the distinct time-evolution operators for each time interval is computed with the newest time-evolution operator in the left and the oldest on the

right in the matrix product. When we finally want to compute the probability to find the system in a final eigenenergy-state m_f given an initial eigenenergy-state m_i, we compute the probability matrix, given by

$$P_{m_f m_i}(\tau) = \left| \left(V^\dagger(\xi_f) U(t) V(\xi_i) \right)_{m_f m_i} \right|^2, \tag{5.15}$$

while if the initial and final states, given by the vectors v_i and v_f in the Hilbert space respectively, are not eigenenergy-solutions but some arbitrary composed states, the probability is

$$P(f, i, \tau) = \left| v_f^\dagger U(\tau) v_i \right|^2. \tag{5.16}$$

5.1.2 Oscillations

A possible effect that may arise from sudden quenches in *finite systems* is that of oscillations in the survival probability. Such oscillations can be understood in the context of repeated reflections internally in the system. Thus, if a wave packet does not disperse too much during the traversal of the system after a quench, it must eventually appear back where it began with a nonzero overlap with the initial wave function and therefore a nonzero survival probability. Depending on the degree of the dispersion of the wave packet, the survival probability may repeat with the same peak heights or decay as the wave packet is more uniformly distributed inside the finite system. Take for example a MBS at the boundary of a finite system before a quench. This energy eigenstate of the Hamiltonian is prohibited from entering the bulk because of the band gap which is located there. However, if the system is suddenly quenched from this nontrivial topological phase to a trivial one, the in-gap zero-energy states (the Majoranas) disappears and are now located inside the bulk-energy spectrum. In general there is nothing which says that the Majorana modes must overlap mainly with edge states, if they still exist, and we expect that the Majorana modes will overlap with a range of eigenenergy states around the band gap. Since many of these eigenstates will be bulk-states in the new Hamiltonian, the previous Majorana mode now start to move through the bulk. The wave packet form and dispersion will then depend on the dispersion relation for the new Hamiltonian and the details of the overlap between the Majorana modes in the old Hamiltonian and the bulk modes in the new Hamiltonian.

We can take this analysis further and consider various forms of the dispersion relation of the new Hamiltonian and the effects on the dispersion of the resulting wave packet and thereby the behaviour of the survival probability. If we assume that the Majorana modes mainly overlap with the eigenstates closest to zero in energy after the quench, we can describe the result in terms of the dispersion limit close to the edge of the energy band. In this regime, the Hamiltonian can be qualitatively described by two types of fermions: massless (Dirac node) and massive fermions. The difference between the two types of dispersion relations is that the massless type has a constant phase velocity and also group velocity, whereas the massive fermion one has a nonzero double derivative of the dispersion relation with respect to the momentum,

$$\partial_k^2 E(k) \neq 0. \tag{5.17}$$

The difference between these dispersion relations is that the first is non-dispersive whereas the latter is, meaning that a massive wave-packet will widen over time and eventually be uniformly distributed in the finite system after enough reflections. Thus if there are oscillations at all, we can expect a survival probability which is peaked with a constant period but decaying over time.

The long term survival probability of a Majorana mode can be approximated when the system is quenched once such that the topological phase of the ground state is unchanged. This probability is in most cases the constant probability value that the survival probability oscillates around. In that case, if there are, for example, two Majorana modes in the first Hamiltonian, then there will also be two Majorana modes in the second Hamiltonian. We refer to these Majorana modes as $|\gamma_1(\xi_i)\rangle$ and $|\gamma_2(\xi_i)\rangle$ for the Hamiltonian with the parameter set denoted ξ_i. These Majorana modes are numerically chosen as the two eigenenergy solutions with the lowest energy, which due to PH are the two eigenstates in the middle in a list of eigenstates sorted by energy. If we are interested in the long term survival probability of one of the Majorana modes in the initial system, say $|\gamma_1(\xi_0)\rangle$, we compute the overlap of this mode onto the new Majorana modes. Since the initial modes and final modes have 0 energy, the evolution operator will be constant if we focus only on the subspace of states which are the Majorana states. Thus the evolution operator is approximately

$$U(\tau) = |\gamma_1(\xi_1)\rangle\langle\gamma_1(\xi_1)| + |\gamma_2(\xi_1)\rangle\langle\gamma_2(\xi_1)|, \tag{5.18}$$

and the survival probability is then approximately

$$\begin{aligned} P_{\gamma_1,\gamma_1}(\tau) &= \left|\langle\gamma_1(\xi_0)|\, U(\tau)\,|\gamma_1(\xi_0)\rangle\right|^2 && (5.19)\\ &= \left|\langle\gamma_1(\xi_0)|\gamma_1(\xi_1)\rangle\langle\gamma_1(\xi_1)|\gamma_1(\xi_0)\rangle + \langle\gamma_1(\xi_0)|\gamma_2(\xi_1)\rangle\langle\gamma_2(\xi_1)|\gamma_1(\xi_0)\rangle\right|^2 && (5.20)\\ &= \left|\left|\langle\gamma_1(\xi_1)|\gamma_1(\xi_0)\rangle\right|^2 + \left|\langle\gamma_2(\xi_1)|\gamma_1(\xi_0)\rangle\right|^2\right|^2. && (5.21) \end{aligned}$$

We also point out that the sudden approximation can be used to approximate any time-dependent Hamiltonian by dividing the Hamiltonian evolution into small time steps as follows

$$\begin{aligned} U(\tau,\tau') &= U(\tau,\tau-\Delta\tau)U(\tau-\Delta\tau,\tau-2\Delta\tau)\cdots U(\tau-(n-1)\Delta\tau,\tau'), \quad \Delta\tau = (\tau-\tau')/n && (5.22)\\ &\approx \exp\left\{-i\hat{H}(\tau-\Delta\tau)\Delta\tau\right\}\exp\left\{-i\hat{H}(\tau-2\Delta\tau)\Delta\tau\right\}\cdots\exp\left\{-i\hat{H}(\tau')\Delta\tau\right\} && (5.23)\\ &= \sum_{m_1\ldots m_{n-1}m_n} \exp\left\{-i(E_{m_n}(\tau-\Delta\tau)+E_{m_{n-1}}(\tau-2\Delta\tau)+\ldots+E_{m_1}(\tau'))\Delta\tau\right\}\times \\ &\quad \left|\psi_{m_n}(\tau-\Delta\tau)\right\rangle\left\langle\psi_{m_n}(\tau-\Delta\tau)\right|\left|\psi_{m_{n-1}}(\tau-2\Delta\tau)\right\rangle\left\langle\psi_{m_{n-1}}(\tau-2\Delta\tau)\right|\cdots \\ &\quad \left|\psi_{m_1}(\tau')\right\rangle\left\langle\psi_{m_1}(\xi(\tau'))\right|. && (5.24) \end{aligned}$$

This is actually a first order numerical method to solve a differential equation , specifically the forward Euler method. Other methods may be used to solve the differential Schrödinger equation, including higher order solvers as for example the well known Runge-Kutta method of 4th order (Kutta, 1901; Runge, 1895). The relation between the approximation to a continuously changing Hamiltonian and that of quenching the Hamiltonian is that a series of quenches in short succession approximates any Hamiltonian, with the numerical accuracy depending on the number of steps or equivalently the size of $\Delta\tau$.

5.2 Results and discussion

The model that we will consider in this chapter is the elliptical model analysed in the adiabatic limit in chapter 4. Experimentally, the helicity of the magnetic textures of

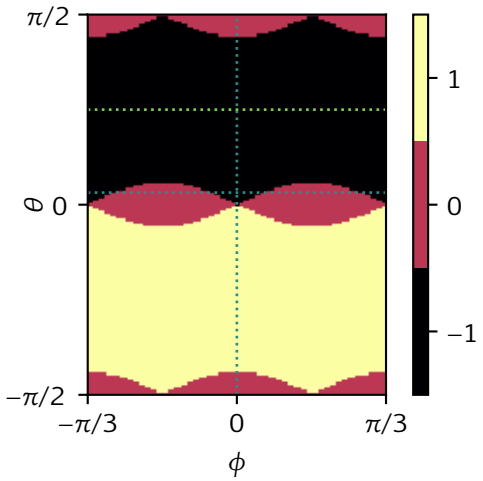

Figure 5.1: Phase diagram of the cases considered in this section. The parameters are $h = -\mu = t$, $p/q = 1/3$ and $h_z = 0$ except when stated otherwise. The lines represent the places of quenches.

such models have been tuned back and forth by external electrical and magnetic fields (Kimura & Tokura, 2008; Murakawa et al., 2008, 19; Yamasaki et al., 2008; Yamasaki et al., 2007). The offset of the spin-texture may also change during transitions or external perturbations to the system. The chemical potential (or equivalently the filling factor) can easily be modified in 1D by the application of electrical potentials and the chiral symmetry of the system can easily be broken by applying external homogeneous magnetic field. All of these methods can be used experimentally or in applications where the control of MBS is necessary, and we will therefore evaluate the robustness of the Majorana states for a range of quenches in these parameters.

5.2.1 Change in helicity

We previously mentioned how flipping the direction of rotation of the magnetic texture has been obtained experimentally for materials like some perovskites. In addition, we have seen that for cases where the unit cell is odd the system can be in a marginal topological phase, where any perturbation in the value of θ will bring the system into a topological nontrivial phase. Thus we want to evaluate the dynamics of the Majorana single particle states after the direction of the magnetic texture has been flipped ($\theta \to -\theta$) both close to and away from the value $\theta = 0$. We do this by considering quenches along the vertical line in fig. 5.1, where the two nontrivial topological phases are connected at $\theta = \phi = 0$.

We consider a sudden flip of the helicity of the magnetic texture, keeping the eccentricity of the elliptical form and without an out-of-plane field, such that the chiral symmetry is conserved. That is,

$$\theta_0 \to \theta_1 = -\theta_0.$$

For very small values of θ_0, close to the marginal region, the initial and final magnetic texture are near identical and we can expect that the initial Majorana states are compatible with the final Majorana states. When θ is increased, the flipping of the magnetic texture helicity will have more significant effects on the eigenstates, since the

y-component of the texture is increasing in size. This is confirmed in the computations shown in fig. 5.2. For a very small value of $\theta = 0.001$, the survival probability barely changes around 1, whereas for a slighly larger value of $\theta = 0.012$, large oscillations in the survival probability occur. At even larger values, the oscillations become more erratic with multiple frequency-components and the peaks no longer go to a maximum of 1. This is also shown in the fourier spectrum of the survival probability in fig. 5.3.

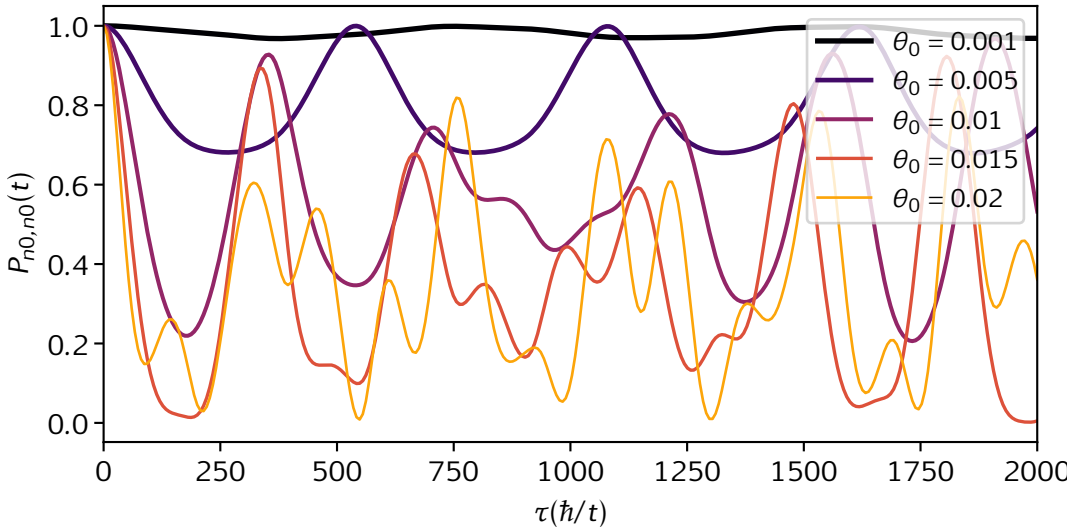

Figure 5.2: Survival probability of a Majorana state after flipping the helicity. The parameters were $h = -\mu = t$, $\phi = 0$ and $p/q = 1/3$.

As the initial θ value increased, the spectrum broadens. This is an effect of the overlap between the initial MBS and the bulk states after the quench, which due to the energy differences leads to oscillations in the probability.

If the process of flipping the direction of rotation in the magnetic texture takes some time, and slowly goes from a positive value of θ to the negative value $-\theta$, passing 0, the sudden approximation can be better approximated by inserting a new step of quenching the Hamiltonian. We can e.g. approximate such a flip as the Hamiltonian first quenching from θ_0 to $\theta_1 = 0$ and then finally to $\theta_2 = -\theta_0$:

$$\theta_0 \to \theta_1 = 0 \to \theta_2 = -\theta_0.$$

By setting the parameter τ_1 right, this is a better approximation then just a sudden quench from θ_0 to $-\theta_0$. This is because now the transitions between Hamiltonian takes half the time since the previous time step is cut in half, and thus the sudden approximation is more accurate. In fig. 5.4 the probability of one of the single particle Majorana modes to overlap with one of the Majorana modes in the final Hamiltonian as a function of the time spent in the middle case is shown. For small values of θ_0, the overlap between the initial case, the middle case and the final case is for a small range of energies close to 0, which leads to the overlap probability being almost constant and equal to 1. For larger values of θ_0 the overlap between the Majorana states in the initial and final case is zero for immediate quenches, as can be seen as the purple and yellow lines starting close to zero in probability. But for even short times in the middle case, τ_1, the overlap between the Majoranas is significant in isolated peaks. This overlap is later repeated as distinct peaks with a constant period. Thus, by tuning the transition time between the initial and final magnetic textures, or by inserting a midpoint where

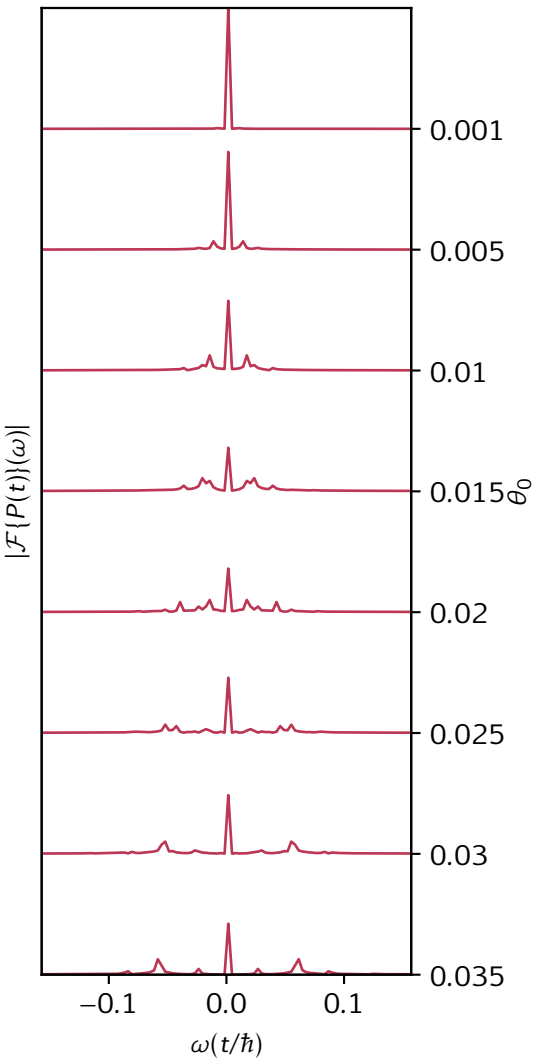

Figure 5.3: Fourier transform of the survival probability after a sudden quench in the helicity of the magnetic texture.

the ellipse is flat, the Majoranas in the initial state can be controlled to either excite a Majorana in the final system or not.

An even better approximation to continuous but fast changes in the Hamiltonian would be to use eq. (5.24) which is an even better approximation that the one used here, where we only used two time steps. A natural transition form would be to use a linear ramp of the parameters over the course of the time τ_1. It would be interesting to see the effects on the Majorana modes by varying the ramping time. From the two-step approximation in the previous paragraph, we have indications that such continuous changes in the Hamiltonian and correct timing are paths to controlling MBS effectively.

5.2.2 Change in ϕ

In the helical case we can easily compute the overlap between the old and the new Majorana states after a quench in ϕ provided that chirality is not broken. First, we note that the Hamiltonian of the model then only includes the Pauli spin matrices σ_0, σ_x and σ_y. This implies that any solution to the eigenenergy problem must have a net

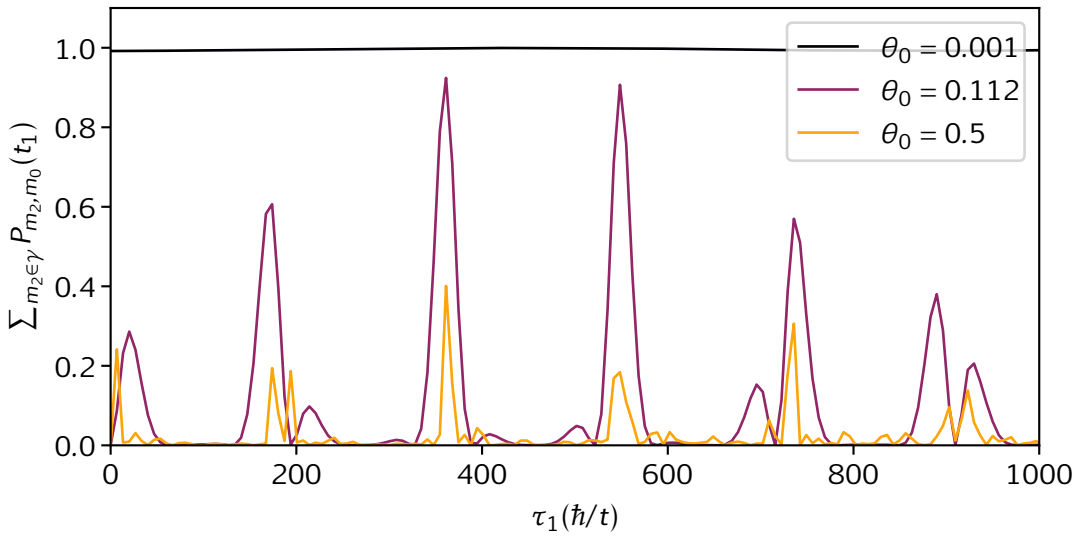

Figure 5.4: Overlap onto the new Majorana states after negating $\theta_0 \to \theta_2 = -\theta_0$ via a midpoint of $\theta_1 = 0$. The parameters were $h = -\mu = t$, $\Delta_0 = 0.3t$, $\phi = 0$ and $p/q = 1/3$.

spin in the xy-plane. Second, we note that a change in the offset ϕ is equivalent to an opposite rotation of the spin of the electrons – they are uniformly connected. The overlap between a Majorana state onto itself after a sudden quench in the parameter ϕ is then equivalent to computing the overlap between two spins rotated by the angle ϕ relative to each other. This computation can be done in any spin-plane, so we choose the xz-spin plain which is easiest. In the initial case we choose the state which is an eigenstate with an eigenvalue of +1 of the operator σ_z. After a rotation of ϕ around the y-axis, this state becomes

$$u = \begin{pmatrix} 1 \\ 0 \end{pmatrix} \to u' = \exp\left(-i\phi\sigma_y/2\right)\begin{pmatrix} 1 \\ 0 \end{pmatrix} = \begin{pmatrix} \cos(\phi/2) \\ \sin(\phi/2) \end{pmatrix}.$$

Thus the overlap between the states is

$$\langle u' \big| u \rangle = \cos(\phi/2).$$

The long-term survival probability is then $|\langle u'|u\rangle|^4 = \cos^4(\phi/2) = (1+\cos(\phi))^2/4$. The remaining question is then how the bulk energy states are exited when the phase of the helical texture is changed, and by extension the time-dependence of the survival probability. It turns out that the spin-flipped Majorana state overlaps significantly with most of the bulk-states, as shown in fig. 5.5a. This means that Majorana survival probability will quickly stabilise to a final value without significant oscillations, as shown in fig. 5.5b.

When $\theta \neq \pi/4$ the value of ϕ becomes more important as seen in for example the phase diagrams (figs. 4.1 and 4.2). Quenches in ϕ now not only rotates the exchange field vectors uniformly in the unit cell, but also changes the length of them non-uniformly. If the initial and final phase after such a quench are the same, there will be a nonzero overlap between the initial and final Majorana bound states (for $\phi \neq (2n+1)\pi, n \in \mathbb{Z}$), and thus we expect the survival probability to vary around this nonzero value. However, if the angle ϕ is changed such that the topological phase changes, we expect the survival probability to decay after some time. If the final state

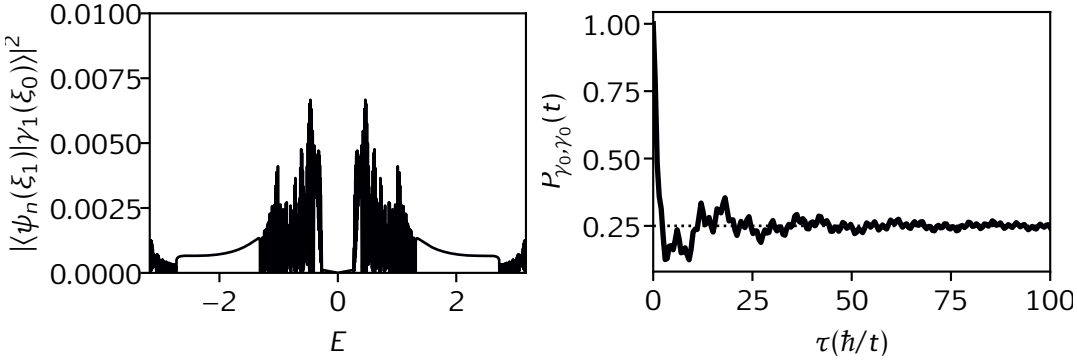

(a) Overlap between a spin-flipped Majorana (orthogonal to itself) and the bulk-energies in a helical system.

(b) Survival probability of a Majorana bound state after a change in ϕ of $\pi/2$. The dashed line is given by $\cos^4(\pi/4) = 0.25$.

Figure 5.5: A quench in the ϕ parameter **(a)** excites a broad range of energies, which leads to **(b)** a quick stabilisation of the survival probability of the original Majorana state without significant oscillations. The parameters were $h = -\mu = t$, $\Delta_0 = 0.3t$, $\theta = \pi/4$, $p/q = 1/3$.

lies between two topological phases, i.e. where the Hamiltonian has a node, the survival probability oscillates as shown in fig. 5.6. Here the system is quenched from to initial values of ϕ_0 which both lie inside the topological nontrivial region to a point where the gap closes. Clear oscillations occur, similar to the dynamics obtained in Sacramento (2016) for critical quenches in other systems. We also see that depending on the amount of change in the parameter ϕ from initial to final state, the frequency in the oscillations vary. In the paper of Sacramento he demonstrated that such a frequency doubling can be explained by whether the Majorana is localised at one or both boundaries, which doubles the frequency in the latter case. However, as seen in fig. 5.6b, both of the Majorana states are localised near both of the edges. When the system is quenched to a critical point, these Majorana states will begin to move through the bulk since the energy gap is closed. Thus, for the resulting wave packets to overlap with their initial form with different oscillation frequencies, they must move with different speeds through the bulk. Since the bulk states and energies are the same in the final Hamiltonian for both cases, we must conclude that the Majoranas excite energystates with different group velocities in the final Hamiltonian.

5.2.3 Chiral breaking

We now consider the effects of suddenly turning on out-of-plane magnetic fields in the system, which we have seen breaks chirality. Although a winding number can not be defined anymore, the parity of the winding number still resides in the Pfaffian of the Hamiltonian at TR invariant momenta. Thus if we go from a nontrivial phase to another by adding a small out-of-plane field, h_z, we can expect that the Majorana bound states at the boundaries will overlap at least somewhat with the new Majorana state. The overlap will in general not be perfect, which means that the old Majorana states must overlap at least partially with the bulk states and thus at of the wave function will begin to move into the bulk of the material. Since the system is of finite size, the moving wave will eventually reach the boundaries again and thus lead to oscillations around a finite non-zero value, similar to the results of Sacramento (2014).

The first quench we consider is to go from a system with chiral symmetry, and

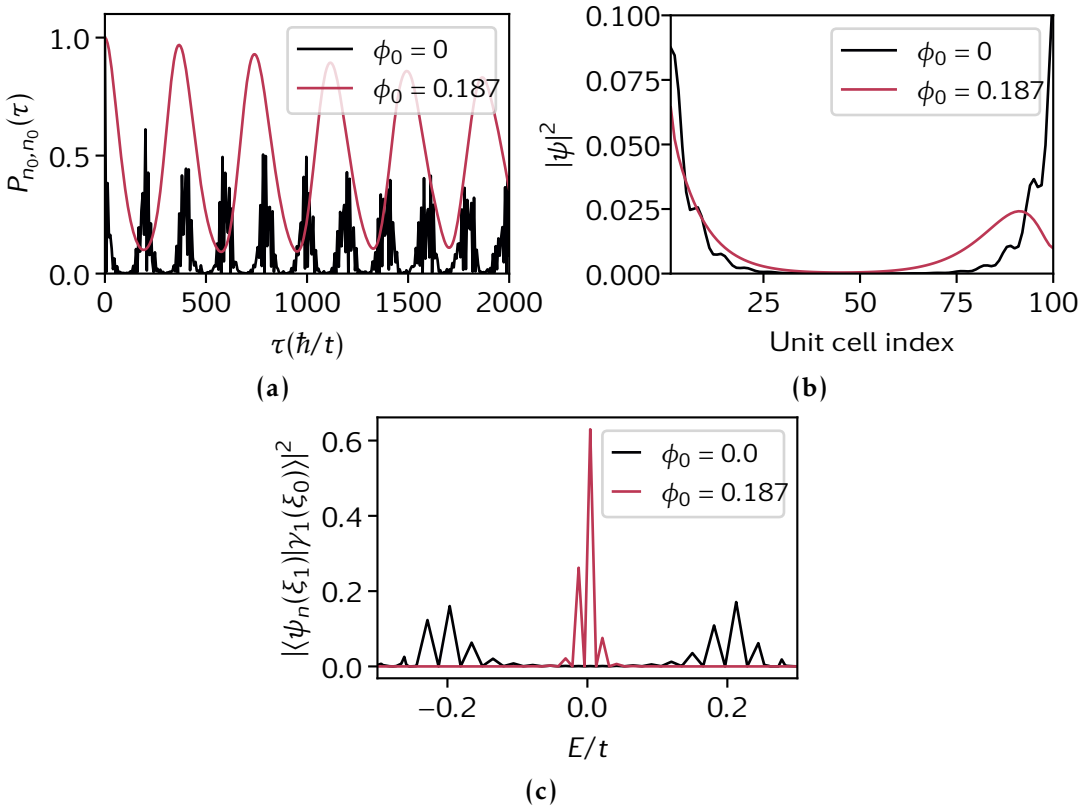

Figure 5.6: Quenching the parameter ϕ to a critical value. **(a)** Survival probability as a function of time, τ. **(b)** Unit cell density of one of the Majorana states. Both cases of initial values of ϕ_0 have peaked densities at each boundary. Thus the increased oscillation frequency in **(a)** can only be explained by an increase in the group velocity of the excited states. This is supported by **(c)** which shows that the excited states lie at significantly different energies. The parameters are $h = -\mu = t$, $\Delta_0 = 0.3t$, $\theta = 0.1$ and $p/q = 1/3$, and the critical value is $\phi_c \approx .197$.

suddenly break the symmetry by adding an out-of-plane field. We do this both for subcritical field strengths ($|h_{z,1}| < |\Delta_0|$) and critical strengths and beyond. In fig. 5.7 we show the survival probability of one of the Majorana bound states after the chiral symmetry has been broken, but without changing the Pfaffian topological invariant for most of the lines. The system is described by a *helical* exchange field texture in the chain. When the out-of-plane field is increased in strength in the final Hamiltonian, the survival probability in general decreases (on average). For all nonzero values of the out-of-plane field the survival probability decreases rapidly to a steady and constant value, with only minor oscillations.This value is in general kept for a while until around $\tau \approx 450$, where oscillation in the survival probability appears for all the cases. This can be interpreted as the initial Majorana bound state overlaping with the bulk states, which will then begin to propagate throught the system. Eventually it is reflected at the other end and comes back after about 450 time units. But interestingly, instead of oscillation about once and then repeating the cycle, multiple oscillations appear in close succession. This means that multiple wave packets with different group velocities propagate through the system, meaning that the oscillations are from multiple groups. The decreasing long-term survival probability can be more clearly seen

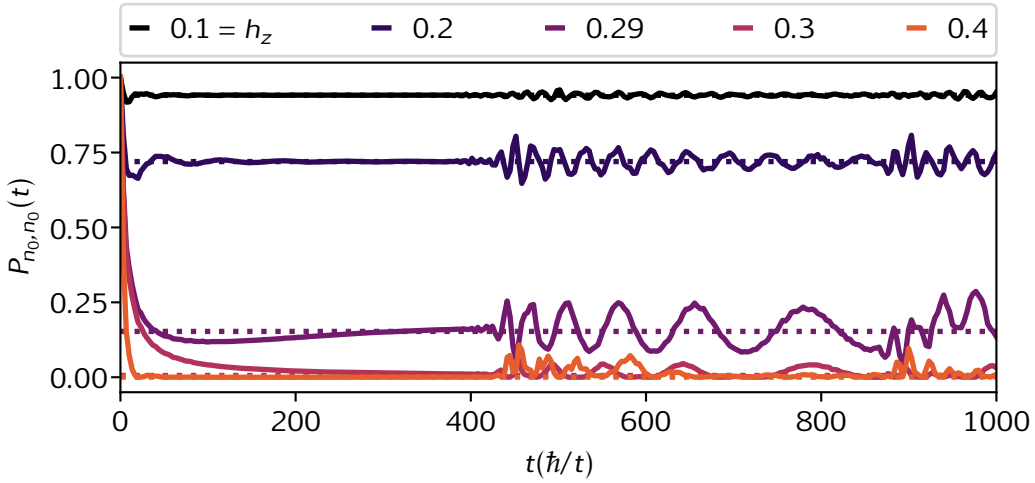

Figure 5.7: Survival probability of one of the Majorana states after a quench which breaks chirality. The different colours differ by the value of the chiral breaking field h_z, and the dashed horizontal lines are the approximated long term survival probability. The parameters were $h = -\mu = t$, $\Delta_0 = 0.3t$, $\theta = \pi/4$, $\phi = 0$, N_{UC} and $p/q = 1/3$.

in fig. 5.8a which shows it as a function of the final out-of-plane field. We note that the critical value of $|h_z| = |\Delta_0|$ is also a clear point in this figure where the long term survival probability goes to zero. We also point out that the Pfaffian invariant is nontrivial still after this critical value, but the Hamiltonian is gapless which makes it irrelevant. As the figure shows, the decrease in the survival probability is minor for small values of h_z but is increasing as h_z becomes bigger. This means that the MBSs are quite robust against small perturbations in the chiral breaking field. This could perhaps also be expected from the previous analysis in the following way. We previously explained that the electrons must have a spin expectation value lying in the xy-plane since none of the Pauli matrices are of the form σ_z. This means that for small additions of an out-of-plane field, the initial wave functions will still be good approximations to the new Hamiltonian after the perturbation if $|h_z|^2 \ll |h|^2$. This is because on average the exchange field vectors are $|h|\hat{\boldsymbol{n}}_{\parallel} + h_z\hat{\boldsymbol{z}}$, which creates an angle of approximately $h_z/|h|$ with the plane. If we then assume that the electrons are approximately parallel to the exchange field vectors, the overlap between a purely in-plane spin and a spin with the angle $h_z/|h|$ from the plane will be $\cos(h_z/|h|) \approx 1 - \frac{h_z^2}{2h^2}$, which is approximately equal to 1 as long as $|h_z| \ll |h|$. This last argument, although hand-wavy, gives a possible interpretation of the effects of turning on small chiral breaking fields and also fits the results as presented here, but does not explain the behaviour close to $h_z = \Delta_0$. This is explained by the fact that the bulk gap closes which delocalises the MBSs which then interact and gain a nonzero energy.

Next we consider quenches beyond the critical out-of-plane field strength. We want to investigate the effects of quenches between a topological system in close proximity to the critical value to a value just above the critical value. The survival probability of one of the Majorana fermions is shown in fig. 5.9, where the dashed line is the long-term survival probability. As expected based on fig. 5.8, we see that the survival probability is small as soon as the out-of-plane field is above the critical value, which is true even

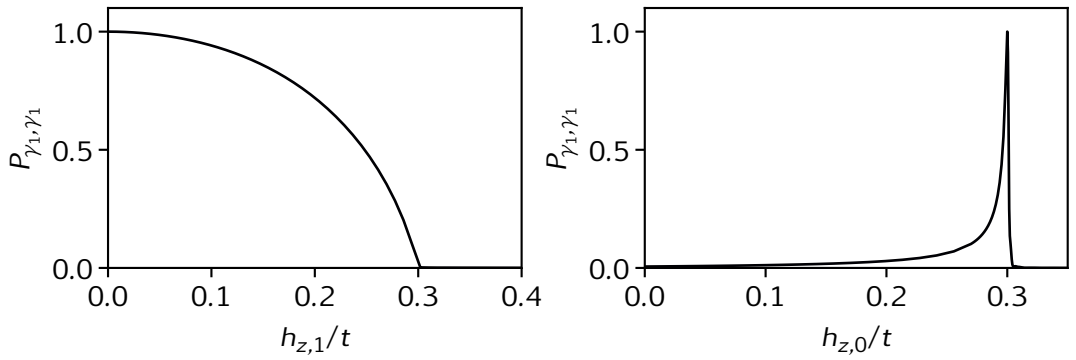

(a) Long-term survival probability of a Majorana state as a function of $h_{z,1}$ when $h_{z,0} = 0$.

(b) Long-term survival probability of a Majorana state as a function of $h_{z,0}$ when $h_{z,1} = 0.3 = \Delta_0$.

Figure 5.8: Long-term survival of the Majorana states for sudden quenches **(a)** from the chiral symmetric system, **(b)** and to the critical value $h_z = \Delta_0$. The parameters were $h = -\mu = t$, $\Delta_0 = 0.3t$, $\theta = \pi/4$, $\phi = 0$, N_{UC} and $p/q = 1/3$.

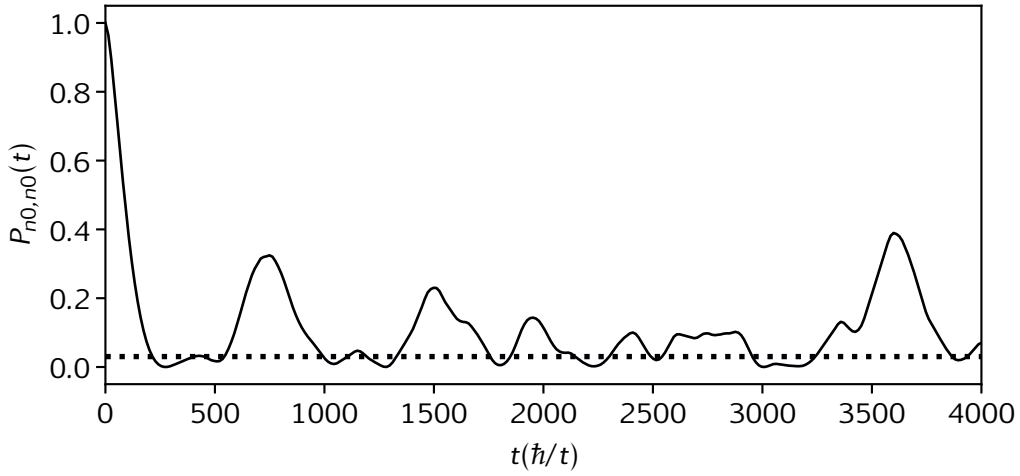

Figure 5.9: Survival probability when quenching a system with a barely subcritical out-of-plane field to a barely supercritical one. The parameters were $h_{z,0} = 0.29t$, $h_{z,1} = 0.31t$, $h = -\mu = t$, $\Delta_0 = 0.3t$, $\theta = \pi/4$, $\phi = 0$, N_{UC} and $p/q = 1/3$.

if the initial system is quite close to the critical value. This leads to oscillations in the survival probability close to zero. The oscillations are erratic which implies that the excited states after the quench correspond to a massive dispersion relation. In fig. 5.10 the energy bands for the system is shown when the out-of-plane field strength is larger than the critical value of $|\Delta_0|$. The energy bands are characterised by two sets of point nodes in the Hamiltonian in close proximity to each other, one set in the rightmost part of the 1BZ, and the other in the left most part. The chiral breaking is easy to see as the fact that the transformation $\hat{H}(k) \to -\hat{H}(k)$ does not exist. That is, the energy spectrum is not mirror symmetric around the k axis. However, PH symmetry can be seen by going from k to $-k$ which negates the energies. The red region indicates the energies which are significantly excited in the new Hamiltonian with $h_z = 0.31t$ from the single particle bound Majorana state in the nontrivial system with $h_z = 0.29t$. Close to nodes

the Hamiltonian can be approximated by a massless fermion system, however between the two nodes of each pair the dispersion relation bends significantly, even within the excited energy range. This means that the massless dispersion relation approximation is not valid for this quench, and since the bending ($\partial_k^2 E_k$) is significant, we expect the resulting wave packet which is excited from the old Majorana edge state to disperse significantly and the survival probability will not have well defined oscillations since the edge state will only partially overlap with the (after a while) uniformly distributed wave function.

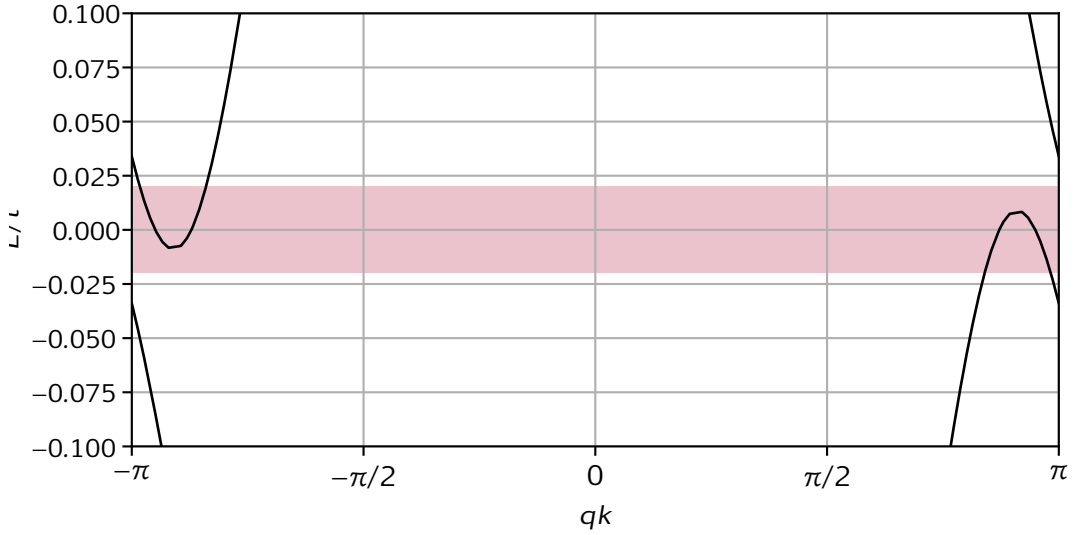

Figure 5.10: Bulk energy bands in the Brillouin zone for an out-of-plane field which is supercritical. The parameters were $h = -\mu = t$, $h_z = 0.31t$, $\Delta_0 = 0.3t$, $\theta = \pi/4$, $\phi = 0$, and $p/q = 1/3$. The red region indicates the energies which are significantly excited in the new Hamiltonian after quenching from $h_z = 0.29t$ to $h_z = 0.31t$, computed as the standard deviation.

5.3 Conclusion

The MBSs in the elliptical system have proven to be both robust and quite sensitive to quenches in the Hamiltonian parameters depending on the type of perturbation, the strength and the similarity between the initial and final state. Changing the helicity of the magnetic texture quickly led to erratic behaviour of the survival probability for larger values of θ_0 due to the increased significance of the y-component of the exchange field vectors which flips when the helicity flips. By introducing an intermediate step of $\theta_1 = 0$ we showed that he initial MBSs can excite MBSs in the final state with opposite helicity. However, this requires correct timing as the overlap has narrow peaks in time. A natural next step to the dynamics of quenches in the helicity would be to analyse the effects of a continuous ramp instead of a sudden quench in the parameter. This might be a more realistic process. In that case the length of the ramp would be another factor which affects the fate of the MBSs. Thus if the transition time can be experimentally controlled, it can be a path to controlling the Majorana state in the system.

Quenches in the global offset of the magnetic texture in the material had different effects depending on the eccentricity of the elliptical pattern. When the ellipse was circular (helical), the overlap between the Majorana states and the bulk was very broad,

leading to a fast decay of the survival probability as the time went, and reaching a stable long term probability with only minor erratic oscillations. In this case the final value of the survival probability is given by the overlap probability squared of two spins rotated by ϕ relative to each other. When the ellipse was more flat, the overlap between the MBSs and the bulk was considerably narrower, thus the survival probability in quenches in ϕ oscillated less erratic. The energy of the excited states were not necessarily concentrated around 0 energy when quenched to a critical value of ϕ between the trivial and topological phase, and as a result the frequency of oscillations of the survival probability varied depending on the initial value of ϕ.

The MBSs were very robust against the application of out-of-plane ferromagnetic fields which breaks the chirality, but the overlap between the initial and final MBSs continuously decreased towards 0 as the out-of-plane field went towards the critical value $h_z = \Delta_0$, where the Majoranas were completely killed and overlapped heavily with the the bulk states. This happens over a short time scale of the order of $\hbar/t$. Thus the application of an external out-of-plane exchange field can prove to be a very effective control mechanism for turning on and off the MBSs states in a finite size system.

We did not check the time dependence of the MBSs after quenches in the superconducting order parameter. This has been done by for example Sacramento (2014) for multiple types of systems, and in many cases lead to well defined oscillations in the survival probability of the Majorana states. However, this still has to be confirmed for this specific system.

A natural next step to the analysis in this chapter would be to investigate more natural time-dependent changes in the Hamiltonian, like for instance continuous ramping of the potential, thereby using eq. (5.24). We have already seen implications that this can change the dynamics of the system as in the case of an intermediate step in the quench of θ.

6 | Summary and outlook

We have now investigated the emergent topology in magnetic chains in contact with conventional and unconventional superconductivity. One of the novel ideas of this thesis has been the search for non-accidental and robust topological systems defined as being between two topological phases such that any symmetry conserving perturbation immediately drives the systems into topological nontrivial phases. These marginal topological superconductors were obtained in p-wave superconductors in ferromagnetic fields, but not when the magnetic field was purely antiferromagnetic. They were also obtainable in conventional superconductors in non-collinear exchange fields when the exchange fields vectors either were aligned on a linear line or when other geometric criteria were fulfilled. Marginal topological superconductors can potentially be an important tool in devices where control of, creation of and annihilation of MBSs is required, as only minor changes in the parameters of the system can lead to localisation of the MBSs on the edges. We have not investigated whether marginal topology can exist in 2D or 3D systems or not. In 1D systems with a winding number topological invariant, we were able to find non-accidental regions where the imaginary part of the winding curve was zero. This is not immediately applicable to, for instance, 3D where the Hamiltonian is a mapping to the 3-sphere and is not anymore a complex number. Also, systems with other symmetries defined by, for instance, a Pfaffian invariant, does not easily lead to equation for when the Hamiltonian is gapless and marginal topological. Therefore future research needs to be conducted into marginal topological superconductors in more dimensions than 1D.

It is also not immediately clear how to experimentally achieve the marginal topological phases. For instance, in the s-wave superconductor in a noncollinear and inhomogeneous exchange field we are dependent on a unit cell of at least three atoms where the exchange field vectors are different enough, and the gap opening perturbations needs to be local in the unit cells, only affecting the exchange field at a few of the sites or affecting the sites differently.

We investigated the topological properties of conventional superconductors coupled with elliptical exchange fields in 1D magnetic chains. The topological phases were understood in terms of the new symmetries that appear in the 2D and 3D space extended by the synthetic momentum variables θ and ϕ. The nodal points and lines in these spaces are protected by both chiral symmetry and PH symmetry. In the case when the chiral symmetry is present, the nodal points have nonzero winding numbers defined on curves in $k\theta$-space enclosing them. The marginal topological phase in these systems also indicated the importance of and interplay between the TR symmetry and inversion symmetry, where both must be broken for nontrivial topological phases to emerge.

The elliptical system was then analysed in a terms of time-dependent quenches in the Hamiltonian parameters and the dynamics of the Majorana fermions after quenches that were subcritical, critical or supercritical. We demonstrated that quenches across

marginal topological regions were dependent of the characteristic length scale of the transition of the parameters. The usage of a chiral symmetry breaking term in the Hamiltonian of the elliptical system can also be a potential tool for manipulation of the MBSs. Since this term does not change the topological phase of the system, the MBSs are robust against small in this parameter. However, when the out-of-plane field reached a critical value of Δ_0, the system is gapless in many cases and effectively kills the MBSs.

Other time-dependent phenomena in both the elliptical magnetic chain system and other marginal topological systems would be an interesting research topic in the future, where for instance periodic driving is an interesting alternative to sudden quenches in the parameters.

Bibliography

Alicea, J. (2012). New directions in the pursuit of Majorana fermions in solid state systems. *Reports on Progress in Physics*, *75*(7), 076501. doi:10.1088/0034-4885/75/7/076501. arXiv: 1202.1293 [cond-mat.supr-con]

Alicea, J., Oreg, Y., Refael, G., von Oppen, F. & Fisher, M. P. A. (2011). Non-Abelian statistics and topological quantum information processing in 1D wire networks. *Nature Physics*, *7*, 412–417. doi:10.1038/nphys1915. arXiv: 1006.4395 [cond-mat.mes-hall]

Altland, A. & Zirnbauer, M. R. (1997). Nonstandard symmetry classes in mesoscopic normal-superconducting hybrid structures. *Physical Review B*, *55*, 1142–1161. doi:10.1103/PhysRevB.55.1142. arXiv: cond-mat/9602137 [cond-mat]

Amorim, C. S., Ebihara, K., Yamakage, A., Tanaka, Y. & Sato, M. (2015). Majorana braiding dynamics in nanowires. Phys. Rev. B, *91*(17), 174305. doi:10.1103/PhysRevB.91.174305

Balian, R. & Werthamer, N. R. (1963). Superconductivity with Pairs in a Relative p Wave. *Physical Review*, *131*, 1553–1564. doi:10.1103/PhysRev.131.1553

Bao, J.-K., Liu, J.-Y., Ma, C.-W., Meng, Z.-H., Tang, Z.-T., Sun, Y.-L., ... Feng, C.-M. (2015). Superconductivity in Quasi-One-Dimensional $K_2Cr_3As_3$ with Significant Electron Correlations. *Physical Review X*, *5*(1), 011013. doi:10.1103/PhysRevX.5.011013. arXiv: 1412.0067 [cond-mat.supr-con]

Bardeen, J., Cooper, L. N. & Schrieffer, J. R. (1957). Theory of Superconductivity. *Physical Review*, *108*, 1175–1204. doi:10.1103/PhysRev.108.1175

Bargmann, V. (1964). Note on Wigner's Theorem on Symmetry Operations. *Journal of Mathematical Physics*, *5*, 862–868. doi:10.1063/1.1704188

Bermudez, A., Patanè, D., Amico, L. & Martin-Delgado, M. A. (2009). Topology-Induced Anomalous Defect Production by Crossing a Quantum Critical Point. Phys. Rev. Lett. *102*(13), 135702. doi:10.1103/PhysRevLett.102.135702. arXiv: 0811.3843 [cond-mat.str-el]

Bihlmayer, G., Rader, O. & Winkler, R. (2015). Focus on the Rashba effect. *New Journal of Physics*, *17*, 050202. doi:10.1088/1367-2630/17/5/050202

Bloch, F. (1929). Über die Quantenmechanik der Elektronen in Kristallgittern. *Zeitschrift fur Physik*, *52*, 555–600. doi:10.1007/BF01339455

Bogoliubov, N. N. (1958). On a new method in the theory of superconductivity. *Il Nuovo Cimento*, *7*, 794–805. doi:10.1007/BF02745585

Bonnes, L., Essler, F. H. L. & Läuchli, A. M. (2014). "Light-Cone" Dynamics After Quantum Quenches in Spin Chains. Phys. Rev. Lett. *113*(18), 187203. doi:10.1103/PhysRevLett.113.187203. arXiv: 1404.4062 [cond-mat.str-el]

Braunecker, B. & Simon, P. (2013). Interplay between Classical Magnetic Moments and Superconductivity in Quantum One-Dimensional Conductors: Toward a Self-

Sustained Topological Majorana Phase. Phys. Rev. Lett. *111*(14), 147202. doi:10.1103/PhysRevLett.111.147202. arXiv: 1307.2431 [cond-mat.mes-hall]

Chen, W. & Schnyder, A. P. (2015). Majorana edge states in superconductor-noncollinear magnet interfaces. Phys. Rev. B, *92*(21), 214502. doi:10.1103/PhysRevB.92.214502. arXiv: 1504.02322 [cond-mat.supr-con]

Chiu, C.-K. & Schnyder, A. P. (2014). Classification of reflection-symmetry-protected topological semimetals and nodal superconductors. *Physical Review B*, *90*, 205136. doi:10.1103/PhysRevB.90.205136. arXiv: 1408.4642 [cond-mat.mes-hall]

Chiu, C.-K., Teo, J. C. Y., Schnyder, A. P. & Ryu, S. (2016). Classification of topological quantum matter with symmetries. *Reviews of Modern Physics*, *88*, 035005. doi:10.1103/RevModPhys.88.035005. arXiv: 1505.03535 [cond-mat.mes-hall]

Choy, T., Edge, J. M., Akhmerov, A. R. & Beenakker, C. W. J. (2011). Majorana fermions emerging from magnetic nanoparticles on a superconductor without spin-orbit coupling. Phys. Rev. B, *84*(19), 195442. doi:10.1103/PhysRevB.84.195442. arXiv: 1108.0419 [cond-mat.mes-hall]

Claveau, Y., Arnaud, B. & Di Matteo, S. (2014). Mean-field solution of the Hubbard model: the magnetic phase diagram. *European Journal of Physics*, *35*(3), 035023. doi:10.1088/0143-0807/35/3/035023. arXiv: 1403.2259 [cond-mat.str-el]

Cooper, L. N. (1956). Bound Electron Pairs in a Degenerate Fermi Gas. *Physical Review*, *104*, 1189–1190. doi:10.1103/PhysRev.104.1189

de Gennes, P. G. (1964). Boundary Effects in Superconductors. *Reviews of Modern Physics*, *36*, 225–237. doi:10.1103/RevModPhys.36.225

Deng, M. T., Yu, C. L., Huang, G. Y., Larsson, M., Caroff, P. & Xu, H. Q. (2012). Anomalous Zero-Bias Conductance Peak in a Nb-InSb Nanowire-Nb Hybrid Device. *Nano Letters*, *12*, 6414–6419. doi:10.1021/nl303758w

Fossheim, K. & Sudbø, A. (2005). *Superconductivity: Physics and applications*. John Wiley & Sons.

Fu, L. & Kane, C. L. (2008). Superconducting Proximity Effect and Majorana Fermions at the Surface of a Topological Insulator. Phys. Rev. Lett. *100*(9), 096407. doi:10.1103/PhysRevLett.100.096407. arXiv: 0707.1692 [cond-mat.mes-hall]

Hubbard, J. (1963). Electron Correlations in Narrow Energy Bands. *Proceedings of the Royal Society of London Series A*, *276*, 238–257. doi:10.1098/rspa.1963.0204

Jérome, D., Mazaud, A., Ribault, M. & Bechgaard, K. (1980). Superconductivity in a synthetic organic conductor $(TMTSF)_2PF_6$. *J. Phys Lett*, *41*(4), 95–98. doi:10.1051/jphyslet:0198000410409500

Kimura, T. & Tokura, Y. (2008). Magnetoelectric phase control in a magnetic system showing cycloidal/conical spin order. *Journal of Physics Condensed Matter*, *20*(43), 434204. doi:10.1088/0953-8984/20/43/434204

Kirilyuk, A., Kimel, A. V. & Rasing, T. (2010). Ultrafast optical manipulation of magnetic order. *Reviews of Modern Physics*, *82*(3), 2731–2784. doi:10.1103/RevModPhys.82.2731

Kitaev, A. Y. (2003). Fault-tolerant quantum computation by anyons. *Annals of Physics*, *303*, 2–30. doi:10.1016/S0003-4916(02)00018-0. arXiv: quant-ph/9707021 [quant-ph]

Kitaev, A. Y. (2001). Unpaired Majorana fermions in quantum wires. *Physics Uspekhi*, *44*, 131. doi:10.1070/1063-7869/44/10S/S29. arXiv: cond-mat/0010440 [cond-mat.mes-hall]

Kittel, C. (2005). *Introduction to solid physics* (8th ed.). John Wiley & Sons.

Klinovaja, J. & Loss, D. (2013). Giant Spin-Orbit Interaction Due to Rotating Magnetic Fields in Graphene Nanoribbons. *Physical Review X*, *3*, 011008. doi:10.1103/PhysRevX.3.011008. arXiv: 1211.2739 [cond-mat.mes-hall]

Klinovaja, J., Stano, P. & Loss, D. (2012). Transition from Fractional to Majorana Fermions in Rashba Nanowires. Phys. Rev. Lett. *109*(23), 236801. doi:10.1103/PhysRevLett.109.236801. arXiv: 1207.7322 [cond-mat.mes-hall]

Kramer, H. A. (1930). Théorie générale de la rotation paramagnétique dans les cristaux. *Proc. Amst. Acad. 33*, 959–972.

Kreyzig, E. (2011). *Advanced engineering mathematics* (10th ed.). Wiley.

Kutta, W. (1901). *Beitrag zur näherungsweisen integration totaler differentialgleichungen*.

Lebed, A. G. & Sepper, O. (2013). Possible triplet superconductivity in the quasi-one-dimensional conductor $Li_{0.9}Mo_6O_{17}$. Phys. Rev. B, *87*(10), 100511. doi:10.1103/PhysRevB.87.100511

Lee, E. J. H., Jiang, X., Houzet, M., Aguado, R., Lieber, C. M. & de Franceschi, S. (2014). Spin-resolved Andreev levels and parity crossings in hybrid superconductor-semiconductor nanostructures. *Nature Nanotechnology*, *9*, 79–84. doi:10.1038/nnano.2013.267. arXiv: 1302.2611 [cond-mat.mes-hall]

Lee, I. J., Brown, S. E., Clark, W. G., Strouse, M. J., Naughton, M. J., Kang, W. & Chaikin, P. M. (2002). Triplet Superconductivity in an Organic Superconductor Probed by NMR Knight Shift. Phys. Rev. Lett. *88*(1), 017004. doi:10.1103/PhysRevLett.88.017004

Leggett, A. J. (1975). A theoretical description of the new phases of liquid ^{3}He. *Reviews of Modern Physics*, *47*(2), 331–414. doi:10.1103/RevModPhys.47.331

Linder, J. [J.], Amundsen, M. & Risinggård, V. (2017). Intrinsic superspin Hall current. *Physical Review B*, *96*(9), 094512. doi:10.1103/PhysRevB.96.094512. arXiv: 1704.07381 [cond-mat.mes-hall]

Linder, J. [Jacob]. (2017). *Intermediate quantum mechanics* (1st ed.). bookboon.com.

Ludwig, A. W. W. (2016). Topological phases: classification of topological insulators and superconductors of non-interacting fermions, and beyond. *Physica Scripta Volume T*, *168*, 014001. doi:10.1088/0031-8949/2015/T168/014001. arXiv: 1512.08882 [cond-mat.mes-hall]

Lutchyn, R. M., Sau, J. D. & Das Sarma, S. (2010). Majorana Fermions and a Topological Phase Transition in Semiconductor-Superconductor Heterostructures. Phys. Rev. Lett. *105*, 077001. doi:10.1103/PhysRevLett.105.077001. arXiv: 1002.4033 [cond-mat.supr-con]

Majorana, E. (1937). Teoria simmetrica dellelettrone e del positrone. *Il Nuovo Cimento*, *14*, 171.

Marra, P. & Cuoco, M. (2017). Controlling Majorana states in topologically inhomogeneous superconductors. *Physical Review B*, *95*, 140504. doi:10.1103/PhysRevB.95.140504. arXiv: 1606.08450 [cond-mat.supr-con]

Maxwell, E. (1950). Isotope Effect in the Superconductivity of Mercury. *Physical Review*, *78*, 477–477. doi:10.1103/PhysRev.78.477

Mercaldo, M. T., Cuoco, M. & Kotetes, P. (2018). Magnetic manipulation of topological states in p-wave superconductors. *Physica B Condensed Matter*, *536*, 730–733. doi:10.1016/j.physb.2017.11.007. arXiv: 1710.05567 [cond-mat.supr-con]

Mercaldo, M. T., Cuoco, M. & Kotetes, P. (2016). Magnetic-field-induced topological reorganization of a p -wave superconductor. *Physical Review B*, *94*, 140503. doi:10.1103/PhysRevB.94.140503. arXiv: 1607.03539 [cond-mat.supr-con]

Mercaldo, M. T., Kotetes, P. & Cuoco, M. (2018). Topological signatures of the coexistence of antiferromagnetism and odd-parity spin-triplet superconductivity. *AIP Advances*, *8*, 101303. doi:10.1063/1.5042830. arXiv: 1806.07140 [cond-mat.supr-con]

Mourik, V., Zuo, K., Frolov, S. M., Plissard, S. R., Bakkers, E. P. A. M. & Kouwenhoven, L. P. (2012). Signatures of Majorana Fermions in Hybrid Superconductor-Semiconductor Nanowire Devices. *Science*, *336*, 1003. doi:10.1126/science.1222360. arXiv: 1204.2792 [cond-mat.mes-hall]

Murakawa, H., Onose, Y., Kagawa, F., Ishiwata, S., Kaneko, Y. & Tokura, Y. (2008). Rotation of an Electric Polarization Vector by Rotating Magnetic Field in Cycloidal Magnet $Eu_{0.55}Y_{0.45}MnO_3$. *Phys. Rev. Lett. 101*, 197207. doi:10.1103/PhysRevLett.101.197207

Nadj-Perge, S., Drozdov, I. K., Bernevig, B. A. & Yazdani, A. (2013). Proposal for realizing Majorana fermions in chains of magnetic atoms on a superconductor. Phys. Rev. B, *88*(2), 020407. doi:10.1103/PhysRevB.88.020407

Oreg, Y., Refael, G. & von Oppen, F. (2010). Helical Liquids and Majorana Bound States in Quantum Wires. Phys. Rev. Lett. *105*, 177002. doi:10.1103/PhysRevLett.105.177002. arXiv: 1003.1145 [cond-mat.mes-hall]

Perfetto, E. (2013). Dynamical Formation and Manipulation of Majorana Fermions in Driven Quantum Wires in Contact with a Superconductor. Phys. Rev. Lett. *110*(8), 087001. doi:10.1103/PhysRevLett.110.087001. arXiv: 1207.6888 [cond-mat.str-el]

Pyka, K., Keller, J., Partner, H. L., Nigmatullin, R., Burgermeister, T., Meier, D. M., … Zurek, W. H. (2013). Topological defect formation and spontaneous symmetry breaking in ion Coulomb crystals. *Nature Communications*, *4*, 2291. doi:10.1038/ncomms3291

Quezel, S., Tcheou, F., Rossat-Mignod, J., Quezel, G. & Roudaut, E. (1977). Magnetic structure of the perovskite-like compound TbMnO $_3$. *Physica B+C*, *86-88*, 916–918. doi:10.1016/0378-4363(77)90740-9

Rashba, E. I. & Sheka, V. I. (1959). Symmetry of energy bands in crystals of wurtzite type ii. Symmetry of bands with spin-orbit interaction included. *Soviet Phys. Solid State*, *2*, 162–176. English translation: Supplemental Material to the paper by Bihlmayer, G., O. Rader, and R. Winkler, 'Focus on the Rashba effect', New J. Phys. 17.

Runge, C. (1895). *Mathematische Annalen*, *46*(2), 167–178. doi:10.1007/BF01446807

Ryu, S., Schnyder, A. P., Furusaki, A. & Ludwig, A. W. W. (2010). Topological insulators and superconductors: tenfold way and dimensional hierarchy. *New Journal of Physics*, *12*, 065010. doi:10.1088/1367-2630/12/6/065010. arXiv: 0912.2157 [cond-mat.mes-hall]

Sacramento, P. D. (2016). Edge mode dynamics of quenched topological wires. Phys. Rev. E, *93*, 062117. doi:10.1103/PhysRevE.93.062117. arXiv: 1601.05476 [cond-mat.mes-hall]

Sacramento, P. D. (2014). Fate of Majorana fermions and Chern numbers after a quantum quench. Phys. Rev. E, *90*, 032138. doi:10.1103/PhysRevE.90.032138. arXiv: 1404.5141 [cond-mat.stat-mech]

Sato, M., Takahashi, Y. & Fujimoto, S. (2010). Non-Abelian topological orders and Majorana fermions in spin-singlet superconductors. *Physical Review B*, *82*, 134521. doi:10.1103/PhysRevB.82.134521. arXiv: 1006.4487 [cond-mat.supr-con]

Scheurer, M. S. & Shnirman, A. (2013). Nonadiabatic processes in Majorana qubit systems. Phys. Rev. B, *88*(6), 064515. doi:10.1103/PhysRevB.88.064515. arXiv: 1305.4923 [cond-mat.mes-hall]

Sedlmayr, N., Aguiar-Hualde, J. M. & Bena, C. (2015). Flat Majorana bands in two-dimensional lattices with inhomogeneous magnetic fields: Topology and stability. *Physical Review B*, *91*, 115415. doi:10.1103/PhysRevB.91.115415. arXiv: 1410.1734 [cond-mat.mes-hall]

Shiozaki, K., Sato, M. & Gomi, K. (2016). Topology of nonsymmorphic crystalline insulators and superconductors. Phys. Rev. B, *93*(19), 195413. doi:10.1103/PhysRevB.93.195413. arXiv: 1511.01463 [cond-mat.mes-hall]

Sigrist, M. & Ueda, K. (1991). Phenomenological theory of unconventional superconductivity. *Reviews of Modern Physics*, *63*, 239–312. doi:10.1103/RevModPhys.63.239

Slater, J. C. & Koster, G. F. (1954). Simplified LCAO Method for the Periodic Potential Problem. *Physical Review*, *94*, 1498–1524. doi:10.1103/PhysRev.94.1498

Sticlet, D. C. (2012). *Edge states in chern insulators and majorana fermions in topological superconductors* (Ph. D. thesis, Université Paris-Sud XI).

Sudbø, A. (n.d.). Lecture notes in 'FY8302 Quantum theory of Solid'.

Tewari, S. & Sau, J. D. (2012). Topological Invariants for Spin-Orbit Coupled Superconductor Nanowires. Phys. Rev. Lett. *109*(15), 150408. doi:10.1103/PhysRevLett.109.150408. arXiv: 1111.6592 [cond-mat.mes-hall]

Thomas, L. H. (1926). The Motion of the Spinning Electron. *Nature*, *117*, 514. doi:10.1038/117514a0

Timm, C. (2015). Theory of magnetism [lecture notes]. Technische Universität Dresden, Institute for Theoretical Physics. Technische Universität Dresden, Institute for Theoretical Physics. Retrieved from https://www.physik.tu-dresden.de/~timm/personal/teaching/thmag_w09/lecturenotes.pdf

Valatin, J. G. (1958). Comments on the theory of superconductivity. *Il Nuovo Cimento*, *7*, 843–857. doi:10.1007/BF02745589

Wigner, E. P. (1959). *Group theory: And its application to the quantum mechanics of atomic spectra*. Academic press.

Yamasaki, Y., Sagayama, H., Abe, N., Arima, T., Sasai, K., Matsuura, M., ... Tokura, Y. (2008). Cycloidal Spin Order in the a-Axis Polarized Ferroelectric Phase of Orthorhombic Perovskite Manganite. Phys. Rev. Lett. *101*(9), 097204. doi:10.1103/PhysRevLett.101.097204

Yamasaki, Y., Sagayama, H., Goto, T., Matsuura, M., Hirota, K., Arima, T. & Tokura, Y. (2007). Electric Control of Spin Helicity in a Magnetic Ferroelectric. Phys. Rev. Lett. *98*(14), 147204. doi:10.1103/PhysRevLett.98.147204

Glossary

1BZ First Brillouin zone.

AFM antiferromagnetic.

AZ Altland-Zirnbauer [table].

BCS Bardeen-Cooper-Schrieffer.

BdG Bogoliubov-de Gennes.

CCW counterclockwise.

CW clockwise.

FM ferromagnetic.

LDoS Local density of states.

MBS Majorana bound state.

OP Order Parameter.

PH Particle-Hole.

SC superconductor.

SDW spin-density wave.

SOC spin-orbit coupling.

TR Time Reversal.

Kristian Løvås Svalland

Topological phases in proximised magnetic superconductors and related time dependent phenomena

NTNU
Norwegian University of
Science and Technology

SPIN